TAMPEREEN TEKNILLINEN YLIOPISTO
TAMPERE UNIVERSITY OF TECHNOLOGY

SASU RUOKANGAS
RUBBER - PHASE CHANGE MATERIAL COMPOSITES FOR
HEAT STORAGE APPLICATIONS

Master of Science Thesis

ABSTRACT

SASU RUOKANGAS: Rubber - Phase Change Material Composites for Heat Storage Applications
Master of Science Thesis, 97 pages
January 2018
Master's Degree Programme in Materials Engineering
Major: Polymers and Biomaterials
Examiners: Asst. Prof. Essi Sarlin and Postdoctoral Researcher Minna Poikelispää

Keywords: phase change material, rubber, heat storage, latent heat, composite

Because of the universal concern over accelerated climate change and increasing price of fossil fuels, renewable energy sources and energy efficiency has become more and more important. These both make use of heat storage. Heat can be stored by either sensible heat or latent heat, of which latent heat offers multiple heat storage capacity. The materials that can store or release large amounts of heat during a phase change are called phase change materials (PCM). The majority of PCMs are so-called solid-liquid phase change materials. For practical applications, the leakage of the PCMs at their liquid phase must be prevented. The most cost-efficient way to do this is to disperse the PCM in a matrix material. This kind of composites are called shape stabilized phase change materials (SSPCM).

The main goal of the theory part of this thesis was to research previous studies concerning SSPCMs with polymeric matrix. The understanding of these previous studies was important in order to provide the scope and reference to the experimental part of this thesis. The purpose was to figure out the used matrix materials, phase change materials as well as the most important properties of different material combinations. The most important properties of SSPCMs are the phase change temperature and the latent heat, as they determine the application temperature and heat storage capacity of the material. Another important thermal property is thermal conductivity, which influences the heat transfer between the SSPCM and the environment, thus restricting the efficiency of the heat storage. These previous studies were important to provide the scope and reference to the experimental part of this thesis. Besides thermal properties, mechanical properties such as tensile strength and elasticity are important in certain applications.

The aim of the experimental part of this thesis was to prepare SSPCMs with NR and latex matrixes, to study their properties and to find the most compatible PCM/matrix combinations and optimal PCM contents. It was found that the heat storage capacity of the SSPCMs increases with increasing PCM content. By contrast, mechanical properties deteriorate when PCM content is increased. Thus, the PCM content of the SSPCM should be optimized according to the requirements of the application. In this study, an optimal PCM content to offer sufficient heat storage capacity while still retaining satisfactory mechanical properties was found to be 50 phr (parts per hundred rubber). Paraffins were found to be the most compatible PCM group to be mixed with rubber, as they maintained their heat storage capacity more effectively than other options. Moreover, paraffins did not seem to change the mechanical properties of rubber as much as other PCMs.

TIIVISTELMÄ

SASU RUOKANGAS: Kumi-faasimuutosmateriaalikomposiitit lämmön varastointisovelluksiin
Diplomityö, 97 sivua
Tammikuu 2018
Materiaalitekniikan diplomi-insinöörin tutkinto-ohjelma
Pääaine: Polymeerit ja biomateriaalit
Tarkastajat: Assistant Professor Essi Sarlin ja tutkijatohtori Minna Poikelispää

Avainsanat: faasimuutosmateriaali, kumi, lämmön varastointi, latenttilämpö, komposiitti

Energiatehokkuuteen ja uusiutuviin energianlähteisiin on viime vuosina kiinnitetty entistä enemmän huomiota ilmastonmuutoksen kiihtymisen ja fossiilisten polttoaineiden vähenemisen ja kallistumisen takia. Sekä uusiutuvan energian tuotannossa että energiatehokkuuden parantamisessa hyödynnetään lämmön varastointia. Latenttilämpö on tehokkain tapa varastoida lämpöä. Materiaaleja, jotka varastoivat tai luovuttavat suuren määrän latenttilämpöä faasimuutoksessa kutsutaan faasimuutosmateriaaleiksi (PCM). Suurin osa faasimuutosmateriaaleista ovat neste-kiinteä – faasimuutosmateriaaleja, joiden valuminen sulana on estettävä käytännön sovelluksia varten. Kustannustehokkain tapa estää faasimuutosmateriaalin valuminen on sekoittaa se polymeerimatriisiin. Tällaisia komposiittimateriaaleja sanotaan muotopysyviksi faasimuutosmateriaaleiksi (SSPCM).

Tämän diplomityön teoriaosan päätavoite oli aiempien tutkimusten perusteella selvittää, mitä matriisi- ja faasimuutosmateriaaleja näissä komposiiteissa on käytetty ja millä pitoisuuksilla, sekä mitkä ovat komposiittien tärkeimmät ominaisuudet sovelluskohteita ajatellen. SSPCM:ien tärkeimmät ominaisuudet ovat latenttilämmön varastointikyky ja faasimuutoslämpötila, jotka määrittävät materiaalin sovelluslämpötilan ja lämmönvarastointikapasiteetin. Tärkeä ominaisuus on myös lämmönjohtavuus, joka vaikuttaa SSPCM:n ja ympäristön väliseen lämmönsiirtoon rajoittaen lämmön varastoinnin tehokkuutta. Näiden termisten ominaisuuksien lisäksi mekaaniset ominaisuudet kuten vetolujuus ja elastisuus ovat tärkeitä tietyissä sovelluksissa.

Tämän diplomityön kokeellisen osan tavoitteena oli valmistaa SSPCM:iä kumimatriisilla, tutkia niiden ominaisuuksia ja löytää sopivimmat kumi/PCM –yhdistelmät sekä niiden optimaaliset PCM-pitoisuudet. Tutkimuksissa selvisi, että SSPCM:ien lämmönvarastointikapasiteetti kasvaa, kun niiden PCM-pitoisuutta kasvatetaan. Mekaaniset ominaisuudet sen sijaan heikentyvät PCM-pitoisuuden kasvaessa. PCM-pitoisuus tulisikin optimoida SSPCM:n suunnitteluvaiheessa sovelluskohteen materiaalivaatimusten mukaan. Tässä tutkimuksessa optimaaliseksi PCM-pitoisuudeksi, jolla oli kohtalainen lämmönvarastointikapasiteetti mutta silti riittävät mekaaniset ominaisuudet, valikoitui 50 phr (parts per hundred rubber). Sopivin PCM-ryhmä kumin kanssa sekoitettavaksi oli parafiinit, jotka säilyttivät lämmönvarastointikyvyn sekoitettaessa muita materiaaleja paremmin. Parafiineilla vaikutti myös olevan vähiten kumin mekaanisia ominaisuuksia huonontava vaikutus.

PREFACE

In Tampere, Finland, on 15 December 2017

Sasu Ruokangas

TABLE OF CONTENTS

LIST OF SYMBOLS AND ABBREVIATIONS

C20	N-eicosane
CA	Capric acid
Cu NW	Copper nanowire
DCP	Dicumyl peroxide
DMA	Dynamical mechanical analysis
DSC	Differential scanning calorimetry
EC	Ethyl cellulose
EG	Expanded graphite
EGP	Expanded graphite plate
EPDM	Ethylene-propylene-diene monomer
EVA	Ethylene-vinyl acetate copolymer
FESEM	Field emission scanning electron microscope
FG	Fiberglass
GNP	Graphene nanoplatelet
GP	Graphite powder
HDPE	High-density polyethylene
LA	Lauric acid
LDPE	Low-density polyethylene
LFA	Laser flash analysis
MA	Myristic acid
MC	Methyl cellulose
MH	Magnesium hydroxide
MP	Mass portion
MWCNT	Multi-wall carbon nanotube
NAO	Nano-Al_2O_3
NG	Nano-graphite
NPG	Neopentylglycol
NR	Natural rubber
OM	Optical microscope
PA	Palmitic acid
PANI	Polyaniline
PCM	Phase change material
phr	Parts per hundred rubber
PMMA	Poly(methyl methacrylate)
POE	Ethylene-octane copolymer
PP	Polypropylene
PVA	Polyvinyl alcohol
PVC	Polyvinyl chloride
RP	Red phosphorus
SA	Stearic acid
SBS	Styrene-butadiene-styrene copolymer
SEBS	Styrene-ethylene-butylene-styrene copolymer
SEM	Scanning electron microscope
SIS	Styrene-isoprene-styrene copolymer
SMA	Styrene maleic anhydride copolymer
SR	Silicone rubber
SSPCM	Shape stabilized phase change material
TD	1-tetradecanol

Wax FT	Hard paraffin wax (Fischer-Tropsch)
Wax S	Soft paraffin wax
a	Thermal diffusivity
a_m	Fraction melted
C_p	Specific heat
ΔH_c	Latent heat of crystallization (solidification)
ΔH_m	Latent heat of fusion (melting)
k	Thermal conductivity
Q	Quantity of heat stored
Q_l	Quantity of latent heat stored
S	Entropy
T_c	Crystallization temperature
T_f	Final temperature of a heating process
T_i	Initial temperature of a heating process
T_m	Melting temperature

1. INTRODUCTION

Because of the constantly increasing levels of greenhouse gas emissions and increasing price of fossil fuels, the use of renewable energy sources and increased energy efficiency has become more and more important in the recent years. Thermal energy storage is important in the effective use of renewable energy, and it also helps to improve the energy efficiency of various applications and processes. Thermal energy storage is used for example to store heat obtained by solar energy during sunlight and release it during the night. Another important use of thermal energy storage is in space heating systems to improve the energy efficiency of buildings. [1,2]

The classification of thermal energy storage materials is presented in Figure 1. Basically, thermal energy can be stored in two ways. Sensible heat storage stands for storage of heat by increasing the temperature of the storage material. By contrast, latent heat storage means the storage of energy when a material changes phase from one to another, most commonly from solid to liquid. Latent heat storage is generally considered as the most efficient method of storing thermal energy, as it offers much higher energy storage density with a narrower temperature range between storing and releasing heat than sensible heat storage. [3-5]
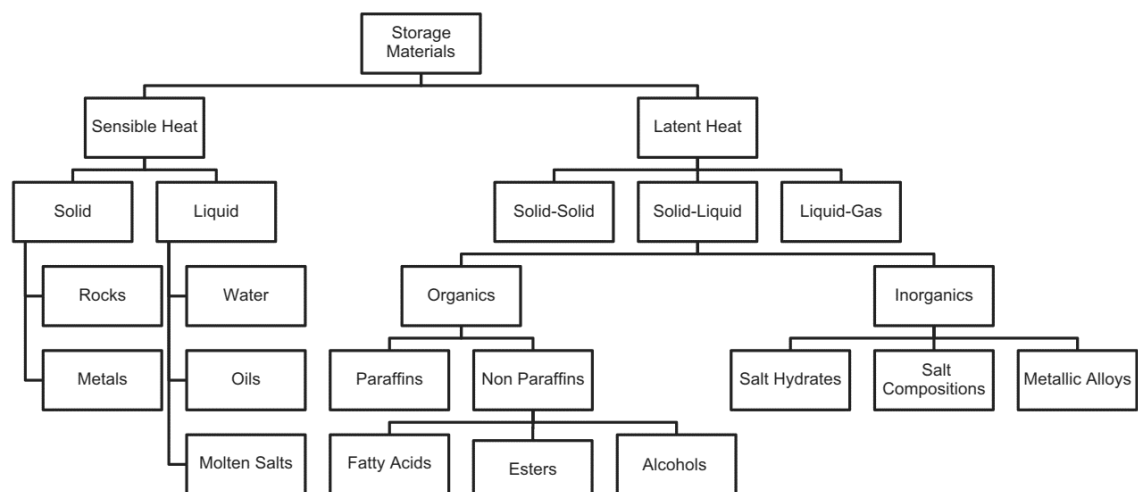
Figure 1. *Classification of thermal energy storage materials [6].*

The materials that are able to store or release large amounts of latent heat at a certain temperature are called phase change materials (PCM). The most important PCM groups commercially are paraffins, fatty acids and salt hydrates. These PCMs are solid-liquid PCMs, meaning that they store and release latent heat during melting and crystallization, respectively. For practical uses, the flowing of these materials at their molten phase must

be prevented. One possible way to do this is to encapsulate the PCM for example in aluminum boxes (macroencapsulation) or micro-sized polymer capsules (microencapsulation). However, the capsulation increases the weight and cost of PCMs. A more cost-effective way to prevent the leakage of PCMs is to disperse them in a matrix material, most commonly a polymer. This kind of composite materials, with a PCM as the latent heat storage material and a matrix material to support the PCM and prevent its leakage at the molten phase, are called shape stabilized phase change materials (SSPCM). [7-10]

SSPCMs with plastic matrix have been studied extensively, with high-density polyethylene (HDPE) being the most commonly used matrix material [10-13]. Also thermoplastic elastomers have been used as matrix materials [14-17]. On the other hand, SSPCMs with rubber matrix have been studied scarcely. However, characteristic properties of rubber, such as the elasticity and damping capability, could be advantageous for SSPCMs. Considering that, the aim of this thesis was to fabricate SSPCMs with natural rubber (NR) and NR latex as matrix materials and to study mechanical and thermal properties of the SSPCMs. Since a thesis (Pönkä, Faasimuutosmateriaalien käyttö energian varastoinnissa, 2012) concerning PCMs has already been published, the emphasis of the theory part of this thesis is in SSPCMs with polymeric matrix materials.

In Chapter 2 of this thesis, important requirements of PCMs are presented. One of the most important requirements is high latent heat, and that is why the basic principles of latent heat and its determination are discussed. In addition, Chapter 2 discusses the classification of PCMs, and the typical properties of each class. Chapter 3 presents the earlier studies concerning polymer-based SSPCMs. Chapter 4 discusses the enhancement of the thermal conductivity of SSPCMs with the addition of fillers. Chapter 5, which is the last chapter of the theory part of this thesis, presents two potential applications for elastomer-based SSPCMs. Chapter 6 presents the raw materials and methods used for the preparation of the SSPCMs in the experimental part of this thesis. Furthermore, the test methods used for characterization of the SSPCMs are presented. The results of the tests are presented in Chapter 7. Finally, Chapter 8 concludes the most important findings of this thesis.

2. PHASE CHANGE MATERIALS

Phase change material (PCM) is a material that can absorb or release large amounts of heat during the phase change at a certain temperature. The stored or released heat is called the latent heat. In the case of solid-liquid phase change, also term "heat of fusion" may be used. PCMs with solid-liquid phase change are usually preferred because of their large latent heat and small volume change (usually less than 10%) during the phase change. However, also some potential solid-solid PCMs exist. Their volume change during the phase change is minimal, but their latent heat is usually lower than that of solid-liquid PCMs. Liquid-vapor phase change of materials has also usually large latent heats. Unfortunately, high vaporization temperatures and very large volume change during vaporization make the exploitation of liquid-vapor phase change impractical. [1,18,19]

The two main prerequisites for PCMs are a suitable phase change temperature for a certain application and a large latent heat [1]. There are also several other requirements, the importance of which depending on a selected application. These requirements may be divided into thermal, physical, kinetic, chemical and economic properties, and they are presented in Table 1.

Table 1. The requirements of PCMs [20,21].

Requirements	Example measurement technique
Thermal properties:	
Suitable phase change temperature	Differential scanning calorimetry (DSC)
High latent heat	DSC
High thermal conductivity	Laser flash analysis (LFA)
High specific heat	DSC
Physical properties:	
Small volume change on phase change	Dilatometry
Low vapor pressure	Isoteniscope
Congruent melting	DSC
High density	Density scale
Kinetic properties:	
Low supercooling	DSC
High crystallization rate	DSC
Chemical properties:	
Long-term chemical stability	DSC
No corrosivity	Corrosion cell
No toxicity	Lethal dose (LD_{50})
No flammability	Cone calorimetry

In addition to the properties presented in Table 1, a PCM should also be easily available at low cost. In practice, none of the currently known PCMs meets all these requirements. For example, most of the PCMs have low thermal conductivity, and especially salt hydrates show significant supercooling during crystallization. Consequently, during materials selection, the material properties must be optimized for the selected application. [1]

2.1 Latent heat

Latent heat, or phase change enthalpy, of materials indicates the amount of energy absorbed or emitted during the phase change of a material. Typically, the phase change from solid to liquid or vice versa, i.e. the melting and solidification of materials, is used to store latent heat. Because solid-liquid PCMs are by far the most commonly used PCMs, the theory of latent heat of solid-liquid phase change is presented here. Considering solid-solid PCMs, the solid-liquid phase change is replaced by solid-solid phase transition, but the theory is otherwise mostly applicable. [1]

2.1.1 Latent heat of solid-liquid phase change

The melting and solidification processes are presented in a simplified manner in Figure 2. During melting, the material absorbs energy (heat) with no increase in its temperature. The energy absorbed increases the vibrational state of the atoms or molecules of the material. At the melting temperature, the covalent bonds between the atoms loosen and the material melts. Correspondingly, energy is emitted during solidifying as the atoms or molecules arrange and lose their energy. [19]
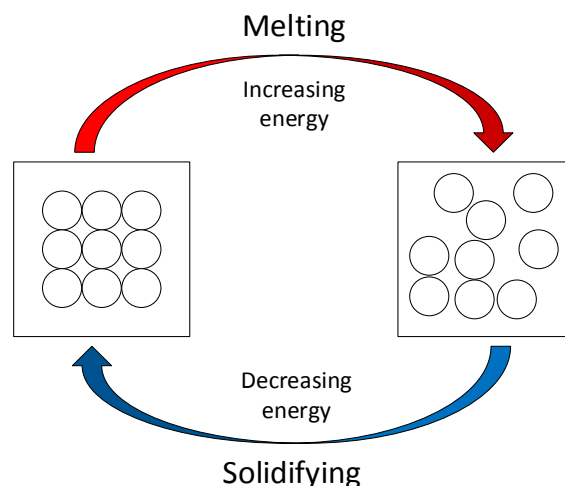

Figure 2. The melting and solidification processes.

Figure 3 shows a generalized heating curve of a PCM. When a PCM is heated at its solid state, it stores heat as sensible heat. Sensible heat is defined as the heat that changes the temperature of the material. When the PCM is further heated to its melting point, the

phase change from solid to liquid occurs. During this phase change, the PCM can store a large amount of latent heat while its temperature remains constant. [1,19] The amount of latent heat stored can be calculated by the equation: [22]

$$Q_l = ma_m\Delta H_m, \tag{1}$$

where Q_l is the quantity latent of heat stored (J), m is the mass of the PCM (kg), a_m is the fraction melted and ΔH_m is the latent heat of fusion (J/kg).
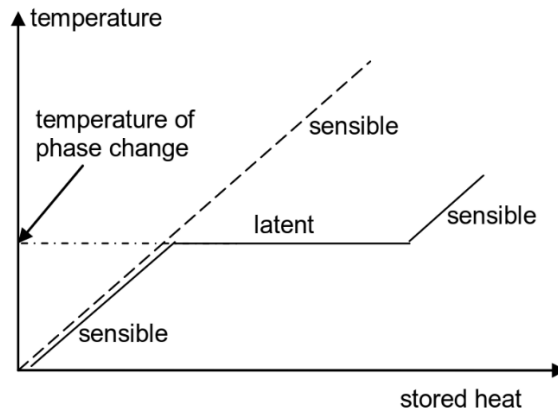

Figure 3. A general heating curve of a PCM showing the latent heat of solid-liquid phase change [1].

If the heating is continued after all the PCM has melted, the temperature of the PCM increases again and the heat is stored as sensible heat. Thus, the total amount of heat stored during the heating process, including both the sensible and latent heat, may be calculated by the equation: [22]

$$Q = \int_{T_i}^{T_m} mC_p dT + ma_m\Delta H_m + \int_{T_m}^{T_f} mC_p dT, \tag{2}$$

where Q is the quantity of heat stored (J), T_i is the initial temperature (K), T_m is the melting temperature of the PCM (K), T_f is the final temperature and C_p is the specific heat of the PCM (J/Kg·K). In the equation (2), the first and the last term result from sensible heat, while the middle term represents the latent heat of fusion.

The latent heat storage capacity of PCMs is often superior compared to heat storage capacities of sensible heat storage materials. Water is a good illustrative example, although its usage as a PCM is restricted because of its low melting temperature. Water has a heat capacity of 4.2 kJ/kg·K, so when the temperature of 1 g of water is increased by 1 °C, 4.2 J heat is stored. The latent heat of fusion of water is 330 kJ/kg, so when 1 g of water is melted so that the temperature rises 1 °C during the process, 334 J heat is absorbed (combined latent heat and sensible heat). Thus, in the case of water, about 80 times more heat is stored as latent heat than as sensible heat. [23]

2.1.2 Determination of the latent heat and phase change temperature

Because the latent heat and the phase change temperature are the most essential properties of PCMs, it is important to understand how they are measured and how the measurement data should be interpreted. There are several different methods to determine the latent heat and the phase change temperature of PCMs (see Table 1). In the studies concerning SSPCMS, the most commonly used method is differential scanning calorimetry (DSC).

In DSC, the difference in heat flux between a sample and a reference is monitored against time or temperature, while they are subjected to a controlled temperature program. The sample is placed in a sample pan to avoid the leakage of the sample at the molten phase. To exclude the effects of the pan to the measurement, a reference pan is used. The sample and the reference are heated or cooled in an oven by a constant (dynamic mode) or variable (step mode) heating rate. Dynamic mode is more commonly used with PCMs. When the temperature reaches the phase change temperature, heat is absorbed (in the case of melting) or released (in the case of crystallization) by the sample, causing an endothermic or exothermic peak on the DSC curve, respectively.

Figure 4 shows a schematic of a DSC curve of a PCM. The latent heat may be calculated from the area of the corresponding peak (lined area in Figure 4). The determination of the phase change temperature is somewhat subject to interpretation, as PCMs generally melt/crystallize at temperature ranges rather than precise phase change temperatures. If a single value for the phase change temperature is persisted, the starting temperature or peak temperature of the phase change peak may be used. [1,18,24,25]

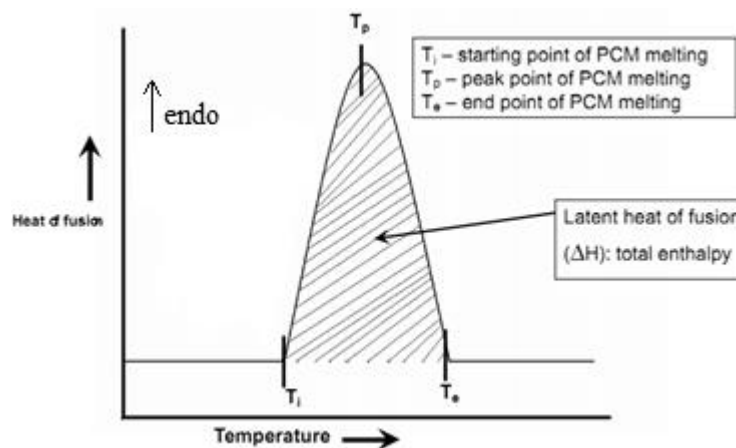*Figure 4.* Schematic of DSC curve of PCM. Adapted from [26].

Certain characteristics and properties of PCMs cause difficulties in DSC measurements. Firstly, some PCM – salt hydrates in particular – show significant supercooling during solidification. Supercooling means that the PCM solidifies at a temperature much lower than its melting temperature. Supercooling may depend on the sample size and hence

cause uncertainties in the measurements. Another challenge is that the sample should be at thermodynamic equilibrium during the measurement. The equilibrium can be disturbed by supercooling, and low thermal conductivity of most PCMs further delays reaching the equilibrium. This problem can be prevented by using adequately slow heating/cooling rates during the measurement. [1]

Besides the measurements, the characteristics of PCMs may cause problems also in the interpretation of the results of the DSC measurements. In addition to the ambiguity in the determination of the melting point, hysteresis of the heating-cooling cycle may also cause confusion in the interpretation of the data. Hysteresis means that the heating and cooling data of the PCM are dissimilar, often due to supercooling. Consequently, both the heating and cooling data should be presented to avoid misinterpretations. [1]

2.2 Classification of PCMs

PCMs can be classified into two major groups: organic and inorganic. Organic PCMs include paraffins, fatty acids, esters, alcohols and glycols. Inorganic materials include salt hydrates, salts, metals and metal alloys. Some of these materials can also be combined to form eutectic compositions. Of all the materials mentioned above, paraffins, fatty acids and salt hydrates are the commercially most commonly used. [7,8] They were also included in the experimental studies presented later in this thesis. In addition, the experimental work included neopentylglycol (NPG), which is a solid-solid phase change material. Thus, the basic characteristics of paraffins, fatty acids, salt hydrates and NPG-based PCMs are presented in the following subchapters. The presented PCM groups and their most important properties are summarized in Table 2. It should be noted that the values are approximate, and may vary according to reference. To be concise, the comparison of the most important advantages and disadvantages of different PCM groups is presented in Table 3.

Table 2. *The most commonly used PCM groups and their important properties. Adapted from [20,27,28].*

PCM	Phase transition temperature (°C)	Latent heat (kJ/kg)	Thermal conductivity (W/m·K)	Density solid/liquid (kg/m³)
Paraffins	-12…135	60-269	0.2	760/900
Fatty acids	-7…187	125-250	0.2	878/1004
Salt hydrates	-33…120	86-328	0.7	1937/2180
NPG-based PCMs	25…187	5-296	no reference	

Table 3. *Advantages and disadvantages of the PCM groups [20].*

PCM	Advantages	Disadvantages
Paraffins	High latent heat	Low thermal conductivity
	Low supercooling	Low density
	Chemically stable	High volume change
	Non-corrosive	Inflammable
	Cheap	Broad melting range
Fatty acids	High latent heat	Low thermal conductivity
	Sharp melting point	Inflammable
	Low supercooling	Instable at high temperatures
		Toxic and corrosive
		Expensive
Salt hydrates	High latent heat	Corrosive
	High thermal conductivity	High supercooling
	High density	Phase separation
	Small volume change	Toxic
	Sharp melting point	
	Cheap	
NPG-based PCMs	Very small volume change	Low latent heat

2.2.1 Paraffins

Paraffins are saturated hydrocarbons (alkanes) characterized by the formula C_nH_{2n+2}. In commercial applications, blends of paraffins with different chain lengths are usually used. These blends are called paraffin waxes. Paraffin waxes are relatively cheap, which is the main reason why paraffins are commercially the most common PCMs. The melting temperature of paraffins increases with the increasing number of carbon atoms. Consequently, the melting temperature of paraffins is easy to tailor for desired application by varying the length of the carbon chain. Typical melting temperatures of paraffins vary between 35-70 ºC, though also lower and higher temperatures are possible, as seen in Table 2. To be more precise, paraffins rather melt at a 5-10 ºC wide temperature range than at one sharp temperature. One clear advantage of paraffins is that they do not show (or show very little) supercooling. They also have relatively good heat of fusion (generally 160-200 kJ/kg). Unfortunately, paraffins have also several drawbacks. The volume increase during melting can be as high as 20%, which must be taken into account in the design of the heat storage system. The thermal conductivity of paraffins − like almost all PCMs − is low, typically below 0.2 W/m·K. The density of paraffins is low, which might be a problem in applications requiring the compactness of the PCM. Moreover, paraffins are inflammable, so fire retardant is needed in high-temperature applications. [27,29,30]

Figure 5 shows a typical DSC heating curve of a paraffin. It is seen that the DSC curve of paraffin has two phase change peaks. The high peak near 58 ºC corresponds to the solid-liquid phase change of paraffin, and the low peak near 40 ºC represents the solid-solid phase change of paraffin. Since the area of the phase change peak corresponds to the latent heat, the majority of heat is absorbed during the solid-liquid phase change of paraffin.
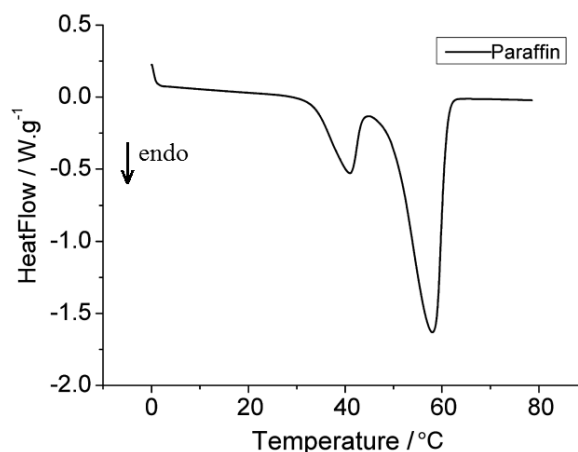

Figure 5. A typical DSC heating curve of a paraffin [31].

2.2.2 Fatty acids

Fatty acids are characterized by the formula $CH_3(CH_2)_{2n}COOH$. The thermal properties of fatty acids are quite similar to those of paraffins. The melting temperature range of fatty acids is narrower than that of paraffins. They have good cyclic stability and show little or no supercooling. Fatty acids are often used as mixtures of two or more acids, which makes it possible to tailor the thermal properties according to the requirements. Unfortunately, they are 2-2.5 times more expensive than paraffins, which limits their commercial usage. Fatty acids are also inflammable and instable at high temperatures. [19,27,29] For example, the fatty acid used in the experimental part of this thesis decomposed at temperatures above 140 ºC. As an example of the melting behavior of fatty acids, a DSC heating curve of palmitic acid is shown in Figure 6. It is seen that unlike paraffins, fatty acids do not show solid-solid phase transformation prior to melting.
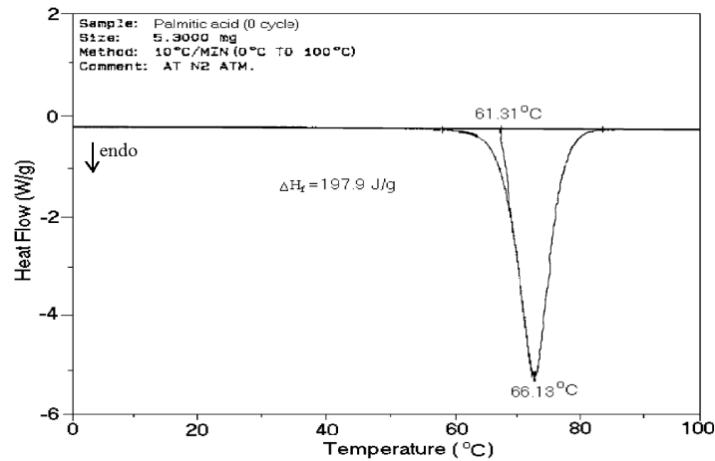
Figure 6. A DSC heating curve of palmitic acid [32].

2.2.3 Salt hydrates

Salt hydrates consist of salts and water of crystallization forming a well-defined, stable crystal structure. The typical melting temperatures of salt hydrates are 5-120 ℃. Salt hydrates have two major advantages compared to paraffins and fatty acids. Firstly, salt hydrates have high heat of fusion, which may be over 300 kJ/kg. Secondly, the thermal conductivity of salt hydrates is high for a PCM, reaching 0.7 W/m·K. In addition, salt hydrates have sharp melting point and low volume change during melting. However, they also have some drawbacks. As salt hydrates are not single-component systems, phase separation during repeated heating-cooling cycles may be a problem. This is seen in Figure 7 as the two cooling curves of calcium chloride hexahydrate are dissimilar. In addition, salt hydrates have high tendency to supercooling, which is also seen in Figure 7. Supercooling may yet be reduced by adding nucleating agents to the materials. Moreover, salt hydrates are corrosive, which restricts their usage in contact with metals. [1,27,30]
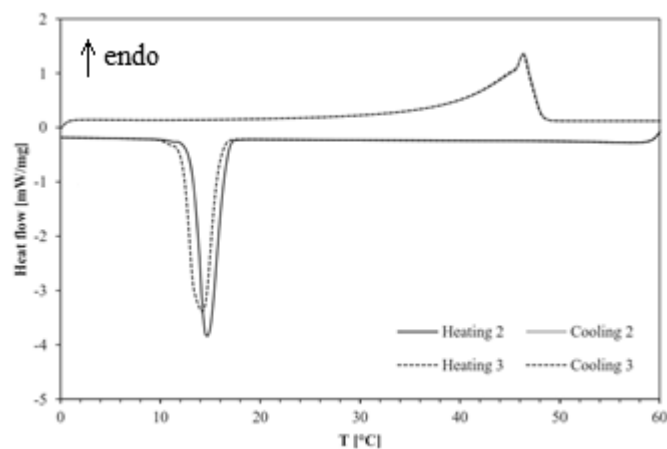

Figure 7. DSC heating and cooling curves of calcium chloride hexahydrate [33].

2.2.4 Solid-solid PCMs

Polyalcohols, such as glycerine, pentaglycerine and neopentylglycol (NPG) can store considerable amounts of energy during their phase transformation at solid state. These materials have been studied and used scarcely because of their lower latent heat compared to solid-liquid PCMs.

3. SHAPE STABILIZED PHASE CHANGE MATERIALS

A major problem in using solid-liquid PCMs as they are is their leakage at the liquid state, which may contaminate the thermal energy storage system, weaken its efficiency and even make it dysfunctional. The most commonly used way to avoid the leakage of the PCM is to encapsulate it. The encapsulation is divided into macro- and microencapsulation, based on the size of the capsule. In macroencapsulation, the diameter of the capsules is bigger than 1 cm, whereas in microencapsulation the diameter is less than 1 mm. Besides the prevention of leakage, microencapsulation improves the processability and heat transfer (due to large surface area) of the PCM. Unfortunately, encapsulation has also some disadvantages. Macrocapsules, which may be for example aluminum containers, increase the weight of the system considerably. Microencapsulation, on the other hand, is often relatively costly due to advanced and complicated capsulation techniques. [9]

One way to avoid the extra costs resulting from the microencapsulation of PCMs is to disperse the PCM in a matrix material. The purpose of the matrix is to act as a supporting material and prevent the leakage of the PCM when it is at the molten phase. These composite materials are called shape stabilized phase change materials (SSPCMs). Also name form-stable phase change material is used in literature to describe similar materials. The most commonly used SSPCMs consist of a PCM dispersed in polymeric matrix. A less researched and utilized subdivision of these is SSPCMs with elastomeric matrix. SSPCMs can also be fabricated by impregnating porous graphite or aluminum matrix with a PCM, but this thesis focuses on SSPCMs with elastomeric or polymeric matrix. [10]

Since the shape of the composite should remain unchanged, the operating temperature of plastic composite materials is limited by the melting temperature of the matrix material. In case of rubber matrix, the operating temperature is dictated by the thermal decomposition of the rubber. Elevated temperatures may also cause over-crosslinking, which may result in the loss of elasticity of the rubber. [12]

In the following subchapters, previous studies about SSPCMs with rubbers, thermoplastic elastomers and plastics are presented. Since the present work focuses on composites of rubbers and PCMs, the researches about SSPCMs with rubbery matrix are the most relevant. However, the amount of studies on these materials is limited. A few more researches have been performed on SSPCMs with thermoplastic elastomers as a matrix material. SSPCMs with plastic matrix, instead, have been widely studied in the previous

years, and they are also included in the present work to offer wider perspective of SSPCMs.

3.1 PCMs in rubber matrix

In the following subchapters, the previous studies concerning rubber-based SSPCMs are presented.

3.1.1 PCMs in NR matrix

Phadungphatthanakoon et al. [34] developed a shape stabilized PCM by mixing microencapsulated n-eicosane (C20, paraffin with 20 carbon atoms within a molecule) with natural rubber (NR) latex. C20 was encapsulated by a polymer blend containing ethyl cellulose (EC) and methyl cellulose (MC) (2:1). The encapsulated PCMs contained 80% or 91% C20 by weight. Water slurry of this encapsulated PCM was mixed with the latex so that the PCM microcapsule contents in the final SSPCMs were 20, 50 and 70%. With the PCM content of 20%, the formed slurry was easily poured into a mold. The dry PCM/NR sample looked homogenous under visual inspection. Figure 8 shows a SEM (scanning electron microscope) picture of the sample. It is seen that the dispersion of PCM particles in the NR was good and homogenous, with no visible agglomerates or density variations. The adhesion between the PCM and the matrix seemed to be relatively low, since the fracture surface mostly follows the PCM-matrix interface.
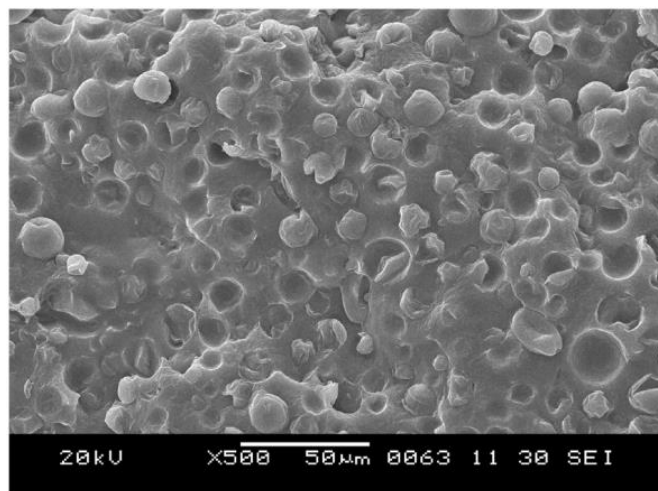

Figure 8. *SEM-image of the PCM/NR SSPCM (PCM-content 20%) [34].*

When the PCM content was raised to 50%, the components were still easily mixable. By contrast, when the PCM content was further raised to 70%, the sample cracked easily. Tensile tests were done for the 50% sample and the control sample (pure NR) to determine how the PCM addition affects to the mechanical properties of the NR. An interesting fact is that the tensile strength of the PCM/NR SSPCM was greater than that of the pure NR. In addition, the hardness of the NR increased when PCM was added. Thus, it was

concluded that the PCM fillers improved the mechanical strength of the NR, as long as the PCM content was not too high. The reason for this unusual reinforcement was supposed to be the novel EC/MC encapsulation material.

The high-temperature stability of the PCM/NR SSPCM was evaluated by keeping the sample at 80 ℃ for 10 minutes. Since there was no visible leakage of the PCM from the sample, the SSPCM was presumed to be stable at 80 ℃. This stability was accounted for the support that the NR matrix provides for the thin-walled PCM microcapsules.

Phadungphatthanakoon et al. tested the thermal storage capacity of the PCM/NR SSPCM (50% PCM-content) and the reference NR by heating and cooling the samples and monitoring the temperature of the samples by thermal camera. The samples were circular, with a radius of 5.2 cm and thickness of 0.315 cm. Figure 9 shows that when the room-temperature (28 ℃) samples were placed onto a heated surface at 50-52 ℃, the temperature of the PCM/NR sample was 40 ℃ or below for 20 minutes, whereas the reference sample heated up to 50 ℃ after 9 minutes. When the samples at 46 ℃ were placed to a surface at 28 ℃, the temperature of the PCM/NR stayed above 30 ℃ for 40 minutes, whereas the temperature of the reference sample decreased to 29 ℃ after 15 minutes. Even though the test was merely approximate, it highlights the potential of the PCM/NR SSPCM to store heat and to equalize differences in temperature. Thus, the thermal properties of the SSPCM should be studied in more detail.
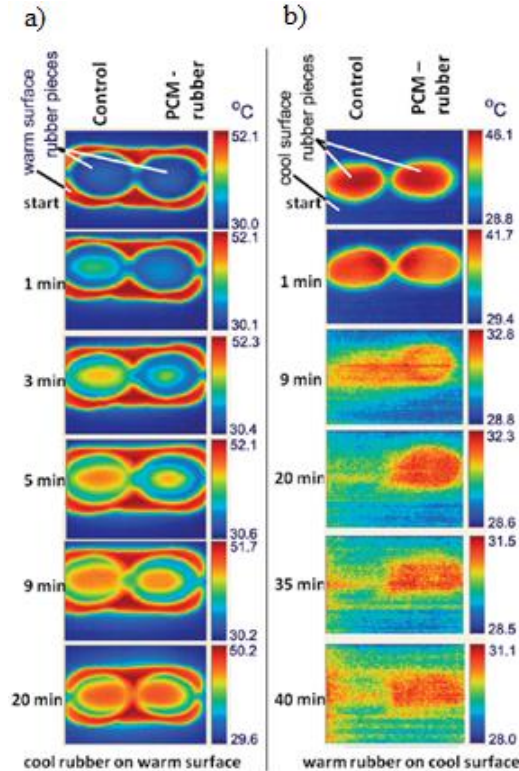

Figure 9. *Thermal camera images of the PCM/NR SSPCM and the reference sample (pure NR). (a) The 28 ℃ samples were placed on a 50 ℃ surface. (b) The 46 ℃ samples were placed on a 28 ℃ surface. [34]*

3.1.2 PCMs in EPDM matrix

Song et al. [35] fabricated and studied SSPCMs with paraffin and ethylene-propylene-diene monomer (EPDM) as matrix material. Most of the samples contained also nano-structured magnesium hydroxide (nano-MH) and red phosphorus (RP) to enhance the fire properties of the material. Table 4 shows the composition of the samples.

Table 4. *The compositions of the SSPCM samples. Adapted from [35].*

Sample	Composition (in mass portions, MP)
I	Paraffin (100 MP) + EPDM (100 MP)
II	Paraffin (50 MP) + EPDM (100 MP) + nano-MH (100 MP) + RP (10 MP)
III	Paraffin (100 MP) + EPDM (100 MP) + nano-MH (100 MP) + RP (10 MP)
IV	Paraffin (100 MP) + EPDM (60 MP) + nano-MH (100 MP) + RP (10 MP)

Figure 10 shows a SEM micrograph of cross-section of the sample IV. It is seen that EPDM forms a three-dimensional network structure, with paraffin evenly distributed within it.
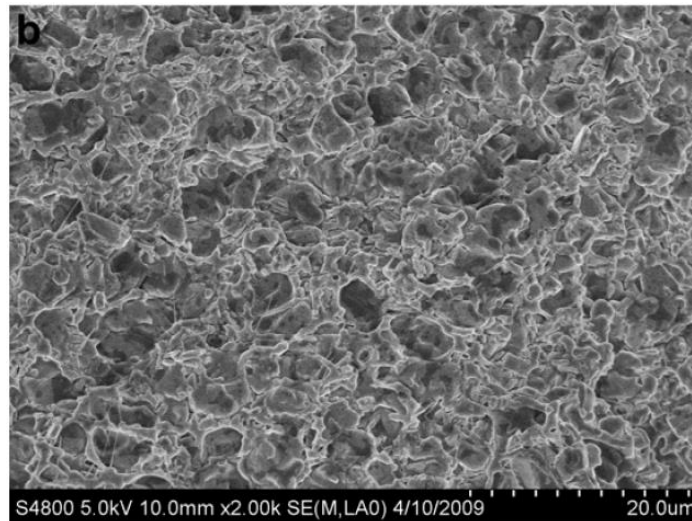

S4800 5.0kV 10.0mm x2.00k SE(M,LA0) 4/10/2009   20.0um

Figure 10. *A SEM micrograph of cross-section of the sample IV at 2000x magnification [35].*

The DSC curves of the samples, as well as typical curves of bulk paraffin and EPDM, are shown in Figure 11. The DSC curves of the samples I-IV all had the phase change peaks typical of paraffin. As supposed, the higher the paraffin content of the sample, the larger the areas of the phase change peaks were. The supercooling effect is also visible in the Figure 11, as the samples solidified at lower temperatures than they melted.
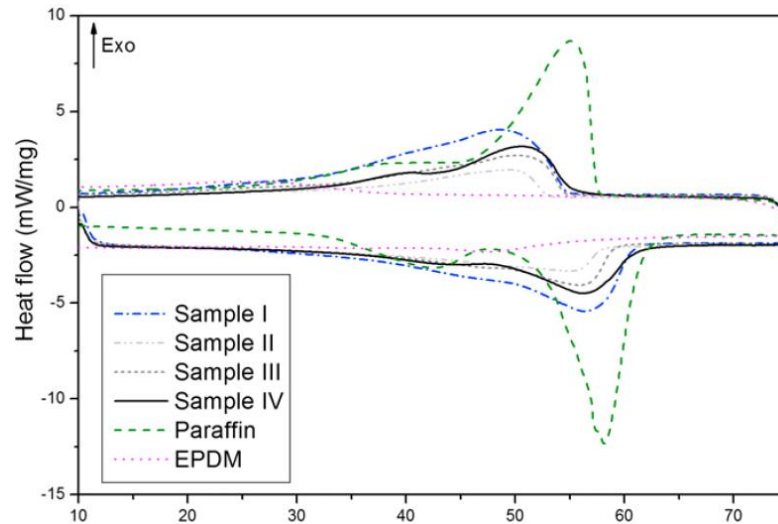
Figure 11. *The DSC curves of the samples, bulk paraffin and EPDM [35].*

The thermal properties of the samples, obtained from the DSC curves in Figure 11, are shown in Table 5. In Table 5, T_m and T_c are the peak temperatures of melting and crystallization and ΔH_m and ΔH_c are the latent heats of melting and crystallization, respectively. Theoretically, the latent heat of an SSPCM should be equal to the latent heat of bulk paraffin multiplied by the mass fraction of the paraffin in the SSPCM. Probably the most important finding in Table 5 is that the latent heat of every SSPCM was smaller than the theoretical value. Thus, the loading level of the SSPCMs, which is defined as the percentage of the actual amount of paraffin compared to the theoretical amount, was always below 100%. The probable reason for this decline in latent heat is the three-dimensional network structure of EPDM, which was supposed to constrict the thermal molecular movements of paraffin during the phase change.

Table 5. *Thermal properties of the samples and bulk paraffin. Adapted from [35].*

Sample	Mass fraction of paraffin (wt%)	T_m (°C)	ΔH_m (kJ/kg)	T_c (°C)	ΔH_c (kJ/kg)	Loading level (%)
I	50.00	56.41	-85.03	48.87	73.57	99.18
II	19.23	55.06	-32.47	49.56	28.15	98.47
III	32.26	55.96	-53.57	50.16	46.34	96.84
IV	37.04	56.20	-61.27	50.51	52.92	96.47
Paraffin	100	58.15	-171.47	55.13	149.39	-

The melting temperatures of the SSPCMs were slightly lower compared to pure paraffin. When the paraffin content of the SSPCMs was increased, the melting temperature approached that of paraffin. During crystallization, both the pure paraffin and the SSPCM blends showed supercooling, which is usually an unwanted property for PCMs. Moreover, the supercooling of SSPCMs was more significant than that of pure paraffin. This complicates the usage of the SSPCMs especially in thermal buffering applications,

as the heat emission during cooling of the PCM starts at much lower temperatures than the heat absorption during the heating of the PCM.

Luo et al. [36] produced SSPCMs with EPDM, ethylene-octane copolymer (POE), ethylene-vinyl acetate copolymer (EVA) and high-density polyethylene (HDPE) as the matrix materials and paraffin as the PCM (60% content of the composite). The substitution of HDPE, which is the most commonly used matrix material for SSPCMs, for the alternative matrix materials was attempted to achieve better processability and stability of the SSPCMs.

High temperature aging test was implemented by heating the samples in an oven at 75 ºC for 5 hours. In the test, the weight loss rate of HDPE/paraffin (9.4%) was significantly higher compared to the SSPCMs with other matrix materials (0.38-0.59%). This implies that EPDM prevents paraffin from leaking effectively at high temperatures. Figure 12 shows the results of the constant temperature water bath test (Figure 12a) and temperature cycle test (Figure 12b). It is seen in the Figure 12a that POE and EVA were the most effective matrix materials to prevent paraffin from leaking in the constant temperature water bath test, while HDPE was the worst. Temperature cycle test, where the temperature fluctuates regularly above and below the phase change temperature of the PCM, simulates well the practical applications of PCMs. In the temperature cycle test, the weight loss rates of EPDM/paraffin, POE/paraffin and EVA/paraffin were below 0.2% for almost every cycle, while the weight loss rate of HDPE/paraffin was above 0.6%.
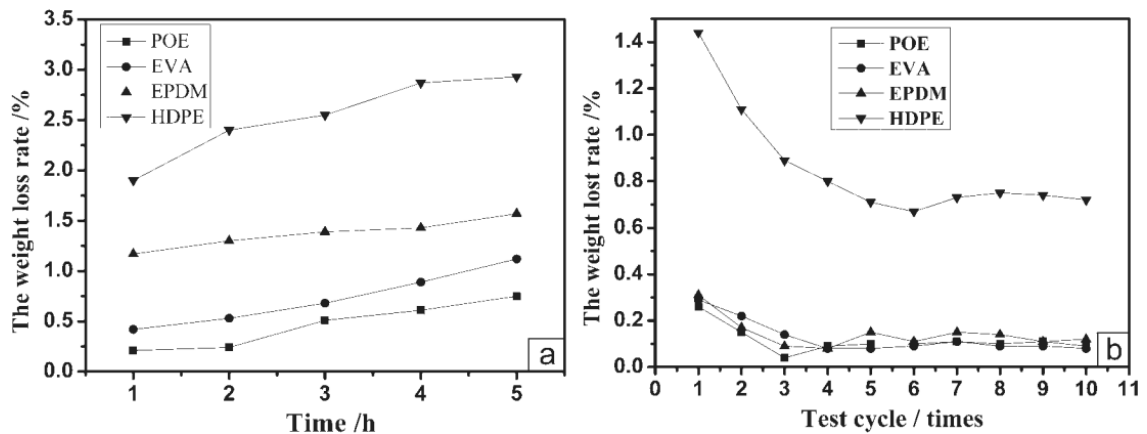

Figure 12. *Weight loss rates of SSPCMs with different matrix materials in (a) constant temperature water bath test and (b) temperature cycle test [36].*

The actual contents of the PCM, determined by DSC, were 58.22% for EPDM/paraffin, 49.75% for POE/paraffin, 58.4% for EVA/paraffin and 42.8% for HDPE/paraffin. Considering that the theoretical PCM content was 60%, these results point out that EPDM, POE and EVA retain the paraffin more effectively than HDPE during press vulcanization. Based on these four tests, it was concluded that EPDM, POE and EVA are more suitable matrix materials for SSPCMs than HDPE.

Wang et al. [37] developed SSPCMs with paraffin (melting temperature of 20 ºC) as the PCM and blends of HDPE and elastomers as the matrix materials. The used elastomers were EPDM, styrene-butadiene-styrene block copolymer (SBS) and styrene-isoprene-styrene block copolymer (SIS). The elastomers were intended to offer good absorption of paraffin, while the purpose of HDPE was to reinforce and support the composite structure. Elastomer/HDPE ratio of 3:1 was found to be the optimal for EPDM/HDPE and SBS/HDPE blends, so that ratio was used in the tests. When the share of elastomer was increased, the composites were too soft to keep the shape at the room temperature. On the other hand, if the share of HDPE was increased, leakage of paraffin at the molten state occurred. Attempts to produce SSPCMs with SIS/HDPE matrix were unsuccessful, as the material was too soft or the paraffin leaked out at the molten state, depending on the mass ratios of the matrix materials.

The latent heats of all the SSPCMs, obtained by DSC, were slightly lower than the theoretical value, probably due to loss of paraffin during the processing. The cyclic stability of the SSPCMs was tested with temperature cycle test. Figure 13 shows the mass loss of the SSPCMs after a number of heating-cooling cycles. It is seen that EPDM and SBS improved the cyclic stability significantly more than pure HDPE. Out of all the tested SSPCMs, the one with EPDM/HDPE had the lowest mass loss, which highlights the superb ability of EPDM to contain the PCM.
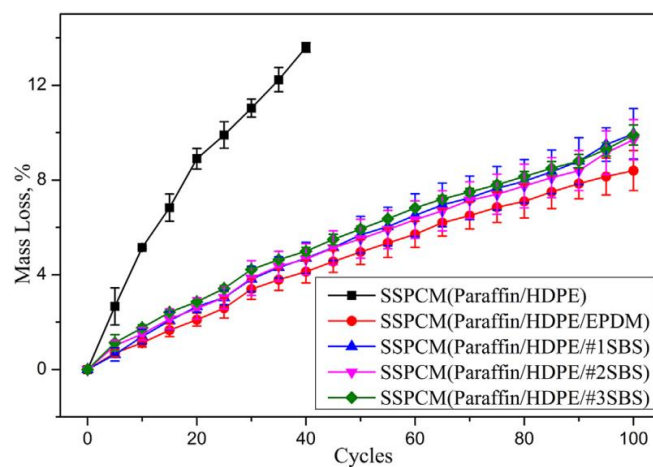

Figure 13. The mass loss ratios of the SSPCMs in temperature cycle test [37].

Besides thermal properties, addition of PCM affected also mechanical properties of the elastomers. Figure 14 shows that the addition of PCM reduced both the tensile strength and elongation at break substantially. However, the tensile strength and elongation at break of the EPDM-based SSPCM were higher than those of the other SSPCMs.
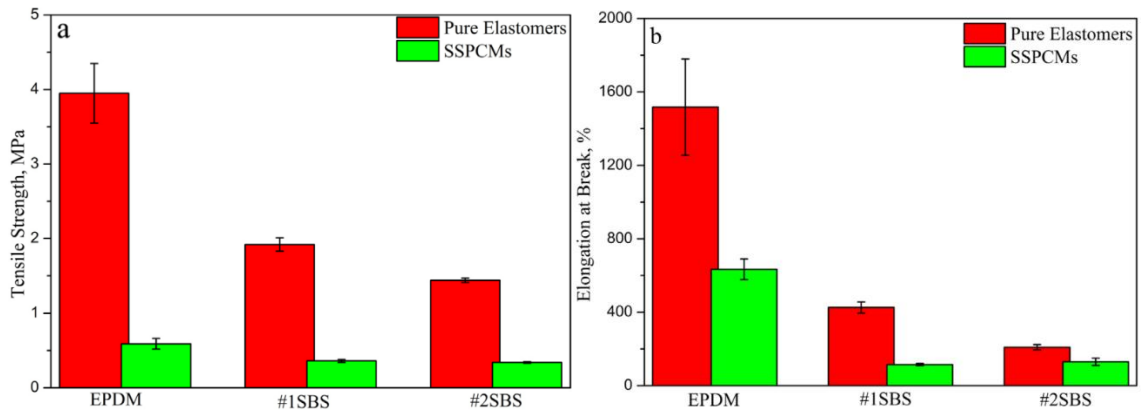
Figure 14. *(a) Tensile strength and (b) elongation at break of the elastomer/HDPE matrix materials and the SSPCMs (60 % paraffin content) [37].*

The SSPCMs were crosslinked by the addition of dicumyl peroxide (DCP) to improve their mechanical properties. Figure 15a shows that crosslinking improved tensile strength of both the EPDM-based and SBS-based SSPCMs. There was also an optimum value of added DCP, after which over-crosslinking occurred and the tensile strength decreased. Figure 15b shows that the effect of crosslinking on the elongation at break was different for the two SSPCMs. Crosslinking improved the elongation at break of the EPDM-based SSPCM (until over-crosslinking), but decreased that of SBS-based SSPCM significantly. Over-crosslinking should be strictly avoided, as it may also cause leakage of paraffin.
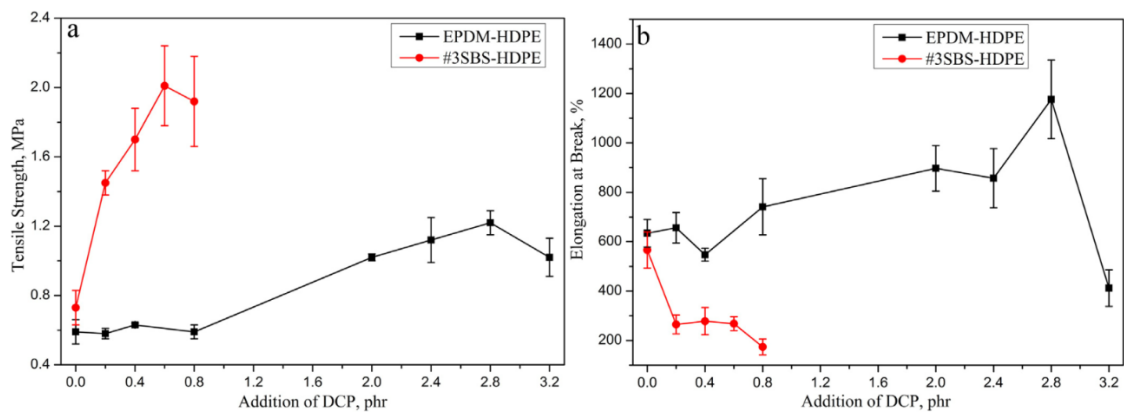

Figure 15. *(a) Tensile strength and (b) elongation at break of the crosslinked SSPCMs [37].*

3.1.3 PCMs in SR matrix

Pause [38] fabricated a novel composite membrane for thermal regulation of different kinds of buildings. The membrane consisted of a fiberglass (FG) base fabric and silicone rubber (SR)/PCM coating. It was fabricated by mixing salt hydrate, which was used as PCM, with SR matrix. The SR/salt hydrate compound (PCM content 40%) was then applied to the base fabric by knife-over-roll coating. Finally, the membrane was vulcanized to crosslink the SR matrix and entrap the salt hydrate particles in it.

The membranes can be tailored for different applications by changing the thickness of the components and amount of the salt hydrate. An example membrane consisted of a 0.4 mm thick FG base fabric with 0.8 mm thick SR/PCM coating on both sides. This kind of fabric had a latent heat storage capacity of 150 kJ/m^2, which is substantially higher compared to conventionally used membranes. The characteristics of this kind of membrane, as well as its advantages in architectural applications, are presented in more detail in Chapter 3.4.1.

3.2 PCMs in thermoplastic elastomer matrix

Because the studies concerning rubber-based SSPCMs are limited, SSPCMs based on other polymers are also discussed in this thesis. In the following sunchapter, the studies concerning SSPCMs based on thermoplastic elastomer matrix are presented.

3.2.1 PCMs in SBS matrix

Zhang et al. [14] prepared SSPCMs with paraffin (T_m = 20.3 ℃) as the PCM and SBS as the supporting matrix material. In most of the samples, some additives were used to offer extra functionality for the SSPCMs. The components were mixed, with the SBS at the molten state, and co-extruded to desired shapes. After co-extruding, the samples were grafted or crosslinked to prevent paraffin from leaking at the molten phase. The distribution of paraffin within the matrix was stated to be homogeneous, and the matrix was able to prevent paraffin from leaking above the melting temperature of paraffin. Considering the relative amounts of SBS and paraffin, 75% was found to be the best concentration of paraffin, as it offered high heat storage capacity and the matrix was still able to support the paraffin. The compositions and thermal properties of the samples, measured by DSC, are presented in Table 6. It is seen that mixing paraffin with SBS and additives changed its melting temperature slightly. An interesting fact is that the theoretical heat of fusion of the SSPCMs was 83.76 kJ/kg. It was not clarified why the heat of fusion of most of SSPCMs was higher than the theoretical value.

Table 6. *The thermophysical properties of the SSPCMs developed by Zhang et al. Adapted from [14].*

Sample	T_m (°C)	ΔH_m (kJ/kg)
Paraffin	20.3	119.66
Paraffin/SBS/wollastonite (70/25/5)	20.0	86.66
Paraffin/SBS/clay-1 (70/25/5)	20.4	88.86
Paraffin/SBS/clay-2 (70/25/5)	21.0	90.37
Paraffin/SBS/clay-3 (70/25/5)	20.3	96.82
Paraffin/SBS/MH (70/10/20)	20.6	82.97
Paraffin/SBS/MH (70/10/10)	20.7	82.17
Paraffin/SBS (70/30)	20.5	87.43

Xiao et al. [15] also used paraffin (T_m = 56-58 °C) and SBS at different mass fractions to create SSPCMs. The mechanical properties and maximum usage temperature of the SSPCMS were reported to decrease with the increase in paraffin content. Figure 16 shows the DSC curves of paraffin and SSPCM with 60% paraffin content. It is seen that the SSPCM exhibited the same phase change characteristics to pure paraffin. The shape of the curves was similar, while the peaks are higher with pure paraffin. Table 7 shows the compositions and latent heats of the SSPCMs. It is seen that the experimental values of latent heat were only slightly lower than the theoretical values, with a maximum difference of 3.1%.
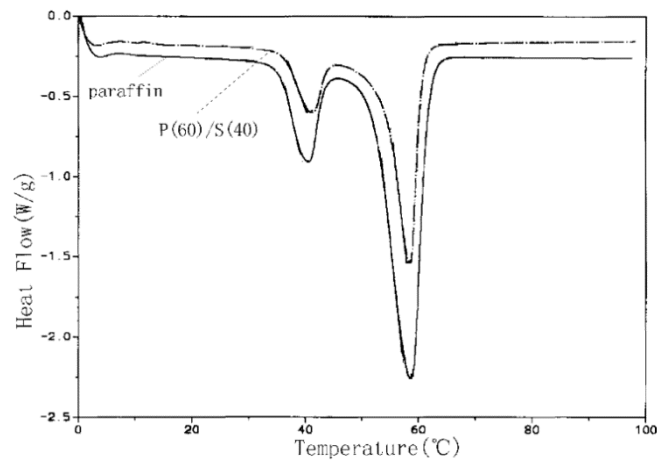

Figure 16. DSC curves of paraffin and SSPCM [15].

Table 7. Latent heats of paraffin and the SSPCMs developed by Xiao et al. Adapted from [15].

Mass percentages of paraffin and SBS	ΔH_m (KJ/kg)		
	Experimental value	Theoretical value	% Difference
40:60	81.6	84.2	3.1
60:40	123.5	126.5	2.4
70:30	146.7	147.4	0.5
80:20	165.2	168.4	1.9
100:0	210.5		

3.2.2 PCMs in SEBS matrix

Peng et al. [16] developed SSPCMs with two paraffin mixtures (melting temperature ranges of 44-58 °C and 50-60 °C) as the PCM and styrene-ethylene-butylene-styrene block copolymer (SEBS) as the matrix material. SEBS and fillers, such as silica, were mixed to molten paraffin, and the blend was solidified in a mold. The PCM contents of the samples were 80% and 50%. Table 8 shows the thermal diffusivities (a) and thermal conductivities (k) of the materials, determined by the transient heat transfer method. It is seen that at the solid state, the thermal conductivity of the SSPCMs were close to pure

paraffin. Moreover, the thermal conductivity of the SSPCMs was higher when the paraffin was at the liquid state than when it was at the solid state. For some reason, data for liquid paraffin was not available.

Table 8. *Thermal diffusivities and thermal conductivities of pure paraffin and the SSPCMs [16].*

Sample	a (m²/s), solid state	k (W/m·K), solid state	a (m²/s), liquid state	k (W/m·K), liquid state
Paraffin	$1.17 \cdot 10^{-7}$	0.22		
80 % Paraffin/SEBS	$1.13 \cdot 10^{-7}$	0.20	$1.36 \cdot 10^{-7}$	0.25
50 % Paraffin/SEBS	$1.08 \cdot 10^{-7}$	0.19	$1.22 \cdot 10^{-7}$	0.22

Figure 17 shows the storage modulus of SEBS, paraffin and the 80% paraffin/SEBS SSPCMs, determined by dynamical mechanical analysis (DMA) by three-point bending. The storage modulus is used to indicate the strength of viscoelastic materials [39]. It is seen that the storage moduli of all these materials decreased with increasing temperature. Paraffin had the highest storage modulus, while that of SEBS was much lower because of its rubbery nature. The rapid decrease in the storage modulus of paraffin near 55 °C resulted from the melting of the paraffin. Correspondingly, the decrease in the storage modulus of SEBS near 50 °C derived from changes in the soft ethylene and butylene blocks in the SEBS polymer. Because the mass fraction of paraffin was as high as 80%, the storage modulus of the paraffin/SEBS composite was close to that of pure paraffin, with the similar decrease in the storage modulus near the melting point of paraffin.
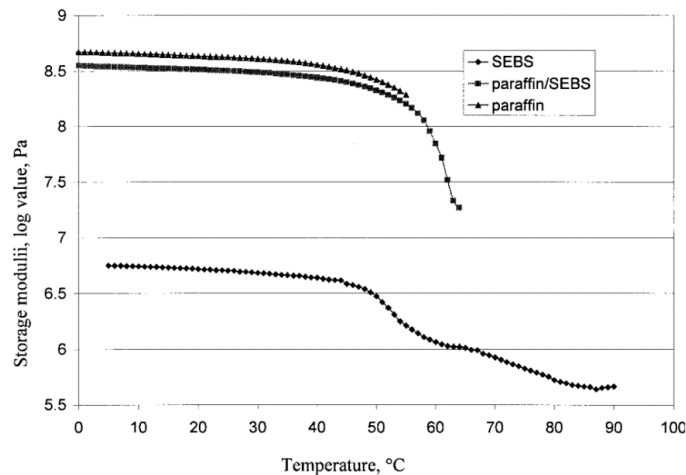

Figure 17. *Storage moduli of paraffin, SEBS matrix and 80% paraffin/SEBS SSPCM [16].*

The loss modulus exhibits the damping (energy absorption) properties of viscoelastic materials [39]. Figure 18 shows the loss moduli of SEBS, paraffin and the 80% paraffin/SEBS SSPCM. It is seen in Figure 18 that of these materials, paraffin had the highest loss modulus while SEBS had the lowest one. Again, like the storage modulus,

the loss modulus of paraffin/SEBS composite was close to that of pure paraffin. The loss modulus curves of paraffin and paraffin/SEBS had a peak near 55 °C, which corresponded to the melting temperature of paraffin. The loss modulus of SEBS has a peak at 50 °C, but that peak is not visible in paraffin/SEBS curve, because it is overwhelmed by the paraffin peak.
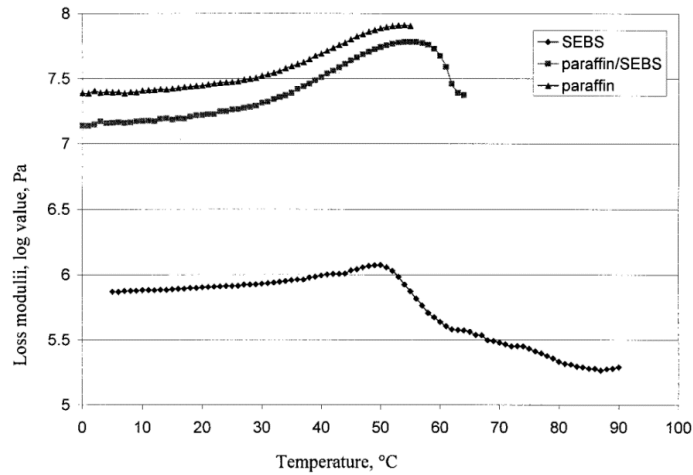

Figure 18. *Loss moduli of paraffin, SEBS matrix and 80% paraffin/SEBS SSPCM [16].*

Zhang et al. [17] used paraffin (melting temperature of 52-54 °C) as the PCM and SEBS as a matrix material to prepare SSPCMs. The SSPCMs contained 80, 85, 90 and 95% paraffin. Figure 19 shows the DSC curves of the samples. It is seen from Figure 19a that the melting peak of paraffin widened, lowered and shifted to slightly higher temperatures when the paraffin content of the SSPCMs was decreased. The solidification peak (Figure 19b), correspondingly, shifted to lower temperatures when the paraffin content was decreased.
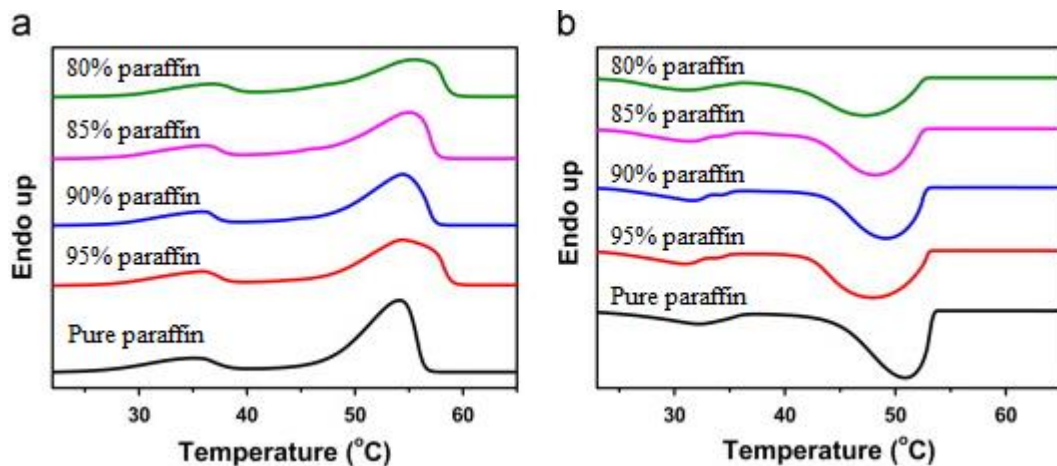

Figure 19. *DSC curves of (a) heating and (b) cooling of the SSPCMs. Modified from [17].*

Figure 20 shows the effect of temperature on the storage modulus of the PCMs, studied by rotational rheometer. For pure paraffin, there was a plateau of storage modulus below

50 °C, demonstrating that the sample was at solid state. When temperature was increased above 50 °C, the storage modulus of paraffin decreased rapidly and diminished. Thus, it was concluded that pure paraffin melts and loses its shape rapidly when the temperature is raised above its melting point. Considering the storage modulus of the SSPCMs, there was similar plateau below 50 °C. There was also a notable decrease in the storage modulus near 50 °C, corresponding to the melting of the paraffin. However, the storage modulus did not diminish but leveled off again, indicating that the samples were at hard gel state. When the temperature was raised to T_1, the storage modulus started to decrease again. This temperature was said to correspond to transition from hard gel to soft gel. After that, when the temperature reached T_2, which was referred as gel-fluid transition temperature, the storage modulus decreased rapidly and eventually diminished. In addition, Figure 20 shows that when the amount of paraffin in the SSPCMs was increased, the transition temperatures T_1 and T_2 shifted to lower temperatures.
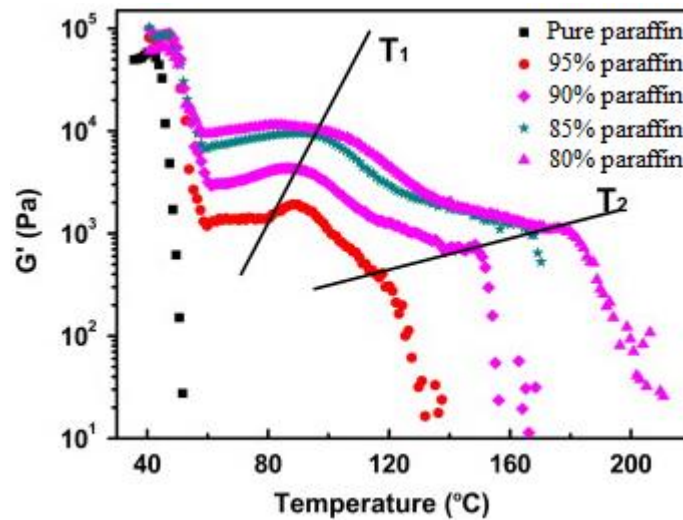

Figure 20. Storage modulus of the SSPCMs. Modified from [17].

To validate the previous assumptions about the phase transitions of the SSPCMs, Zhang et al. took pictures of the sample with paraffin content of 90% at different temperatures. Figure 21 shows that the sample was solid at room temperature, and was able to keep its shape at 80 °C. When the sample was heated to 120 °C, which is between temperatures T_1 and T_2 in Figure 20, the sample started to deform, and its appearance began to change. However, there was no observable leakage of paraffin, so the SEBS matrix was still able to contain the paraffin despite its change of shape. When the temperature was further raised to 150 °C, which is above T_2 in Figure 20, the sample melted and lost its shape. Thus, it was stated that the deformations corresponded well to the changes in storage modulus shown in Figure 20. It may be concluded that the SSPCM retains its mechanical properties below T_1. If mechanical properties are not important in the application, the material could be used also at temperatures between T_1 and T_2.
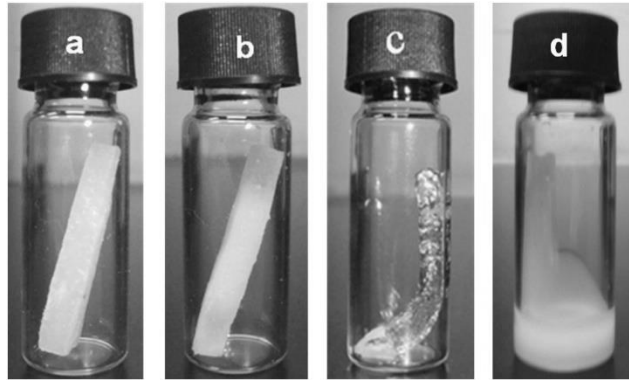
Figure 21. *The picture of the PCM10 sample at (a) room temperature, (b) 80 °C, (c) 120 °C and (d) 150 °C [17].*

3.3 PCMs in plastic matrix

Previous studies concerning SSPCMs based on plastic matrix are discussed in the following subchapters.

3.3.1 PCMS in HDPE matrix

Hong et al. [11] manufactured SSPCMs with paraffin as a PCM and HDPE as a matrix material by simply mixing the molten HDPE with molten paraffin. The PCM content of the SSPCMs was as high as 75%. Figure 22 shows the SEM micrograph of paraffin/HDPE SSPCM. It is seen that the obtained microstructure was homogeneous, with paraffin (dark area) evenly distributed in three-dimensional network of HDPE (white area). The good distribution of paraffin in HDPE was due to paraffin being a homologous compound of HDPE. The latent heat of the SSPCM, measured by DSC, was 157.04 kJ, which is 78.9% of the latent heat of pure paraffin (198.95 kJ). Since the latent heat of the SSPCM was slightly higher than the theoretical value, it was assumed that also the sensible heating of HDPE affected the measured value of latent heat.
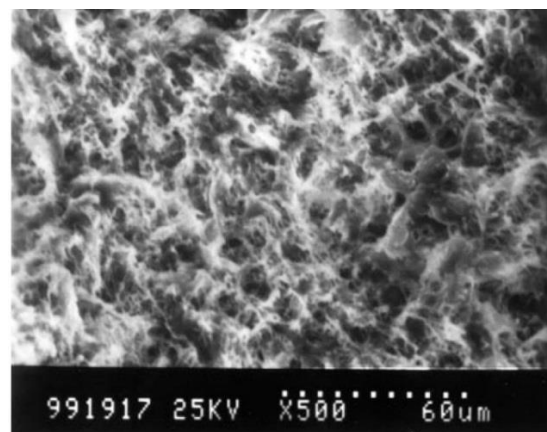

Figure 22. *A SEM image (500x magnification) of a paraffin/HDPE SSPCM (PCM content 75%). Adapted from [11].*

Sari et al. [12] produced paraffin/HDPE SSPCMs with two different paraffins. Paraffins P1 and P2 had melting temperatures of 42-44 °C and 56-58 °C and latent heats of 192.8 and 212.4 kJ/kg, respectively. SSPCMs with different PCM contents were produced, and the maximum PCM content was found to be 77%. When the PCM content was further raised, leakage of paraffin was observed. Figure 23 shows SEM micrographs of P1/HDPE SSPCM. It is seen that paraffin is evenly distributed in HDPE. The morphology of P2/HDPE was found to be similar than that of P1/HDPE.
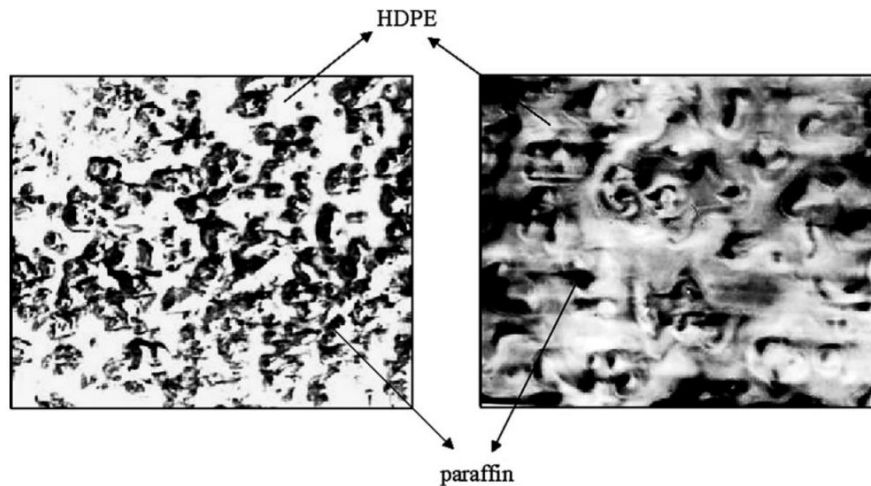

Figure 23. SEM images of paraffin/HDPE SSPCM [12].

The DSC measurements showed that there was little deviation in the melting temperatures of the SSPCMs compared to those of pure PCMs. In addition, the latent heats of the SSPCMs were very close to the theoretical values. Figure 24 shows the DSC curve of P1/HDPE SSPCM with PCM content of 77%. It includes the characteristic solid-solid transition and melting peaks of paraffin at 23.1 °C and 44.3 °C. The peak at 112.5 °C corresponds to the melting of HDPE. Since the characteristic peaks of both the paraffin and HDPE are present, there was no chemical reaction during the mixing of the SSPCM.
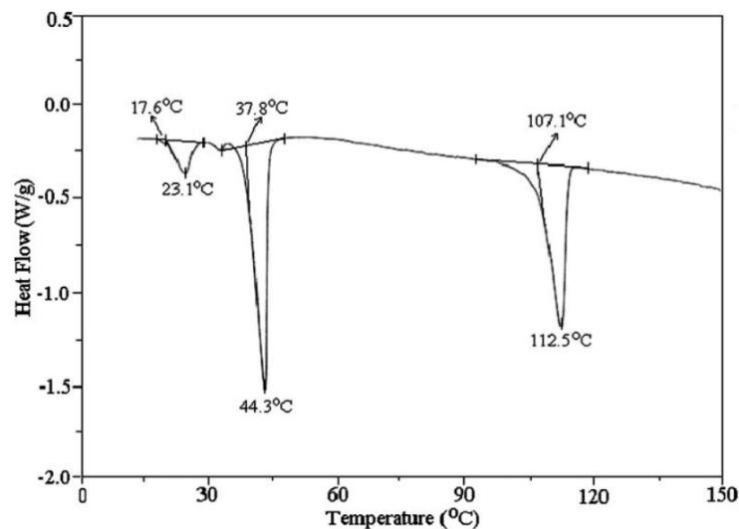

Figure 24. DSC curve of P1/HDPE SSPCM (PCM content 77%) [12].

Karkri et al. [13] produced SSPCMs by mixing microencapsulated paraffin with HDPE. The paraffin content of the microcapsules was 43%, and melamine-formaldehyde was used as shell material. SSPCMs of PCM microcapsule content of 40, 50 and 60% were prepared. Figure 25 shows SEM images of the SSPCM with the microcapsule content of 40%. In Figure 25a, there is an untreated fracture surface, so the microcapsules are mostly covered with HDPE and are not visible. In Figure 25b, the top layer surface was removed with gallium ion beam to improve the visualization of the surface morphology. It is seen that the microcapsules were evenly distributed within the HDPE matrix.
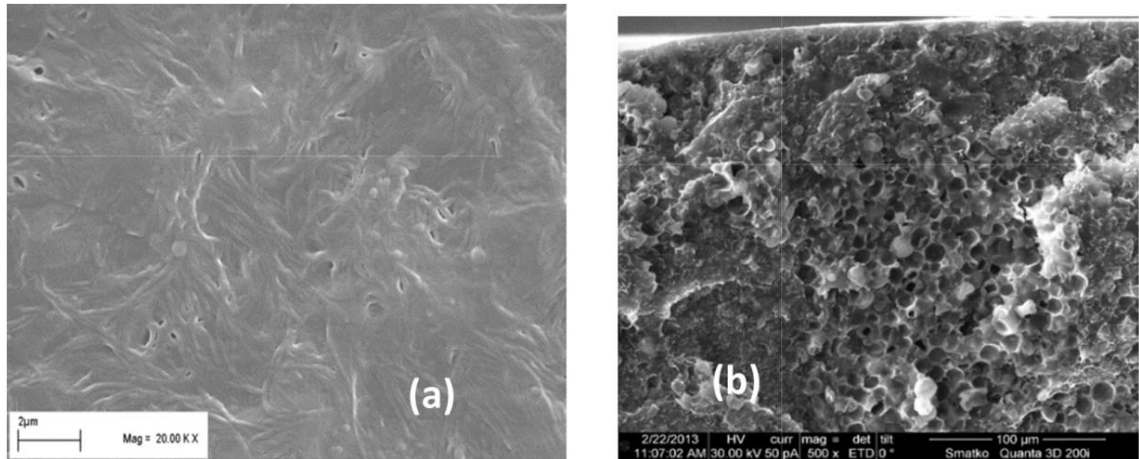

Figure 25. *SEM images of microencapsulated HDPE/paraffin SSPCM (microcapsule content 40%). (a) Untreated fracture surface. (b) Fracture surface treated with gallium ion beam. [13]*

Figure 26 shows the thermal conductivity of the SSPCMs with different microcapsule contents. It is seen that the thermal conductivity of the SSPCMs decreased notably when the microcapsule content was increased. Thus, the microcapsules acted as thermal insulators in the HDPE matrix. It is also seen in Figure 26 that the thermal conductivity of the SSPCM with given microcapsule content was higher at 20 °C than at 55 °C. This decrease in thermal conductivity with increasing temperature has two reasons. Firstly, the thermal conductivity of HDPE decreases with increasing temperature. Secondly, the thermal conductivity of solid paraffin is higher than that of liquid paraffin.
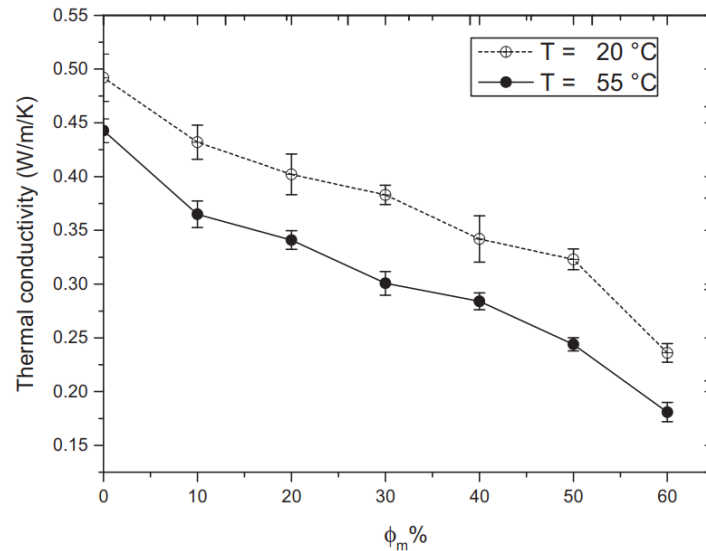
Figure 26. *Thermal conductivity of the microencapsulated paraffin/HDPE SSPCMs with different microcapsule contents [13].*

Tang et al. [40] used myristic acid (MA) and HDPE to develop SSPCMs. The MA contents of the SSPCMs were 60 (HPCM1), 70 (HPCM2), 80 (HPCM3) and 90% (HPCM4). The maximum MA content was found to be 70%, as higher contents resulted in leakage of MA at its molten state.

The DSC curves of heating and cooling of the samples are shown in Figures 27a and 27b, respectively. It is seen that all the SSPCMs exhibited the characteristic DSC peaks of both MA and HDPE, which verifies that no chemical bonds were formed between MA and HDPE. When MA content of the SSPCMs was increased, the area of the peak corresponding to the melting of MA became larger. A notable fact in Figure 27b is that also the supercooling of the SSPCMs increased with increasing PCM content.
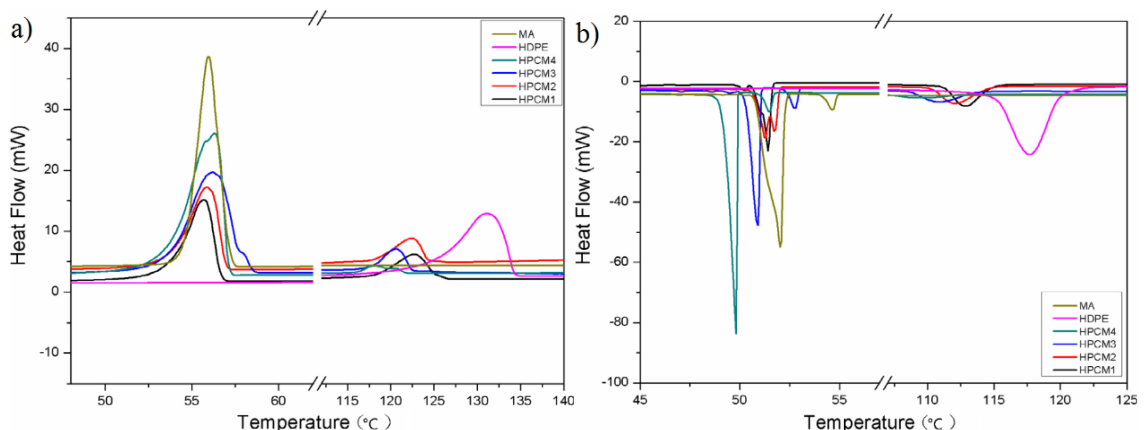

Figure 27. *DSC curves of (a) heating and (b) cooling of pure MA, pure HDPE and MA/HDPE SSPCMs [40].*

3.3.2 PCMs in LDPE matrix

Krupa et al. [41] developed SSPCMs with low-density polyethylene (LDPE) as a matrix material. Two different paraffins, hard (Wax FT) and soft (Wax S), were used as PCMs. Figure 28 shows the SEM images of the SSPCMs with PCM content of 50%. It is seen that the morphology of SSPCMs with different paraffins differed considerably. The LDPE/Wax FT blend (Figure 28a) was much more homogeneous than the LDPE/Wax S blend (Figure 28b). The difference in the dispersion of different paraffins in LDPE was believed to be due to different molecular weights of the paraffins (785 g/mol and 374 g/mol for Wax FT and Wax S, respectively). Wax S has lower molecular weight and consequently lower viscosity than Wax FT, which allowed it to separate more easily during mixing.
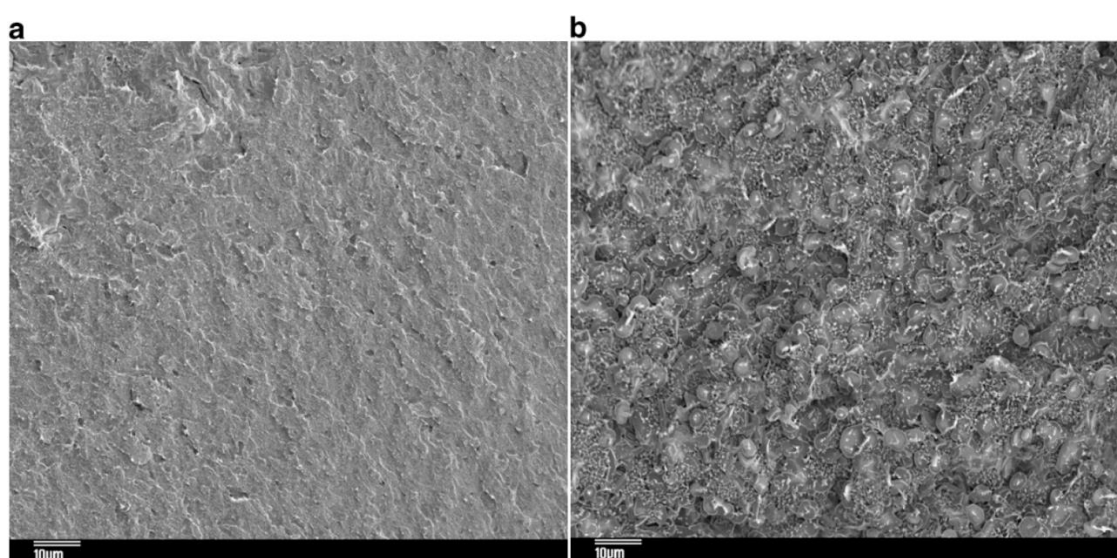

Figure 28. SEM images of (a) LDPE/Wax FT and (b) LDPE/Wax S SSPCMs with PCM content of 50% [41].

Figures 29 and 30 show the DSC curves of LDPE/Wax S and LDPE/Wax FT, respectively. Firstly, it is seen that the latent heat of the SSPCMs with both types of paraffin increased with increasing PCM content. However, there were also differences between the thermal behaviour of the SSPCMs. The DSC peaks of pure Wax S and LDPE/Wax S SSPCMs were notably sharper than those of pure Wax FT and the corresponding SSPCMs. Moreover, Wax FT showed two major overlapping peaks during melting. These differences were said to arise from different molecular weight distributions of the paraffins, with Wax S having relatively narrow molecular weight distribution compared to Wax FT. It is also interesting that the two separate peaks of Wax FT were not clearly visible with the corresponding SSPCMs, which was due to co-crystallization of Wax FT and LDPE.
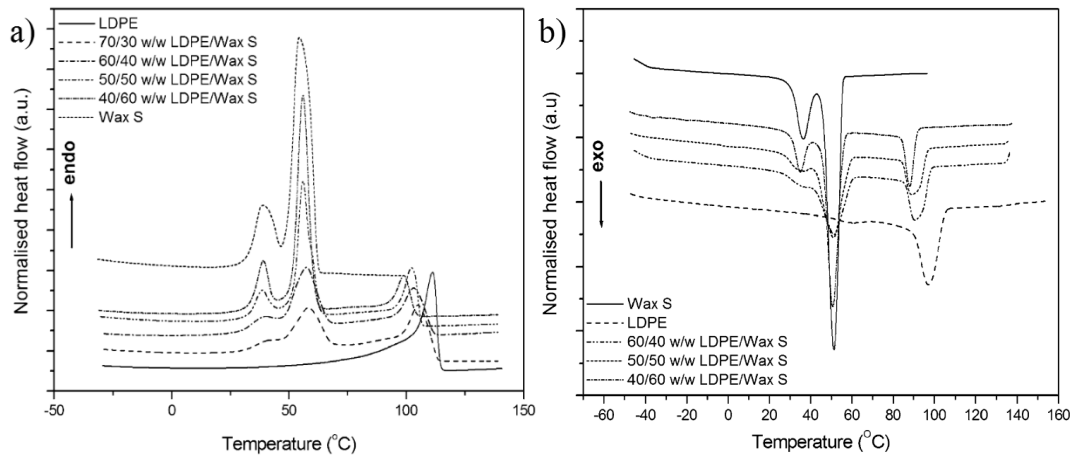
Figure 29. *DSC curves of (a) heating and (b) cooling of Wax S, LDPE and LDPE/Wax S SSPCMs [41].*
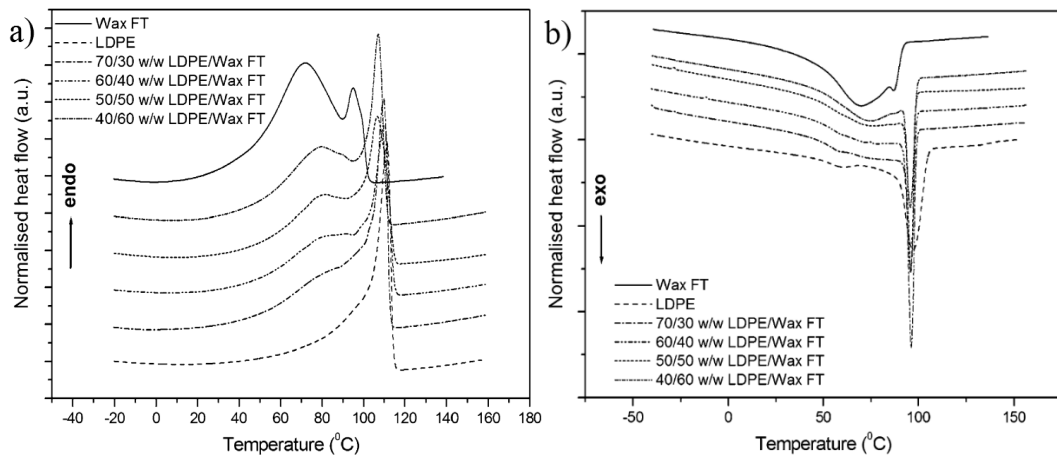

Figure 30. *DSC curves of (a) heating and (b) cooling of Wax FT, LDPE and LDPE/Wax FT SSPCMs [41].*

Figure 31 shows the storage modulus of the SSPCMs as a function of temperature. It is seen that both kinds of paraffin acted as a reinforcing filler in LDPE matrix. The reinforcing effect took place below the melting temperature of paraffin (65 °C for Wax S and 90 °C for Wax FT). In the case of LDPE/Wax S, the level of reinforcement was nearly independent on the paraffin content. In the case of LDPE/Wax FT, the reinforcement was more effective with higher paraffin contents. When the temperature was raised above the melting point of the paraffin, the reinforcement was lost, and the modulus decreased. For both types of SSPCMs, the decrease in modulus was faster in the SSPCMs with high paraffin contents.
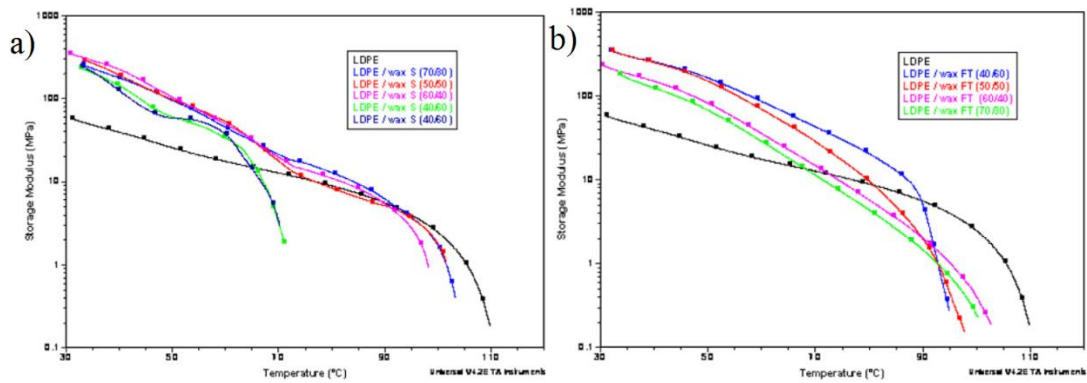
Figure 31. *Storage modulus of (a) LDPE/Wax S and (b) LDPE/Wax FT SSPCMs as a function of temperature [41].*

In the tensile tests of the SSPCMs, two trends were visible. Firstly, the tensile strength and maximum elongation of the SSPCMs reduced as the paraffin content was increased. Secondly, the tensile strength of the SSPCMs with paraffin content of 60% or more decreased significantly with increasing temperature. This decrease in strength resulted from the softening and melting of the paraffin.

3.3.3 PCMs in PP matrix

Krupa et al. [42] developed SSPCMs by mixing paraffin with polypropylene (PP) matrix. Two different paraffins, hard (Wax FT) and soft (Wax S), were used. SEM images showed that both the paraffins were immiscible with PP. DSC heating curves of PP/Wax S and PP/Wax FT are presented in Figure 32. Figure 32a shows that pure Wax S had two distinct DSC peaks common to paraffins. When Wax S was blended with PP, these peaks fused together to form one broader peak, which shifted to higher temperatures as paraffin content was increased. As expected, the latent heat increased notably when paraffin content of the SSPCMs was increased. The melting peak of PP, which was near 160 °C for pure PP, shifted to lower temperatures when paraffin content was increased. This resulted from plasticization of PP by Wax S.

As seen in Figure 32b, the DSC curve of pure Wax FT was notably different to the DSC curve of pure Wax S shown in Figure 32a. The DSC heating curve of pure Wax FT had two overlapping peaks, which were not as distinct as in the case of Wax S. In the DSC curves of the SSPCMs, the peaks were nearly fused together. Similarly to PP/Wax S blends, the melting peak of PP shifted to lower temperatures when the paraffin content was increased, indicating plasticization of PP by Wax FT.
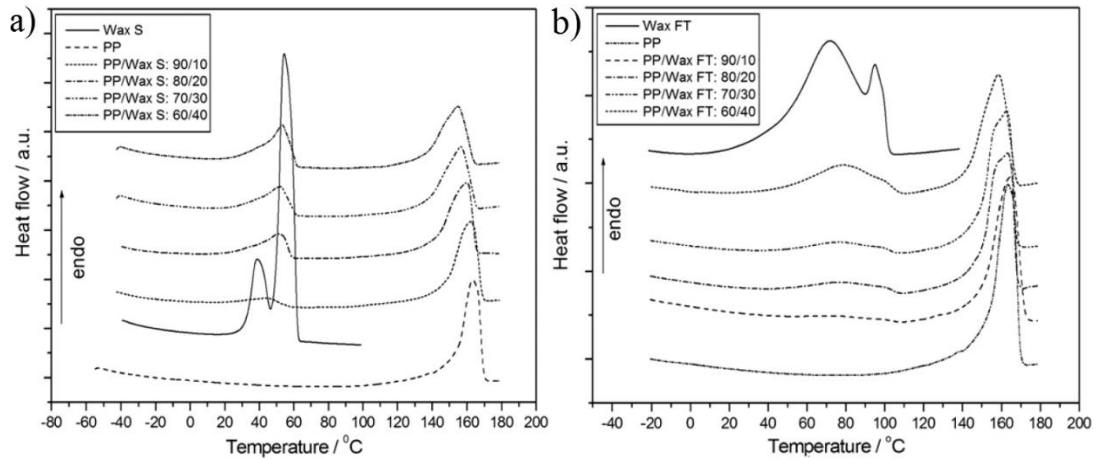
Figure 32. *DSC heating curves of (a) PP/Wax S and (b) PP/Wax FT SSPCMs. Adapted from [42].*

Unfortunately, the latent heat of the SSPCMs were way below the theoretical values. With paraffin content of 40%, the latent heats were 55 kJ/kg and 37 kJ/kg for PP/Wax S and PP/Wax FT, respectively. Theoretically, latent heats should have been 84 kJ/kg and 65 kJ/kg, so the values were surprisingly low. Possible reasons for this inconsistency are for example inhomogeneity of the samples and leakage of paraffin from the matrix during blending of the SSPCMs.

Figure 33 shows the dependence of storage modulus of the SSPCMs on temperature. It can be seen in Figure 33a that the storage modulus of the PP/Wax S SSPCMs decreased when the PCM content was increased, which resulted from plasticization of PP by Wax S. There was also a drop in the storage modulus of the SSPCMs at the melting temperature of Wax S (near 58 °C). Figure 33b shows that in contrast to Wax S, Wax FT at solid state reinforced the PP matrix. According to the storage modulus, PP/Wax FT blends were notably stronger than PP/Wax S blends. Thus, it was stated that Wax FT is more compatible with PP matrix than Wax S.
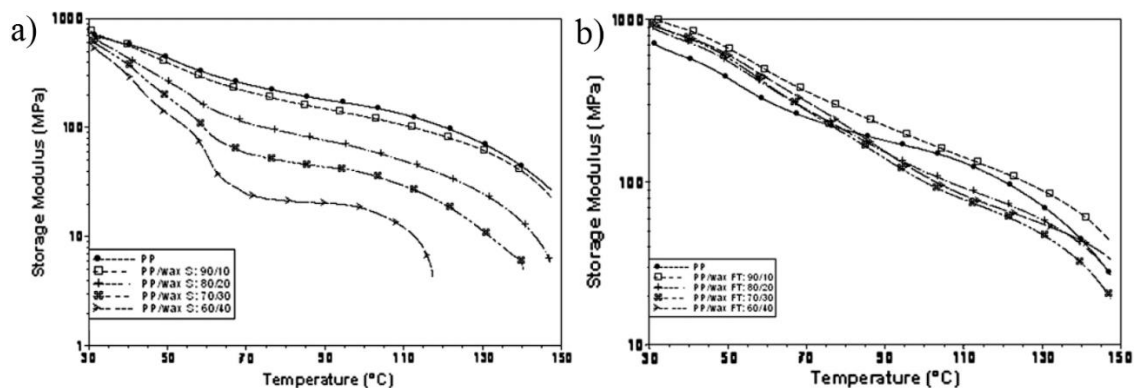

Figure 33. *Storage modulus of (a) PP/Wax S and (b) PP/Wax FT SSPCMs as a function of temperature [42].*

Alkan et al. [43] prepared SSPCMs with paraffin and PP by solution casting method. PCM contents of the prepared SSPCMs were 40, 50, 60, 70, 80 and 90%. The maximum PCM content was found to be 70%, as higher PCM contents resulted in leakage of paraffin. The latent heats of the SSPCM with PCM content of 70% were 136.16 and -136.59 kJ/kg for melting and crystallization, respectively. These values are high enough to make the SSPCM potential for practical applications. To test the thermal stability of the SSPCM, Alkan et al. performed a DSC test with 3000 thermal cycles. After 3000 thermal cycles, the changes in the thermal properties of the SSPCMs were minor, suggesting that the SSPCM was thermally stable.

3.3.4 PCMs in PVC matrix

Sari et al. [44] prepared SSPCMs by mixing fatty acids with polyvinyl chloride (PVC) matrix. Four different fatty acids – lauric acid (LA), myristic acid (MA), palmitic acid (PA) and stearic acid (SA) – were used as PCMs. The maximum PCM content to prevent its leakage was found to be 50% for every PCM, and Sari et al. used that content for the studies. Figure 34 shows the micrographs of PVC/PA and PVC/SA SSPCMs. It is seen that in both cases, the fatty acid (black area)) was distributed in the network of PVC (white area). The textures were similar for both the SSPCMs.
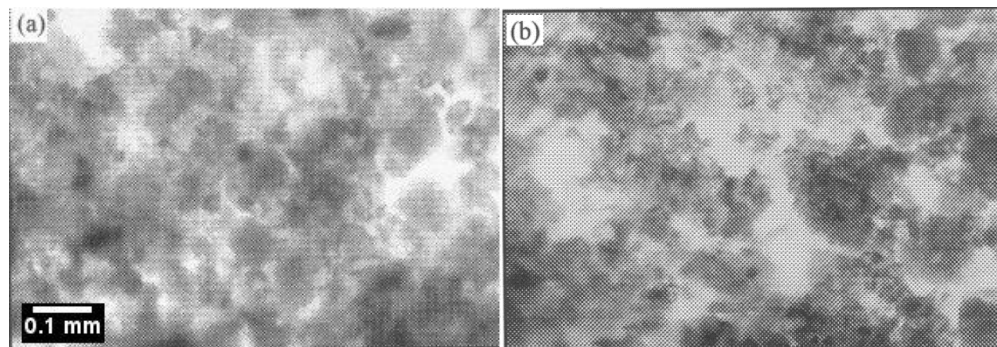

Figure 34. Dissection microscope images of (a) PVC/PA and (b) PVC/SA SSPCMs (PCM contents 50%) [44].

The results of the DSC measurements of the SSPCMs are shown in Table 9. Important trends were found during the measurements. The melting temperatures of the SSPCMs were several degrees lower compared to the corresponding pure PCMs. In addition, the melting temperatures of the SSPCMs approached those of the pure PCMs when the PCM content was increased. Secondly, the latent heats of the SSPCMs were slightly higher than expected theoretically. The reason for that was supposed to be the effect of the sensible heat of the PVC to the measurements. Because of the good thermal properties, the SSPCMs were proposed as potential materials for solar thermal energy storage applications.

Table 9. *Thermal properties of the fatty acid/PVC PCMs [44].*

SSPCM (PCM content 50%)	T_m (°C)	ΔH_m (kJ/kg)
PVC/LA	38.8	97.8
PVC/MA	49.2	103.2
PVC/PA	54.4	120.3
PVC/SA	64.7	129.3

3.3.5 PCMs in PVA matrix

Sari et al. [45] used fatty acids and polyvinyl alcohol (PVA) to prepare SSPCMs. The fatty acids used were LA, MA, PA and SA. The maximum content of every PCM was found to be 50%, as the PCMs started to leak out of the matrix when the PCM content was further increased. Thus, PCM content of 50% was used for inspections. Figure 35 shows micrographs of PVA/PA and PVA/MA. It is seen that the texture is similar in both samples, with fatty acid (black area) dispersed in the PVA matrix (white area).
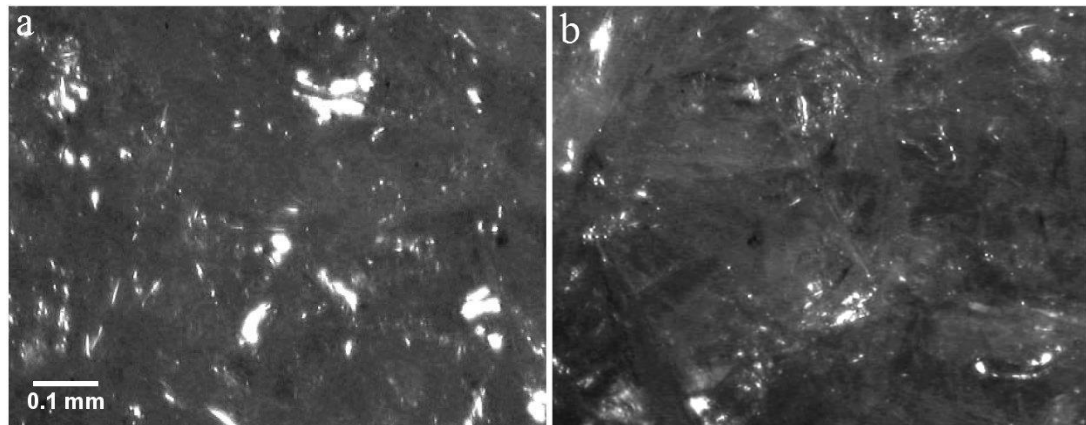

Figure 35. *Dissection microscope images of (a) PVA/PA and (b) PVA/MA SSPCMs (PCM contents 50%) [45].*

The DSC results of the SSPCMs are presented in Table 10. Similarly to the PVC/fatty acid SSPCMs presented in the previous chapter, the melting temperatures of the PVA/fatty acid SSPCMs were a few degrees lower compared to the corresponding pure PCMs. Moreover, the melting temperatures of the SSPCMs approached those of the pure PCMs when the PCM content was increased. The latent heats of the SSPCMs were a little higher than the theoretical values, indicating that the sensible heat of PVA affected the measurements. Because of these satisfactory thermal properties, the SSPCMs were proposed as potential materials for solar thermal energy storage applications.

Table 10. *Thermal properties of the fatty acid/PVA SSPCMs [45].*

SSPCM (PCM content 50%)	T_m (°C)	ΔH_m (kJ/kg)
PVA/LA	39.8	96.4
PVA/MA	50.2	105.3
PVA/PA	56.2	121.6
PVA/SA	67.4	132.6

3.3.6 PCMs in PMMA matrix

Alkan et al. [46] used fatty acids and poly(methyl methacrylate) (PMMA) to develop SSPCMs. Four different fatty acids – LA, MA, PA and SA – were mixed with PMMA by solution casting method. The maximum PCM content to prevent leakage was found to be as high as 80%. Optical microscope (OM) images of the SSPCM with PCM content of 80% showed that the fatty acids were covered by PMMA at the surface of the samples, which enabled the containment of the fatty acids above their melting temperatures. The DSC results of the SSPCMs are shown in Table 11. There was little deviation between the melting temperatures of pure PCMs and the SSPCMs. In addition, the latent heats were only slightly lower than the theoretical values. It should also be noted that the supercooling of the SSPCMs was remarkably low. Considering the good thermal properties, the SSPCMs were suggested as possible materials for applications such as under floor space heating of buildings and solar thermal energy storage.

Table 11. *Thermal properties of the fatty acid/PMMA SSPCMs [46].*

SSPCM (PCM content 80%)	T_m (°C)	ΔH_m (kJ/kg)	T_c (°C)	ΔH_c (kJ/kg)
PMMA/LA	42.14	190.12	42.20	194.23
PMMA/MA	52.44	210.70	52.49	212.65
PMMA/PA	60.45	221.42	59.88	226.56
PMMA/SA	66.87	242.15	66.36	246.74

Wang et al. [47] prepared SSPCMs by mixing fatty acid eutectics with PMMA. Fatty acids were used at eutectic mixtures to reduce their melting temperature. The used eutectics were capric acid (CA)-LA, CA-MA, CA-SA and LA-MA. The maximum PCM content of the SSPCMs was found to be 70%. However, Wang et al. selected PCM content of 50% for inspections, because it was assumed to have the optimal combination of mechanical and thermal properties.

Figure 36 shows SEM images of surface and cross-section of the PMMA/CA-LA SSPCM. It is seen that the surface morphology of the sample was smooth and compact, suggesting that the PCM was covered by PMMA matrix. However, the cross-section was

not equally uniform. The inner structure of the SSPCMs varied slightly depending on the PCM used, but the surface morphology was similar for all the SSPCMs.
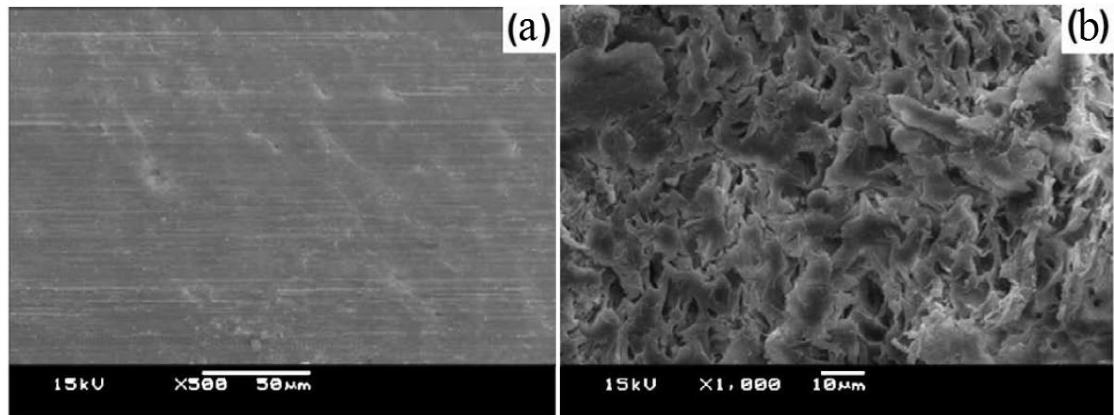

Figure 36. *SEM images of (a) surface and (b) cross-section of the PMMA/CA-LA SSPCM. Adapted from [47].*

The melting temperatures of the SSPCMs were in the range of 21-35 °C, and the latent heats 59-81 kJ/kg. In general, the latent heats were slightly lower than the theoretical values, but still acceptable. The minimal drop in the latent heat was presumed to result from the damage of carbonyl acid dimeric structure following the interactions between fatty acids and PMMA. As a conclusion, the melting temperature range of the PMMA/fatty acid eutectic SSPCMs is suitable for many applications, including building energy conservation and solar thermal energy storage.

3.3.7   PCMs in SMA matrix

Sari et al. [48] prepared SSPCMs by mixing fatty acids (LA, MA, PA and SA) with styrene maleic anhydride copolymer (SMA) by the solution casting method. The maximum PCM content of 85% was achieved with no leakage of the PCM out of the matrix. In the OM images, only one phase was visible, meaning that the fatty acids were covered by SMA.

The DSC measurements showed that the phase change temperatures of the SSPCMs were very close to those of the pure PCMs, deviating less than 1 °C. The latent heats of melting and the melting temperatures of the SSPCMs are shown in Table 12. It is seen that the latent heats were a little lower than the theoretical values, resulting from interactions between the fatty acids and SMA in the SSPCMs. However, when compared to other SSPCMs presented in the previous chapters, the thermal properties of the SMA/fatty acid SSPCMs were satisfying.

Table 12. Thermal properties of the fatty acid/PMMA SSPCMs [48].

SSPCM (PCM content 85%)	T_m (°C)	ΔH_m (kJ/kg)	ΔH_m (kJ/kg), theoretical
SMA/LA	41.48	160.83	161.67
SMA/MA	51.75	176.49	180.00
SMA/PA	60.04	184.54	188.21
SMA/SA	67.35	202.23	205.83

3.3.8 PCMs in PANI matrix

Zeng et al. [49] prepared SSPCMs with MA and polyaniline (PANI). PANI is an organic polymer known for its high electrical conductivity. The maximum MA content in the SSPCMs to prevent the leakage of MA was 82%. Figure 37 shows SEM micrographs of SSPCMs with MA content of 50% (a) and 70% (b). It is seen that with MA content of 50%, PANI covered the MA particles completely. When the MA content was increased to 70%, some uncovered MA particles could be found. However, lipophilic PANI absorbed the molten MA, so that the composite could still maintain its shape without leakage of MA above its melting point. The highest latent heat, 150.63 kJ/kg, was achieved with MA content of 82%.
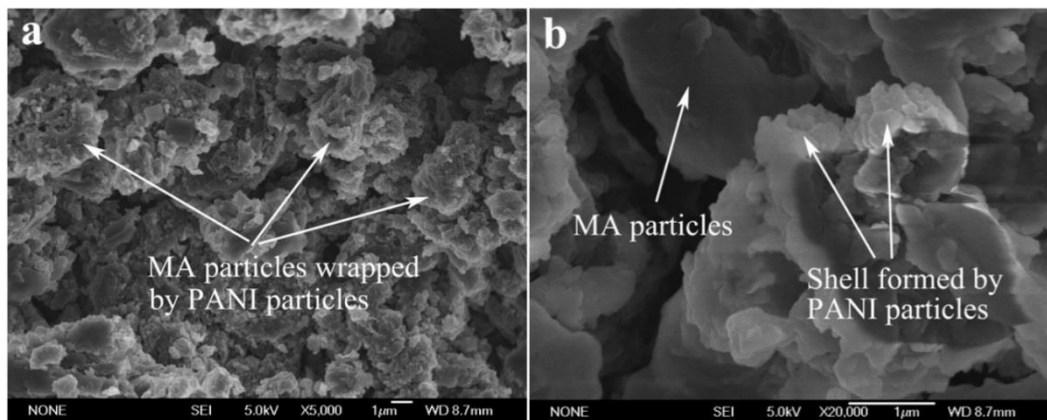

Figure 37. SEM micrographs of MA/PANI SSPCMs with MA content of (a) 50% and (b) 70% [49].

In another work, Zeng et al. [50] developed SSPCMs with 1-tetradecanol (TD) and PANI by in-situ polymerization. TD is a paraffin with melting temperature close to 40 °C. The maximum TD content in the SSPCMs without leakage of TD was found to be 73%. The 73% TD/PANI SSPCM had the latent heat of 162.97 kJ/kg. The latent heat decreased linearly when the TD content was decreased. The thermal conductivities of the SSPCMs are shown in Figure 38. It is seen that the thermal conductivity of the 73% TD/PANI SSPCM was nearly 10% higher than that of pure TD. The thermal conductivity decreased with increasing TD content. At low concentration of PANI, the slow reaction rate resulted in highly crystalline PANI, which acted as a thermal conductivity enhancing filler. When

the concentration of PANI was increased, higher reaction rate resulted in less crystalline PANI, which decreased the thermal conductivity.
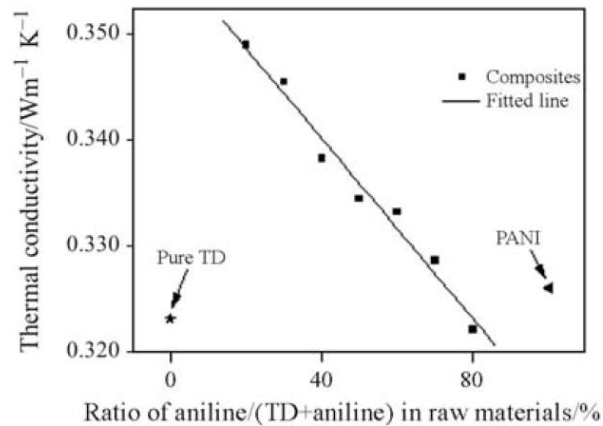

Figure 38. The thermal conductivities of the TD/PANI SSPCMs [50].

Zhu et al. [51] prepared SSPCMs with PA and PANI by surface polymerization. The maximum content of PA in the SSPCM was found to be 80%. The latent heat of the 80% PA/PANI SSPCM was 175 kJ/kg, and the thermal conductivity was 0.377 W/(m·k).

3.4   Summary

Table 13 summarizes the SSPCMs discussed above and their heat storage properties. It is seen that paraffins are by far the most commonly used PCMs in elastomeric SSPCMs, since only one study concerning SSPCMs with elastomeric matrix and a PCM other than paraffin was found. With other polymers as the matrix material, fatty acids have been widely researched as the PCM along with paraffin. The optimal PCM contents of the SSPCMs were between 40 and 90%. In most cases, the maximum PCM content without leakage of the PCM was selected as the optimal content in order to maximize the heat storage capacity of the SSPCM.

There was substantial variation in the phase change temperatures and latent heats of the SSPCMs. The melting and crystallization temperatures of SSPCMs were dictated by the phase change temperatures of the PCMs. The melting temperatures of SSPCMs were usually slightly lower than those of the corresponding pure PCMs, and the crystallization temperatures of SSPCMs were usually a couple of degrees lower than those of the corresponding pure PCMs. These conformities were independent of the matrix material of the SSPCM. Tang et al. [40] validated this reduction in phase change temperature by the entropy formula

$$T_{pc} = \frac{dQ}{dS},$$
(3)

Table 13. *Summary of the SSPCMs discussed above and their thermal properties.*

Matrix	PCM	Optimal PCM content	T_m (°C)	ΔH_m (kJ/kg)	T_c (°C)	ΔH_c (kJ/kg)	Ref
NR latex	Microencaps. n-eicosane (paraffin)	50%					[34]
EPDM	Paraffin	50%	56.4	85.0	48.9	73.6	[35]
	Paraffin	60%		118.3			[36]
SR	Salt hydrate	40%					[38]
SBS	Paraffin	70%	20.5	87.4			[14]
	Paraffin	80%		165.2			[15]
SEBS	Paraffin	90%	54.5	158.5	49.0		[17]
POE	Paraffin	60%		117.5			[36]
EVA	Paraffin	60%		146.1			[36]
HDPE	Paraffin	60%		84.2			[36]
	Paraffin	75%		157.0			[11]
	Paraffin	77%	37.8	147.6			[12]
	Microencaps. paraffin	60%		91.3			[13]
	MA (Myristic acid)	70%	53.8	119.4	52.0	111.5	[40]
LDPE	Paraffin (Wax FT)	50%	80.0	136.0	71.6	146.0	[41]
	Paraffin (Wax S)	50%	56.0	161.0	51.0	176.0	[41]
PP	Paraffin (Wax FT)	40%	99.0	37.0	91.7	45.0	[42]
	Paraffin (Wax S)	40%	52.9	55.0	52.9	49.0	[42]
	Paraffin	70%	45.2	136.2	54.2	136.6	[43]
PVC	LA (Lauric acid)	50%	38.8	97.8			[44]
	MA	50%	49.2	103.2			[44]
	PA (Palmitic acid)	50%	54.4	120.3			[44]
	SA (Stearic acid)	50%	64.7	129.3			[44]
PVA	LA	50%	39.8	96.4			[45]
	MA	50%	50.2	105.3			[45]
	PA	50%	56.2	121.6			[45]
	SA	50%	67.4	132.6			[45]
PMMA	LA	80%	42.1	190.1	42.2	194.2	[46]
	MA	80%	52.4	210.7	52.5	212.7	[46]
	PA	80%	60.5	221.4	59.9	226.6	[46]
	SA	80%	66.9	242.2	66.4	246.7	[46]
SMA	LA	85%	41.5	160.8			[48]
	MA	85%	51.8	176.5			[48]
	PA	85%	60.0	184.5			[48]
	SA	85%	67.4	202.2			[48]
PANI	MA	84%	57.4	150.6			[49]
	PA	80%	62.6	175.0			[51]
	TD (paraffin)	73%	39.8	163.0			[50]

where T_{pc} is the phase change temperature of the PCM, dQ is the melting and solidifying heat change per unit mass, and dS is the entropy change. In SSPCMs, the entropy of the PCM decreases, leading to reduction in the phase change temperatures.

The latent heats of SSPCMs were mainly determined by the latent heats of the corresponding PCMs. Theoretically, the latent heat of an SSPCM is directly proportional to the PCM content of the sample, and approaches that of the pure PCM when the PCM content of the SSPCM approaches 100%. However, this is rarely the case in practice. In the studies discussed above, the latent heats of some SSPCMs were notably lower than the theoretical value, while some even exceeded the theoretical value. The most important reason for the latent heats lower than the theoretical value, especially for the SSPCMs with plastic matrix, is the leakage of the PCM during the processing of the SSPCM, which leads to lower PCM content of the SSPCM than designed. In addition, the polymer network may hinder the thermal movement of the PCM during heating, thus reducing the latent heat. This phenomenon is pronounced with SSPCMs with rubber matrix. inhomogeneity of the samples can also cause variation in the latent heat. On the other hand, the latent heats higher than the theoretical value probably result from the contribution of the sensible heat of the matrix material to the latent heat measurement.

The thermal conductivity of most SSPCMs with paraffin or fatty acid as a PCM is higher below the melting temperature of the PCM than above it, because the thermal conductivity of these PCMs is higher at their solid phase than at their liquid phase. Generally, the thermal conductivity of SSPCMs is low, which limits their efficiency. The thermal conductivity of SSPCMs may be improved by thermal conduction enhancing fillers, which is discussed in Chapter 4.

The addition of a PCM impairs the mechanical properties of matrix materials. Furthermore, mechanical properties of SSPCMs typically decrease with increasing PCM content. For SSPCMs with paraffin or fatty acid as a PCM, increasing temperature worsens the mechanical properties even more, resulting from softening and melting of the PCM. Unfortunately, mechanical properties of SSPCMs have been studied scarcely, since the emphasis of research has been on maximizing their heat storage capacity.

4. ENHANCEMENT OF THE THERMAL CONDUCTIVITY OF SSPCMS

In general, the main factor reducing the efficiency of PCMs is their low thermal conductivity, which retards the melting and solidification processes of the PCM. Consequently, the heat transfer rate between the PCM and the environment is decreased, and significant temperature differences within the PCM may occur. The thermal conductivity of SSPCMs may be enhanced by embedding thermally conductive fillers, such as carbon or metal nanoparticles. In this chapter, previous studies concerning ways to enhance the thermal conductivity of SSPCMs are presented. [52]

Xiao et al. [15] added expanded graphite (EG) to SBS/paraffin SSPCM as an attempt to improve its thermal conductivity, and thus the heat transfer rate. The heat transfer rate of the SSPCMs during the melting and solidification processes was investigated by heating and cooling the samples in a water bath. Figure 39 shows the heating and cooling curves of pure paraffin and SSPCMs with 80% paraffin and 20% SBS. It is seen that during melting (Figure 39a), the heat transfer rate of paraffin/SBS was lower than that of paraffin. During solidification (Figure 39b), however, the heat transfer rate of paraffin/SBS was higher than that of paraffin. The difference resulted from the fact that melting is a convection-dominated process, while solidification is dominated by conduction. Consequently, because natural convection during melting was weakened by the network of SBS, paraffin/SBS melted slower than paraffin. On the contrary, because the thermal conductivity of SBS is higher than that of paraffin, paraffin/SBS solidified faster than paraffin.

It is also seen in Figure 39 that the addition of EG into SSPCMs enhanced the heat transfer rate significantly in both the melting and solidification processes. The difference in heat transfer rate of the SSPCMs filled with EG and EG* is explained by their different morphologies: P(80)/S(20)/EG(5) sample was mixed in a two roll mixer, which broke the graphite into smaller particles. P(80)/S(20)/EG*(3) sample, on the contrary, was manufactured by adding the graphite into molten matrix material, so that the pore structure of the graphite remained unbroken. Consequently, the SSPCM made by the latter method included broader thermally conductive network of graphite, which resulted in higher heat transfer rate.
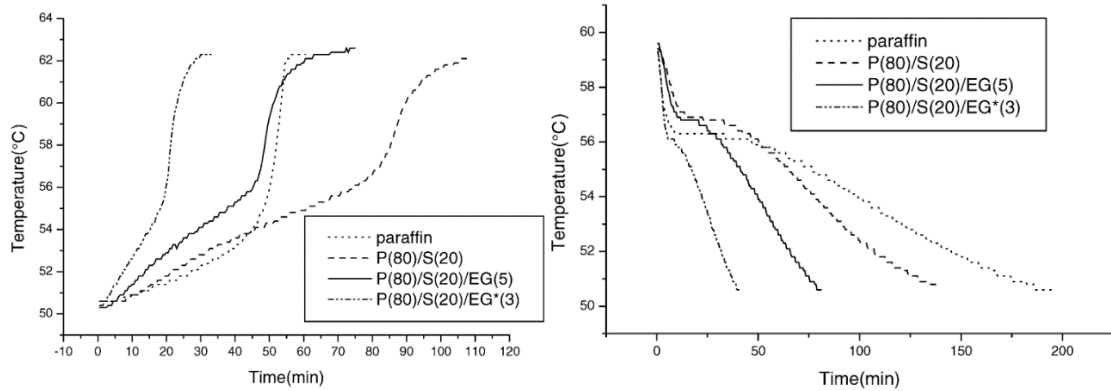
Figure 39. *(a) Heating and (b) cooling curves of paraffin and SSPCMs [15].*

Mhike et al. [53] studied the effect of EG and natural graphite flakes on the thermal conductivity of a paraffin/LDPE SSPCM. The paraffin content of the SSPCMs was 60%. Figure 40 shows the thermal conductivity of the SSPCM with different EG and graphite contents. It is seen that the thermal conductivity of the SSPCM increased almost linearly with increasing EG and graphite contents. Furthermore, the enhancement was more efficient with EG than with natural graphite flakes. With EG content of 10%, the thermal conductivity of the SSPCM increased more than 200%, while the same amount of natural graphite flakes resulted in only 60% increase. The reason for the different efficiencies of the two graphite types are clearly seen in Figure 41. In paraffin/LDPE/EG SSPCM (Figure 41b), graphite (black area) formed more continuous network than in paraffin/LDPE/graphite SSPCM. This network resulted in more efficient heat conduction enhancement.
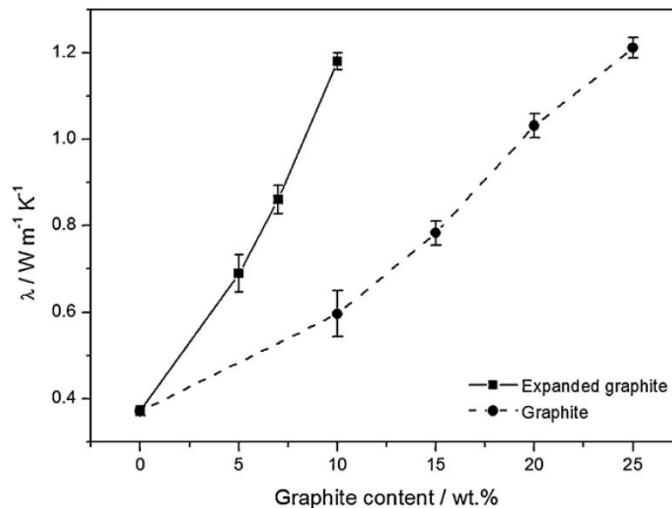

Figure 40. *Thermal conductivity of the paraffin/LDPE SSPCMs with different contents of EG and natural graphite flakes [53].*
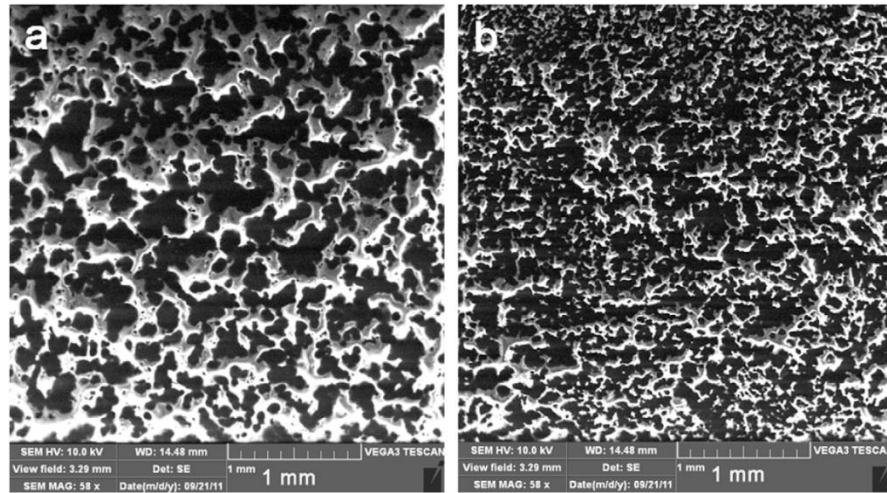
Figure 41. SEM images of (a) paraffin/LDPE/graphite and (b) paraffin/LDPE/EG SSPCMs (graphite/EG content 10%) [53].

The changes in other thermal properties were also investigated with respect to the GP and EG additions. It was found that the latent heat of the SSPCM decreased linearly with increasing additive content, because the relative amount of paraffin was decreased. This is seen as the reduced area of the peak of the DSC curve of the SSPCM, as seen in Figure 42. However, the melting temperature of the SSPCM remained practically unchanged.
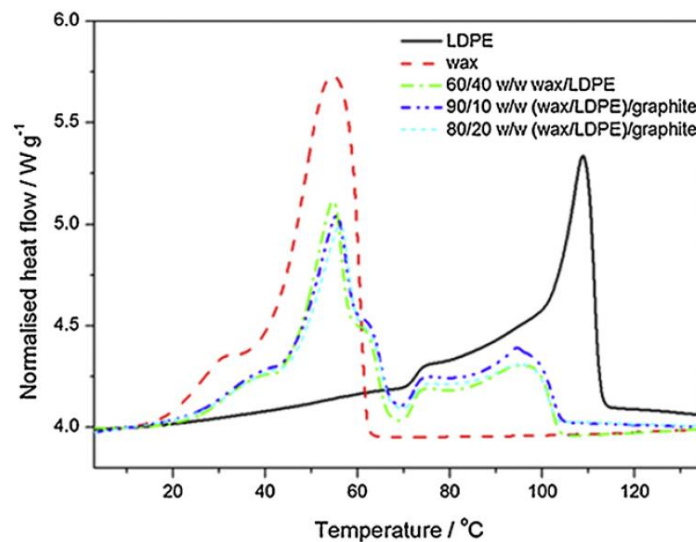

Figure 42. *The effect of graphite filler on the DSC curve of paraffin/HDPE SSPCM [53].*

Cheng et al. [54] studied the effect of graphite powder (GP) end expanded graphite (EG) on the thermal conductivity of a paraffin/HDPE SSPCM. The paraffin content of the SSPCM was 80%. Figure 43 shows the thermal conductivity of the SSPCM with different mass percentages of GP and EG. It is easily seen that EG enhanced the thermal conductivity of the SSPCM much more effectively than GP. Moreover, the thermal

conductivities increased linearly with the filler content. The thermal conductivity of the SSPCM without any filler was 0.31 W/(m·k). With EG content of 4.6%, the thermal conductivity of the SSPCM was as much as 1.36 W/(m·k), indicating over 4-fold increase in the thermal conductivity. On the other hand, the thermal conductivity of the SSPCM with GP content of 16% was only 0.52 W/(m·k). The lower efficiency of GP resulted from insufficient contact between GP particles in the SSPCMs. By contrast, due to higher volume of EG particles, EG formed an effective heat-conducting network even at relatively low contents, resulting in significant increase in thermal conductivity of the SSPCM.
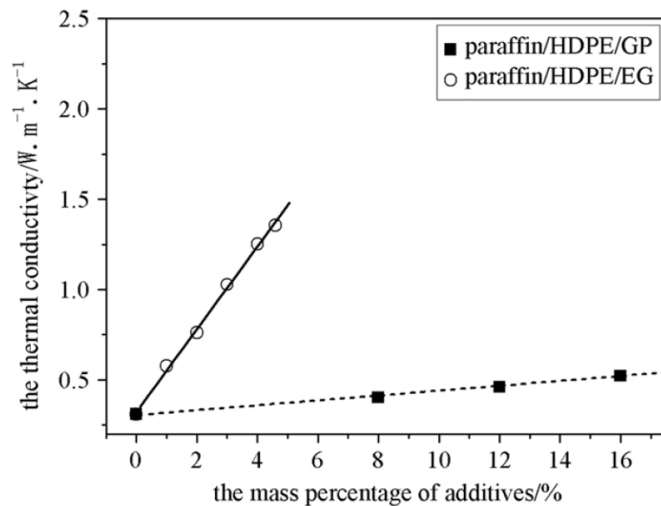

Figure 43. *Thermal conductivity of the paraffin/HDPE SSPCM with different GP and EG contents [54].*

Liu et al. [55] studied the effect of expanded graphite plates (EGP), multi-wall carbon nanotubes (MWCNT) and their combination on the thermal conductivity of an SSPCM. Paraffin with melting temperature of 20-25 °C was used as the PCM and 3:1 blend of SBS and HDPE as the matrix material. Paraffin content of the SSPCM was 60%. Figure 44a shows the thermal conductivity of the SSPCM filled with EGP and MWCNT separately, while Figure 44b shows that of the SSPCM filled with hybrid filler of EGP and MWCNT. The thermal conductivities were measured at 35 °C, with paraffin at the molten phase. It is seen in Figure 44a that the thermal conductivity of the SSPCM increased with the increasing filler content. Moreover, EGP improved the thermal conductivity of the SSPCM much more effectively than MWCNT. The reason for this was that EGP formed better conductive network, while MWCNTs formed aggregates that were separated by the matrix. Figure 44b shows that when the two fillers were used simultaneously, a synergistic effect was obtained. When the weight percentage of EGP was between 4.4 and 9.1, the thermal conductivity of the SSPCM was higher than the theoretical value (dashed blue line in Figure 44b) calculated by the addition law. The synergistic effect of EGP and MWCNT was induced by bridging between evenly distributed fillers, which enabled the formation of effective thermally conductive network.
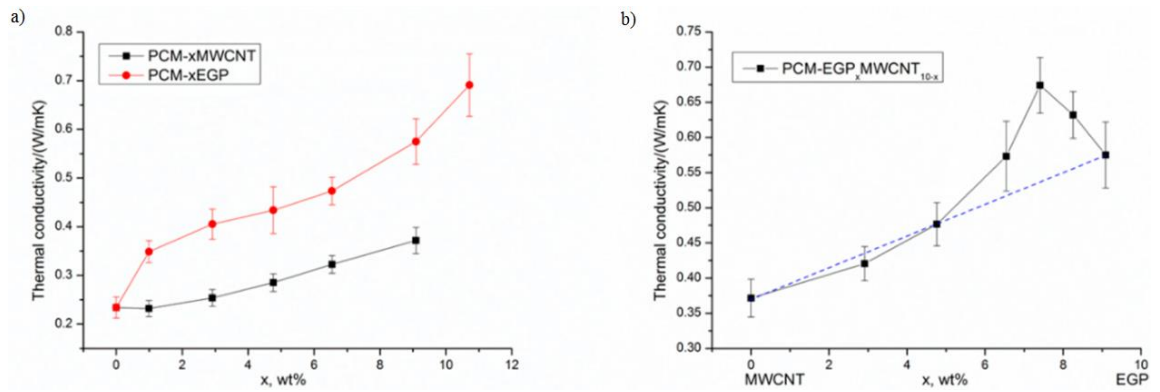
Figure 44. *Thermal conductivities of the SSPCM filled with (a) single filler and (b) hybrid filler [55].*

Figure 45 shows the thermal conductivities of the SSPCM with different fillers at different temperatures. It is seen that no matter the temperature, the thermal conductivity of the SSPCM filled with both EGP and MWCNT was higher than the thermal conductivity of the SSPCM filled with either of the fillers alone. Thus, it was stated that the synergistic effect of EGP and MWCNT takes place at all the temperatures between 35 and 50 °C.
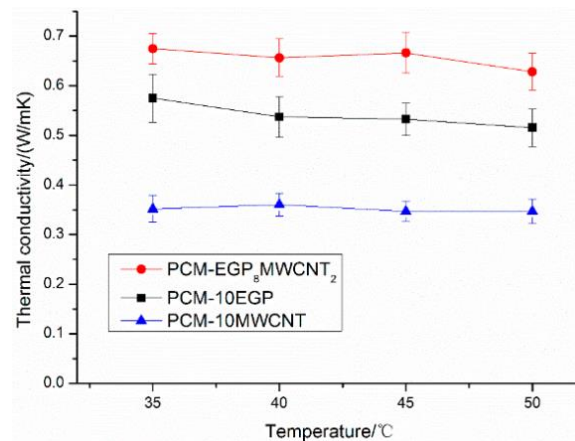

Figure 45. *Thermal conductivity of the SSPCMs with thermally conductive fillers at different temperatures [55].*

Tang et al. [56] studied the effect of graphene nanoplatelets (GNP) on the thermal conductivity of PA/HDPE SSPCM. The PCM content of the SSPCM was 80%. The thermal conductivity of the SSPCM with different GNP contents are presented in Figure 46. It is seen that the thermal conductivity of PA/HDPE SSPCM without GNP was 0.33 W/(m·k), while the addition of 4% of GNP increased it to 0.82 W/(m·k). Thus, the addition of GNP enhanced the thermal conductivity of the SSPCM significantly.
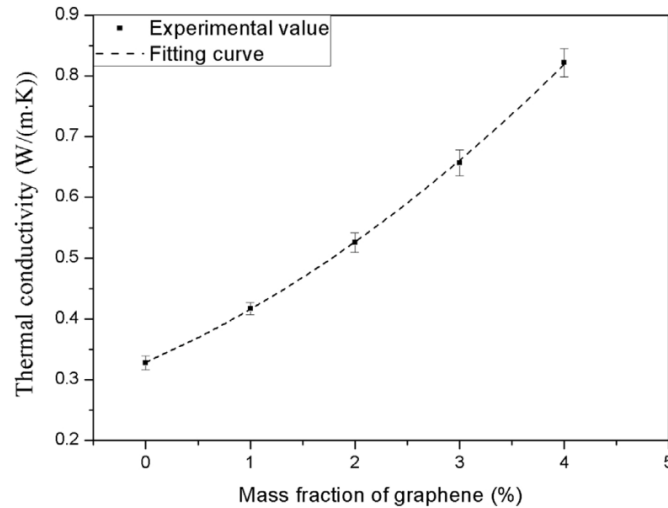
Figure 46. *Thermal conductivity of PA/HDPE SSPCM with different GNP contents [56].*

In another work, Tang et al. [40] studied the effect of nano-graphite (NG) and nano-Al_2O_3 (NAO) on the thermal conductivity of MA/HDPE SSPCM. The PCM content of the SSPCM was 70%. Figure 47 shows the thermal conductivity of the SSPCM with different nano-additive contents with MA at solid (Figure 47a) and at liquid phase (Figure 47b). It is seen that the thermal conductivity of the SSPCM increased when the nano-additive content was increased. In general, the thermal conductivity of the SSPCM was higher when MA was at solid state than at liquid state. In both cases, NG enhanced the thermal conductivity more effectively than NAO. With MA at the solid state, the thermal conductivity of the SSPCM increased from 0.20 W/(m·k) to 0.40 (NAO) and 0.45 W/(m·k) (NG) with the addition of 12% of nano-additives. With MA at the liquid state, the thermal conductivity increased from 0.19 W/(m·k) to 0.35 (NAO) and 0.39 W/(m·k) (NG).
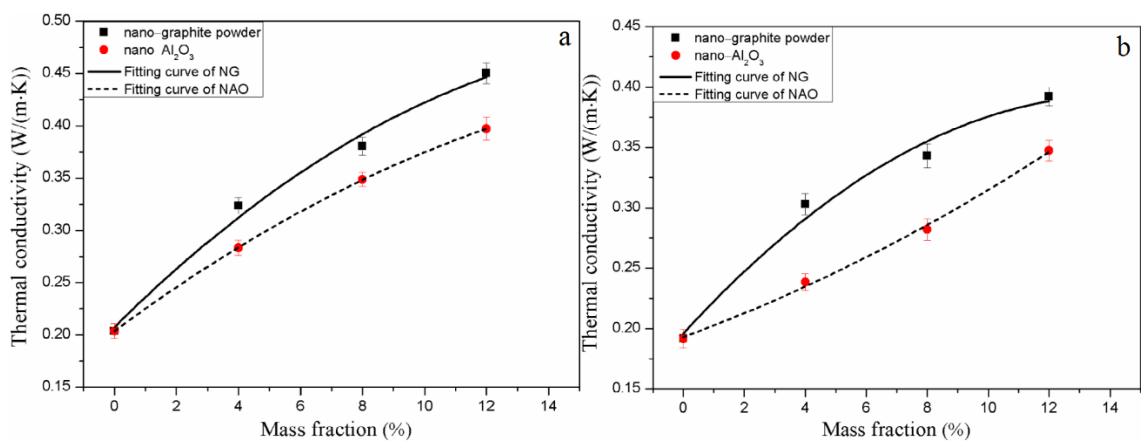

Figure 47. *Thermal conductivity of the MA/HDPE SSPCM with different contents of nanoadditives and with MA at (a) solid and (b) liquid state [40].*

Zhu et al. [51] studied the effect of copper nanowires (Cu NW) on the thermal conductivity of PA/PANI SSPCM. The PCM content before the addition of Cu NWs was

80%. Two different series of materials were prepared. The difference in the series was that the materials of PA/PANI/Cu-E series had ethanol in the final reaction mixture, while the materials of PA/PANI/Cu series did not. Figure 48 shows the thermal conductivity of the SSPCMS with different loadings of Cu NWs. It is seen that at low Cu NW contents, the thermal conductivity of PA/PANI/Cu-E series was lower than that of PA/PANI SSPCM without Cu NWs. However, when the Cu NW content was higher than 3%, the thermal conductivity of PA/PANI/Cu-E became higher than that of PA/PANI. This behavior was attributed to oxidation of Cu NWs at low Cu NW contents, which worsened the thermal conductivity. When the Cu NW content was increased, the amount of unoxidized Cu NWs increased, resulting in formation of thermally conductive paths and increased thermal conductivity. On the contrary, the thermal conductivity of PA/PANI/Cu series was increased with increasing Cu NW content, even at low contents. In conclusion, the thermal conductivity of PA/PANI SSPCM with PCM content of 80% could be increased from 0.377 to 0.455 W/(m·k) by addition of 11.2% of Cu NWs. Hence, it was stated that Cu NWs enhance the thermal conductivity of the SSPCM.
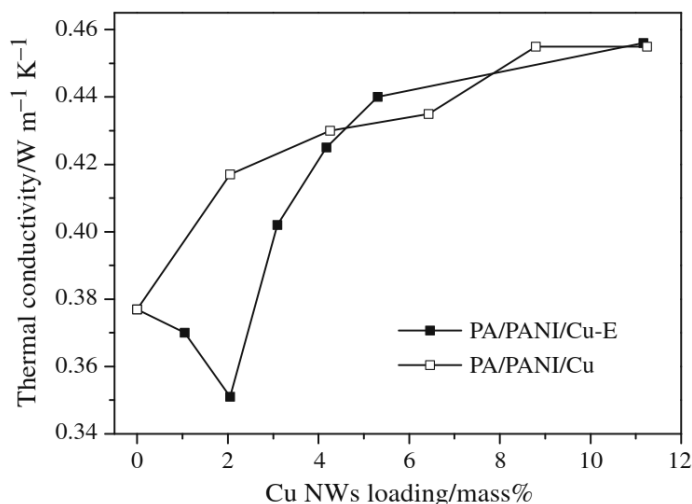

Figure 48. *Thermal conductivity of the PA/PANI SSPCMs with addition of Cu NWs [51].*

The thermally conductive fillers presented in this chapter and their relative enhancement of thermal conductivity are summarized in Table 14. It is seen that expanded graphite in its different forms seems to be the most efficient thermal conductivity enhancing filler for SSPCMs. This superiority results from the formation of thermally conductive graphite network in the SSPCMs. Synergistic effect of EGP and MECNT is also notable, since the addition of MWCNT improves this network even further. On the other hand, Cu NWs improved the thermal conductivity significantly less than the other fillers.

Table 14. *Thermal conductivity enchancing fillers used in SSPCMs.*

Filler	Filler content	Enhancement of thermal conductivity	Reference
Graphite flakes	10%	60%	[53]
EG	5%	85%	[53]
	10%	>200%	[53]
	4.6%	339%	[54]
GP	12%	48%	[54]
	16%	67%	[54]
EGP	10%	148%	[55]
MWCNT	10%	52%	[55]
EGP/MWCNT	10% (8%/2%)	191%	[55]
NG	12%	125%	[40]
NAO	12%	90%	[40]
Cu NW	11.2%	22%	[51]

5. APPLICATIONS OF SSPCMS

Because SSPCMs are relatively novel materials, the commercial applications for them are virtually nonexistent. However, some potential applications have been proposed, but they are still in the development stage. Previous studies concerning possible applications of SSPCMs are presented in this chapter.

5.1 Architectural membranes

Ordinary architectural membranes used in tensile structures have poor thermal insulation capacity compared to other building materials. Consequently, a lot of heat penetrates through the membranes into buildings at daytime, reducing thermal comfort of the buildings. Conversely, the heat escapes from the buildings at night. By enhancing the thermal insulation capacity of the membranes, the need for air-conditioning and heating of buildings could be reduced, resulting in significant energy savings. One feasible way to improve the thermal properties of the membranes is the use of PCMs. [57]

Pause [38] studied the effect of PCM addition to thermal properties of architectural membranes (see Chapter 3.1.3). The membrane was fabricated by mixing PCM with SR and applying the PCM/SR compound as a coating to a FG fabric. In this case, salt hydrate was selected as a PCM because of its large latent heat and fire retardancy. Figure 49 shows the thermal resistance of two ordinary membrane materials and the PCM/SR/FG membrane material. It is seen that the thermal resistance of the membrane can be significantly improved by the addition of PCM. The basic thermal resistance, resulting from sensible heat absorption, of the PCM/SR/FG membrane is higher than that of the other membranes because of its higher thickness and lower density. The biggest contribution to the total thermal resistance of PCM/SR/FG membrane, however, comes from dynamic thermal resistance, corresponding to the latent heat absorption of the membrane.
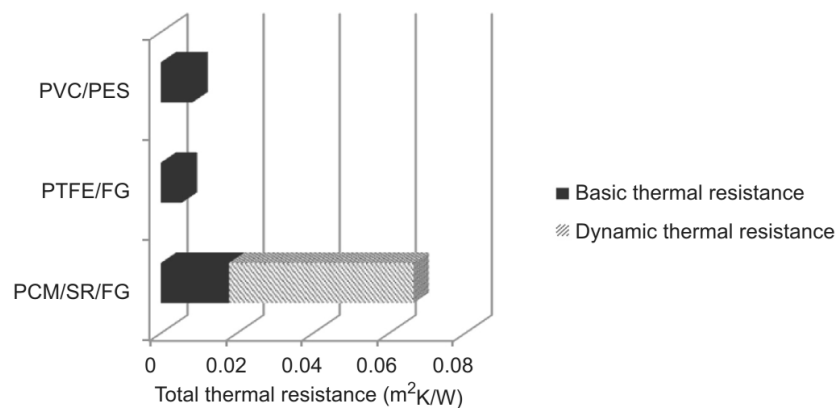

Figure 49. *Thermal insulation properties of different membrane materials [38].*

The effectiveness of the PCM/SR/FG membrane was also tested in practice. The temperature inside two tent structures, one covered with the PCM/SR/FG membrane and the other with an ordinary membrane, was monitored during the same day. The results are shown in Figure 50. It is seen that the temperature increase during the day was notably lower inside the PCM/SR/FG-covered tent. This difference resulted from the latent heat absorption of the PCM/SR/FG membrane, starting at 26 °C. Based on the test results, it was stated that the addition of PCM can reduce the air-conditioning demands of buildings and therefore improve their energy efficiency.
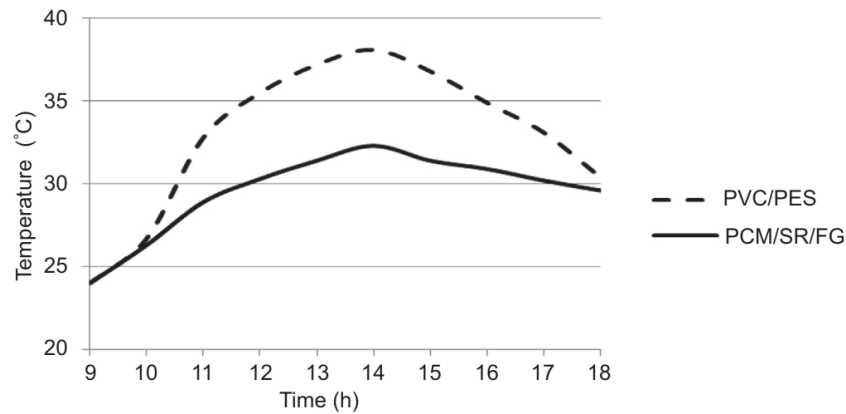

Figure 50. Temperature development inside two model structures [38].

5.2 Spacecraft thermal control

The purpose of spacecraft thermal control system is to maintain the temperature of the spacecraft within acceptable range and therefore avoid misoperations of the spacecraft. The most severe faults usually result from short-term high heat flux, which may seriously damage the thermal control system of the spacecraft. The malfunction of thermal control system may shorten the service life of the spacecraft substantially, or even lead to immediate decommission. [58]

Thermal control coatings are used in spacecraft to reduce the damage by short-term high heat flux. Inefficiency of conventional thermal control coatings has led to deployment of PCMs, of which paraffin is the most commonly used. To avoid leakage of paraffin, it is typically encapsulated in containers, which increases the weight of the system. In addition, leakage of paraffin may appear a problem despite the encapsulation. [58]

To prevent these problems, Wu et al. [58] studied the effectivity of paraffin/HDPE/EG SSPCM as a thermal control coating. It was found that the SSPCM withstood the high energy of the short-term high heat flux. The SSPCM prevented the overheating of the thermal control system and the temperature of the spacecraft remained stable. Even though the results were promising, further research is needed to validate the suitability of SSPCMs in spacecraft thermal control applications.

6. EXPERIMENTAL METHODS

In the experimental part of this thesis, SSPCMs with NR and latex matrixes and various PCMs were prepared and studied. The used raw materials, preparation steps and equipment, as well as test methods are presented in this chapter.

6.1 Raw materials

Two different matrix materials, NR (Standard Malaysian rubber, SMR 10) and NR latex (Revultex MR), were used in this work. The NR was produced by Teh Ah Yau Rubber Factory, and Revultex MR is a full ammonia pre-vulcanized NR latex provided by Nuplex Industries Ltd.

Various PCMs were used as heat storage enhancing fillers. The PCMs used in this work, as well as the published value for their phase change temperatures and latent heats, are presented in Table 15. It is seen that the PCMs encompass all the main PCM classes. The number in the trade name of the PCM means the designed phase change temperature of the PCM, so that for example the phase change of PCM64 should occur at 64 °C. However, all the PCMs change phase at a temperature range rather than at one precise temperature. An important fact considering the PCMs is that PCM64 and RT64HC consist of the same paraffin wax. In PCM64 that wax is microencapsulated, and RT64HC is uncapsulated.

Table 15. The PCMs used in the experiments.

PCM	Material type	Supplier	T_m [°C]	T_c [°C]	$\Delta H_{m,c}$ [kJ/kg]
PCM44	Microencapsulated paraffin wax	MikroCaps d.o.o.	41-44	not published	185-195
PCM64	Microencapsulated paraffin wax	MikroCaps d.o.o.	63-65	not published	172-184
PX52	Paraffin wax bound in silicon dioxide	Rubitherm GmbH	49-53	52-48	100 ± 7.5%
RT54HC	Fatty acid	Rubitherm GmbH	53-54	54-53	200 ± 7.5%
RT55	Paraffin wax	Rubitherm GmbH	51-57	56-57	170 ± 7.5%
RT64HC	Paraffin wax (same paraffin as in PCM64)	Rubitherm GmbH	63-65	64-61	250 ± 7.5%
SP58	Salt hydrate	Rubitherm GmbH	56-59	56-54	250 ± 7.5%
X55	Solid-solid PCM (based on NPG)	PCM Products Ltd	55	55	115

6.2 Preparation of the SSPCMs

All the prepared samples and their characteristics are presented in Table 16. Next, the preparation of the latex-based SSPCMs and NR-based SSPCMs are discussed separately.

Table 16. The prepared samples and their characteristics.

Sample	Matrix	PCM type	PCM content [phr]	Special characteristic
25-PCM44	Latex	Microencapsulated paraffin wax	25	
50-PCM44	Latex	Microencapsulated paraffin wax	50	
75-PCM44	Latex	Microencapsulated paraffin wax	75	
25-PCM64	Latex	Microencapsulated paraffin wax	25	
50-PCM64	Latex	Microencapsulated paraffin wax	50	
75-PCM64	Latex	Microencapsulated paraffin wax	75	
Latex ref	Latex		0	
25-RT64HC	NR	Paraffin wax	25	
50-RT64HC	NR	Paraffin wax	50	
75-RT64HC	NR	Paraffin wax	75	
50-RT55	NR	Paraffin wax	50	
50-RT54HC	NR	Fatty acid	50	
50-RT54HC/140	NR	Fatty acid	50	Cured at 140 °C
50-X55	NR	Solid-solid (NPG-based)	50	
25-PX52	NR	Paraffin wax bound in silicon dioxide	25	
50-PX52	NR	Paraffin wax bound in silicon dioxide	50	
75-PX52	NR	Paraffin wax bound in silicon dioxide	75	
25-PX52+silane	NR	Paraffin wax bound in silicon dioxide	25	Includes silane
50-PX52+silane	NR	Paraffin wax bound in silicon dioxide	50	Includes silane
75-PX52+silane	NR	Paraffin wax bound in silicon dioxide	75	Includes silane
25-PCM64/NR	NR	Microencapsulated paraffin wax	25	
25-PCM64/NR cold	NR	Microencapsulated paraffin wax	25	Cold-mixed
NR ref	NR		0	

6.2.1 PCMs in latex matrix

Microencapsulated PCM44 and PCM64 were primarily mixed with NR latex because water slurries of microencapsulated PCMs were easily dispersed in water-based latex. Because Revultex MR latex is prevulcanized, no other ingredients were needed besides the PCM and the latex. SSPCMs were prepared with PCM concentrations of 25, 50 and 75 phr. PCM slurries were simply added to the latex while stirring. Subsequently, the mixture was poured in a mold, vacuum-treated to eliminate pores and left to cure overnight. In preparation of the reference sample, the latex was diluted with 10% of distilled water to minimize the amount of pores in the sample. The thickness of the latex-based samples was 1 mm.

6.2.2 PCMs in NR matrix

The recipe for preparing SSPCMs with NR matrix is shown in Table 17. In addition to the NR and the PCM, the recipe included stearic acid and ZnO as activators, sulphur as curing agent and CBS as accelerator. The amount of PCM is marked as a number before the trade name of the PCM used: For example, in 25-RT64HC the amount of PCM was 25 phr, and in 50-RT64HC it was 50 phr. Furthermore, PX52+silane –SSPCMs included silane (Si-75) as a coupling agent. In these materials, the amount of silane was 10% of the amount of silica in PX52.

Table 17. *The recipe used in the preparation of the SSPCMs.*

Material	Amount (phr)	Function
NR	100	Matrix material
PCM	0-75	Heat storage enhancing filler
Stearic acid	2	Activator
ZnO	5	Activator
Sulphur	1.5	Curing agent
CBS	1.5	Accelerator

After weighing the components, they were mixed in Brabender mixer 350 E with rotor speed of 60 min^{-1} and barrel temperature of 90 °C (despite in the case of 25-PCM64/NR cold, which was cold-mixed). The mixing scheme is shown in Table 18. Firstly, the NR was masticated, after which the PCM was added. The PCMs (excluding PX52 and X55) had to be added slowly to ensure proper mixing. Stearic acid and ZnO were added after the PCM. Finally, sulphur and CBS were added, and the mixing was continued for three minutes. The reference was mixed similarly to the SSPCMs, but it did not include any PCM. The scheme for PX52-based SSPCMs containing silane was different to the other SSPCMs, because silane required 5 minutes at 135 °C to react with silica. Of the PCMs listed in Table 15, SP58 (salt hydrate) was not successfully mixed with the NR, because

the salt hydrate did not disperse within in the rubber but remained as a molten separate phase.

Table 18. *The mixing scheme of the SSPCMs.*

Regular scheme		Scheme for the SSPCMs containing silane	
Material	Time (min)	Material	Time (min)
NR	0	NR	0
PCM	1.5	PCM	1.5
Stearic acid	9	Stearic acid	4
ZnO	9	ZnO	4
Sulphur	10	(Silane)	7
CBS	10	Sulphur	14
		CBS	14
Total time	13	Total time	16

The vulcanization times of the SSPCMs were determined by Alpha Technologies Advanced Polymer Analyzer 2000 (APA 2000). The measurement time was set to 30 minutes and temperature to 160 °C. RT54HC-based SSPCM was tested also at 140 °C to avoid decomposition of the fatty acid. The vulcanization times of the SSPCMs with NR matrix are shown in Table 19. Finally, the samples were vulcanized to 2 mm thick sheets in a heating press (MKH E 60 M) at their respective curing time.

Table 19. *Vulcanization times of the SSPCMS with NR matrix.*

SSPCM	Vulcanization time (min:s)
25-RT64HC	7:53
50-RT64HC	5:38
75-RT64HC	7:23
50-RT55	9:30
50-RT54HC	21:11
50-RT54HC/140	75:05
50-X55	2:41
25-PX52	9:00
50-PX52	10:52
75-PX52	10:10
25-PX52+silane	9:16
50-PX52+silane	10:59
75-PX52+silane	11:08
25-PCM64/NR	4:23
25-PCM64/NR cold	3:28
Reference	9:46

6.3 Test methods

The test methods used to determine the microstructure, as well as mechanical and thermal properties, are presented in the following subchapters.

6.3.1 Characterization of the microstructure of the SSPCMs

In order to inspect the microstructure of the SSPCMs, their fracture surfaces were studied by field emission scanning electron microscope (FESEM) (Zeiss ULTRAplus). The studied cross-sections were the fracture surfaces of the tensile test specimens. Senior Research Fellow Mari Honkanen prepared the samples and took the images. The SEM samples were prepared by gluing a piece of the sample, with the fracture surface upwards, to the aluminum base with carbon glue. Subsequently, the sample was coated with carbon by an evaporator or with gold by sputtering to offer electrical conductivity. Along with the microstructure, the morphologies of the fracture surfaces were studied by SEM.

6.3.2 Thermal properties

The thermal stability of the samples was tested by keeping them in an oven at 80 °C for 20 minutes. The samples were weighed before and after the heating, and the weight difference was calculated.

The phase change temperatures and latent heats of the SSPCMs were studied by DSC (Netzsch DSC 204 F1). The samples were subjected to two heating and cooling cycles of 0-100 °C with heating and cooling rates of 10 K/min. Furthermore, the cyclic stability of 50-RT64HC sample was tested by subjecting it to 10 heating and cooling cycles.

The thermal conductivity of the SSPCMs were studied by laser flash analysis (LFA) (Netzsch LFA 467 HyperFlash). Circular samples with diameter of 1 cm were used. The samples were coated with thin layer of conductive graphite coating to distribute the heat pulse evenly on the surface of the sample. Each sample was measured five times, and the average values were calculated.

Furthermore, the thermal buffering properties of the SSPCMs was evaluated by heating them from the room temperature to near their melting point and following the temperature rise by a thermal camera (Fluke Ti400).

6.3.3 Mechanical properties

Hardness tests were performed by Bareiss BS61 II hardness tester according to ASTM D 2240 – 00 (Shore A method). To ensure that the thickness was over 6 mm, three sheets (or six in the case of latex-based SSPCMs) were placed one on the other. Hardness was

measured at five different locations of each material, and the mean values and standard deviations were calculated.

Tensile tests were performed by Messphysik tensile testing machine according to ISO 37. The test specimens were type 1 in the case of NR-based SSPCMs and type 2 in the case of latex-based SSPCMs. The traverse speed of the machine was 500 mm/min for specimens of type 1 and 200 mm/min for specimens of type 2. Five specimens were tested of each material.

Dynamic mechanical properties of the SSPCMs were studied by DMA (Mettler Toledo DMA/SDTA861^e). The measurements were done by Research Assistant Mikko Koivula. The circular samples with diameter of 6 mm were sheared with frequency of 1 Hz. The used temperature range was -60 to 80 °C. Based on the DMA results, storage modulus and tan δ of the SSPCMs were determined. Tan δ, also known as the loss factor, is determined as the ratio of loss modulus to storage modulus. It indicates the damping properties of the material so that the higher the tan δ, the more effectively the material absorbs and dissipates energy. [39]

7. RESULTS AND DISCUSSION

In this chapter, the results of the experimental part of this thesis are discussed. The discussion starts from preparation of the SSPCMs and continues with the characterization of the microstructure. After that, the thermal and mechanical properties of the SSPCMs are discussed.

7.1 Preparation of the SSPCMs

Because the preparation process of the latex- and NR-based SSPCMs were different, they are discussed separately in the following subchapters.

7.1.1 PCMs in latex matrix

The preparation of the SSPCMs with latex matrix was relatively straightforward process, since the slurries of microencapsulated PCMs were easily mixed with the latex. Because the latex was pre-vulcanized, no vulcanization of the SSPCMs was needed. The biggest challenge in the preparation of the latex-based SSPCMs was to eliminate the pores resulting from the mixing by vacuum treatment. The problem was emphasized with the reference sample, which needed to be diluted to reduce its viscosity and hence minimize the number of pores.

7.1.2 PCMs in NR matrix

There were significant differences between the ease of the preparation of the SSPCMs with different PCMs. Generally, SSPCMs with PX52 as the PCM were the easiest to prepare. In PX52, the paraffin is bound in silica so that it does not seemingly melt during the mixing. The situation was similar with SSPCMs with X55 (solid-solid PCM) as the PCM. However, the dispersive mixing of X55 was inadequate, and it remained as relatively large particles in the NR. This resulted in decrease in the mechanical properties of the composite. Also PCM64 (microencapsulated paraffin) was relatively easy to mix with NR, because the melamine/formaldehyde shell prevented the molten paraffin from flowing during the beginning of the mixing. The other PCMs were more difficult to mix, because the melting of the PCMs complicated the mixing process. The PCMs had to be added to the NR very slowly to obtain proper mixing. As an example, the mixing curve of 50-RT64HC is presented in Figure 51. If the PCM was added too fast or in too large portions, the PCM did not disperse in the rubber but remained as a separate liquid phase. For the same reason, the mixing of SP58 (salt hydrate) failed.
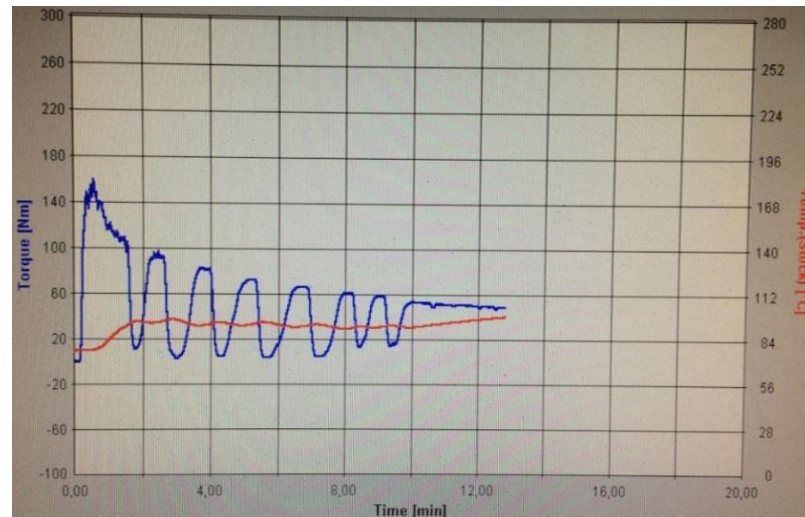
Figure 51. *The mixing curve of 50-RT64HC. The blue curve represents the torque [Nm], and the red curve indicates the temperature [°C] of the stock.*

The vulcanization time of the SSPCMs varied notably depending on the PCM used (see Table 18). Compared to the reference (pure NR), the vulcanization times of 50-X55, 25-PCM64/NR and 25-PCM64/NR cold were significantly shorter. Also SSPCMs with RT64HC as the PCM had lower vulcanization times than the reference. The vulcanization times of the other SSPCMs were close to that of the reference. The PCM content of the SSPCMs did not have notable effect on the vulcanization time.

7.2 Characterization of the microstructure of the SSPCMs

The microstructure of the SSPCMs is discussed in the following subchapters. Because FESEM was found to be superior to stereomicroscope in terms of resolution, only FESEM pictures are used in this thesis.

7.2.1 PCMs in latex matrix

The FESEM images of latex reference, pure (dry) PCM64, 50-PCM64 SSPCM and 75-PCM64 SSPCM are shown in Figure 52. It is seen that the PCM microcapsules seemed to be homogenously dispersed in the latex matrix. The increase in PCM content of the SSPCM did not result in notable changes in the dispersion. Since the shell materials of PCM64 and PCM44 microcapsules were the same, the microstructure of the SSPCMs with PCM44 as a PCM were similar to those with PCM64 as a PCM.
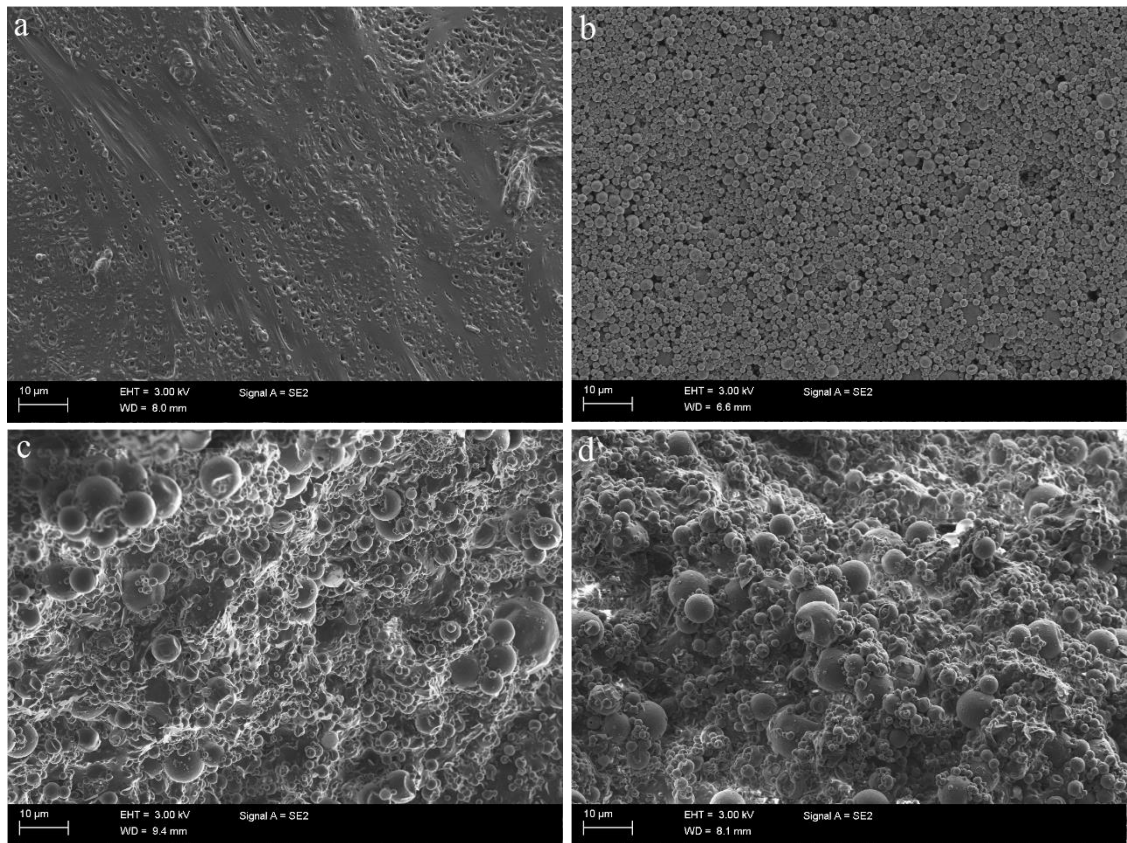
Figure 52. *FESEM images of (a) latex reference, (b) pure PCM64, (c) 50-PCM64 and (d) 75-PCM64.*

7.2.2 PCMs in NR matrix

The FESEM images of the NR reference, pure RT64HC, 25-RT64HC SSPCM and 75-RT64HC SSPCM are shown in Figure 53. It is seen that in 25-RT64 HC, the paraffin was evenly distributed as small flakes within the NR matrix. These flakes were born during the mixing, when the paraffin was melted and solidified again when the temperature of the SSPCM decreased below the melting temperature of the paraffin. By contrast, the microstructure of 75-RT64 HC was very different compared to 25-RT64HC. The paraffin did no longer appear as small flakes, but as larger lumps in the NR matrix. However, these lumps were still somewhat evenly distributed. The microstructure of 50-RT64HC was between those of 25-RT64HC and 75-RT64HC, including both small flakes and large lumps of paraffin within the matrix.
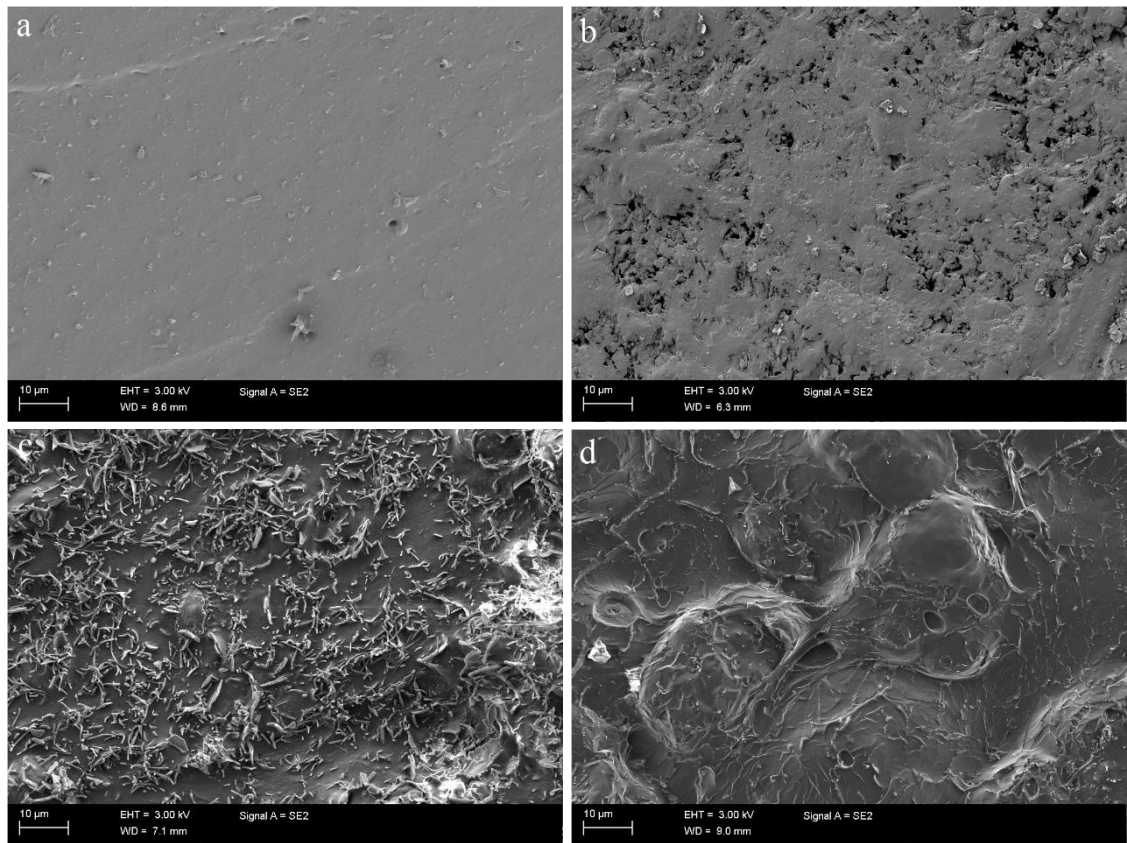
Figure 53. *FESEM images of (a) NR reference, (b) pure RT64HC, (c) 25-RT64HC and (d) 75-RT64HC.*

Figure 54 shows FESEM images of pure RT55 (paraffin), 50-RT55 SSPCM, pure RT54HC (fatty acid), 50-RT54HC SSPCM and 50-X55 (solid-solid PCM) SSPCM. It is seen in Figure 54b that RT55 appeared as nearly spherical inclusions in the NR matrix. The appearance was significantly different to that of the SSPCMs with RT64HC – also a paraffin – as the PCM (see Figure 53). Thus, it seems that different paraffins may disperse differently in NR matrix. Figure 54d shows that RT54HC was dispersed in the matrix as differently sized lumps. In addition, notable porosity is visible, which probably resulted from the decomposition of the fatty acid as it was cured at 160 °C. The microstructure of 50-X55 (Figure 54e) is hard to interpret, because X55 appeared mainly as large macro-sized lumps, which separated from the matrix during the tensile tests and hence were not visible in the FESEM images.
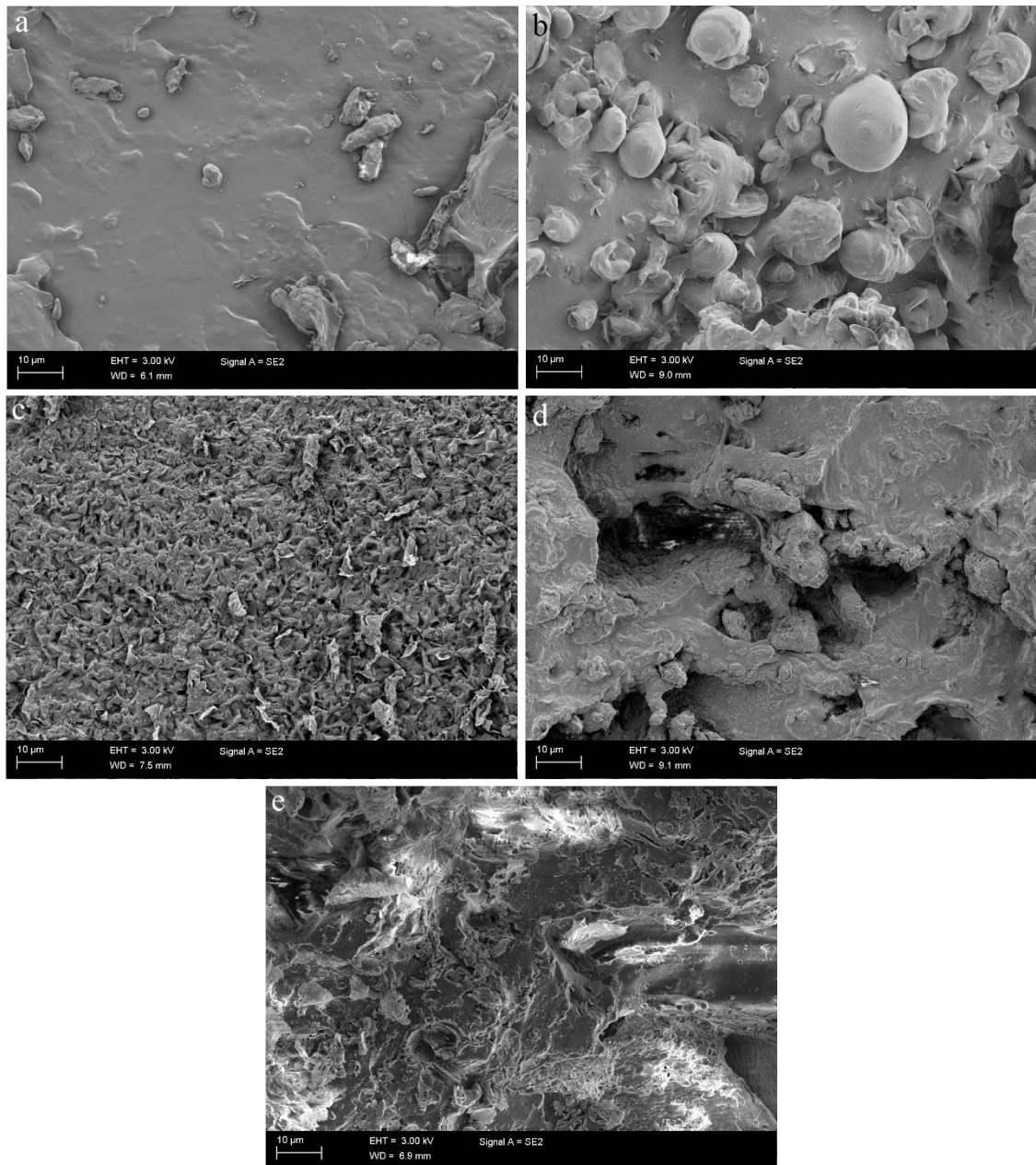
Figure 54. *FESEM images of (a) pure RT55, (b) 50-RT55 SSPCM, (c) pure RT54HC, (d) 50-RT54HC SSPCM and (e) 50-X55 SSPCM.*

The FESEM images of the SSPCMs with PX52 as the PCM are shown in Figure 55. The intention was to evaluate if the addition of silane had an effect on the dispersion of the PX52 within NR matrix or the polymer-filler interaction within the composite. It is seen that when the PCM content was 25 phr, the dispersion of 25-PX52 and 25-PX52+silane were similar. When the PCM content was increased to 50 phr, notable change occurred. In 50-PX52, the PCM did not disperse homogeneously in the matrix but accumulated as stripes. The resulting microstructure seemed to consist of large areas of nearly pure NR and narrow stripes of nearly pure PX52. In 50-PX52+silane, by contrast, the dispersion of PX52 looked homogenous. When the PCM content was raised even further (75 phr),
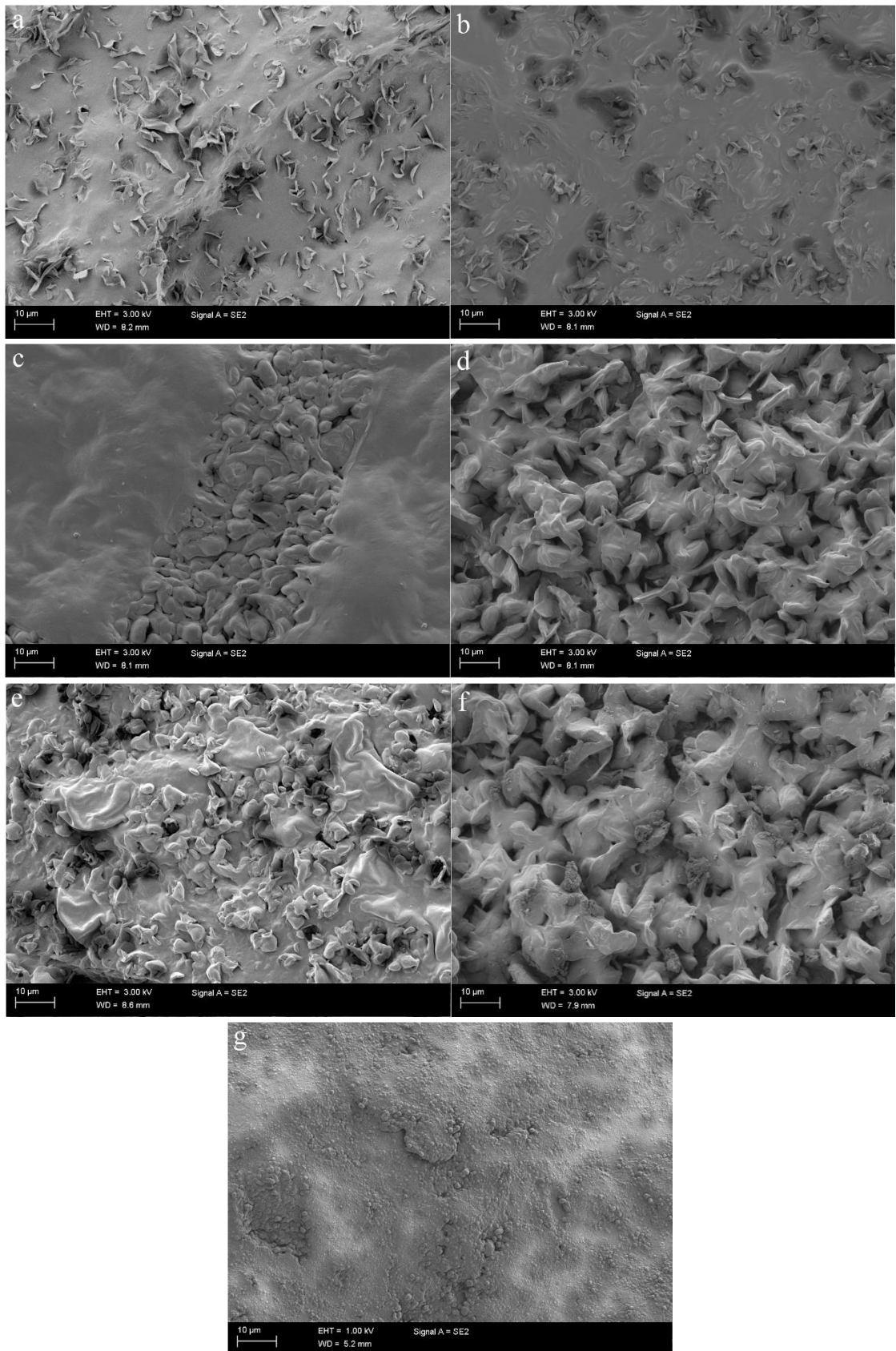
Figure 55. FESEM images of (a) 25-PX52, (b) 25-PX52+silane, (c) 50-PX52, (d) 50-PX52+silane, (e) 75-PX52 and (f) 75-PX52+silane SSPCMs and (g) pure PX52.

the microstructures resembled each other again. However, the addition of silane resulted in slightly more homogeneous dispersion of PX52.

Figure 56 shows FESEM images of the SSPCMs with PCM64 as the PCM and NR as the matrix material. One of these materials (25-PCM64/NR) was prepared the same way as the other NR-based SSPCMs, while the other (25-PCM64/NR cold) was mixed at as low temperature as possible (without heating the mixing chamber). It is seen that the microstructures of these two SSPCMs were similar. The PCM microcapsules were broken in both the samples, and the microstructures consisted of paraffin flakes and pieces of shattered capsule shells homogeneously dispersed within the NR matrix. In addition, the cold-mixed SSPCM included a few unbroken PCM microcapsules. However, since the majority of the microcapsules were broken even in the cold-mixed SSPCM, it seems that they were broken by high shear forces during the mixing rather than too high temperature.
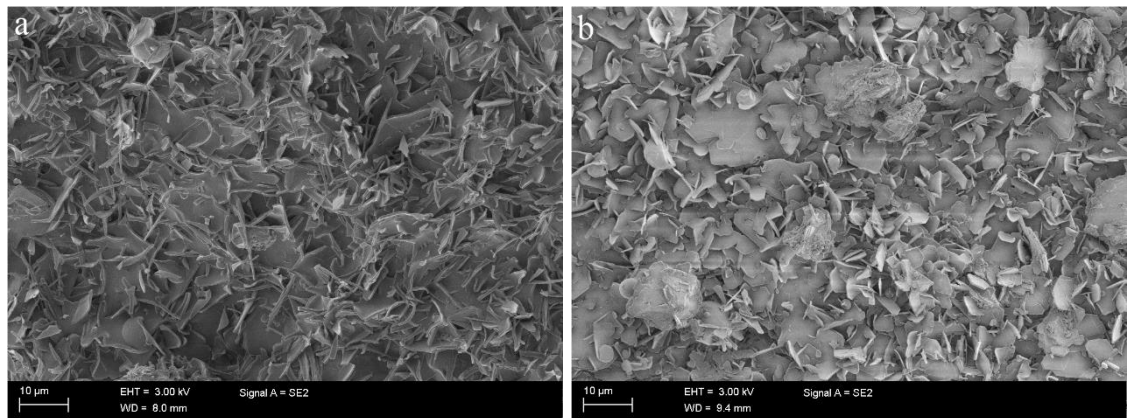

Figure 56. FESEM images of (a) 25-PCM64/NR and (b) 25-PCM64/NR cold SSPCMs.

7.3 Thermal properties

Before testing the thermal properties, the thermal stability of the SSPCMs was studied by keeping the samples in on oven at 80 °C for 15 minutes. None of the SSPCMs showed leakage of the PCM in the oven test, so the SSPCMs were considered stable at 80 °C. Thermal stability was a prerequisite for thermal conductivity measurements, as the samples should remain solid in the LFA measurements. Thermal properties of the SSPCMs are discussed in the following subchapters.

7.3.1 Latent heat and phase change temperature

The results of the DSC measurements of the SSPCMs are shown in Table 20. In addition, in order to illustrate the results more clearly, they are presented through different comparisons.

Table 20. *The phase change temperatures and latent heats of the SSPCMs.*

Sample	T_m (°C)	ΔH_m (kJ/kg)	T_c (°C)	ΔH_c (kJ/kg)
25-PCM44	49.1	30.1	34.3	-30.5
50-PCM44	49.4	46.3	33.9	-45.2
75-PCM44	52.4	70.8	31.1	-70.4
Pure PCM44	53.2	172.8	30.2	-171.2
25-PCM64	70.1	23.7	44.2	-27.1
50-PCM64	70.1	46.7	43.8	-53.7
75-PCM64	72.3	58.9	43.7	-67.6
Pure PCM64	73.0	163.9	36.1	-158.8
25-RT64HC	64.4	36.6	44.8	-37.4
50-RT64HC	65.3	68.2	48.4	-69.6
75-RT64HC	69.7	85.8	46.9	-91.5
Pure RT64HC	72.0	231.1	47.2	-224.7
50-RT55	55.0	47.5	40.7	-46.3
50-RT54HC	41.4	22.01	23.6	-20.3
50-RT54HC/140	52.0	45.8	29.3	-46.6
50-X55	68.9	24.6	32.2	-21.9
Pure RT55	59.9	170.3	40.5	-175.8
Pure RT54HC	64.8	184.7	38.2	-187.3
25-PX52	38.9	9.0	26.2	-8.0
50-PX52	45.9	18.7	31.1	-19.3
75-PX52	49.8	30.0	36.6	-32.0
25-PX52+silane	42.4	13.9	26.5	-14.1
50-PX52+silane	49.7	28.2	28.6	-29.1
75-PX52+silane	51.6	40.7	33.4	-42.8
Pure PX52	54.2	97.7	36.1	-103.9
25-PCM64/NR	70.6	40.0	37.9	-44.9
25-PCM64/NR cold	69.9	40.5	37.9	-44.2

The DSC heating curves of the latex-based SSPCMs are shown in Figure 57. The most important finding is that the latent heat of the SSPCMs increased with increasing PCM content. It is also seen that the melting temperature increased slightly with increasing PCM content. For example, the melting temperature of 25-PCM64 was 70.1 °C, while that of 75-PCM64 was 72.3 °C. That was expected, since the melting temperatures of the SSPCMs should approach that of pure paraffin when the PCM content is increased. Correspondingly, as seen in Figure 58, the crystallization temperature decreased with increasing PCM content. An interesting fact is that the SSPCMs had a single melting peak, but two overlapping crystallization peaks. Furthermore, Table 20 shows that the melting and crystallization temperatures of the SSPCMs approached those of the pure PCMs when the PCM content of the SSPCM was increased. The crystallization temperatures of the SSPCMs were much lower than the melting temperatures, indicating significant supercooling of the SSPCMs. These results comply well with the previous studies presented in Chapter 3.
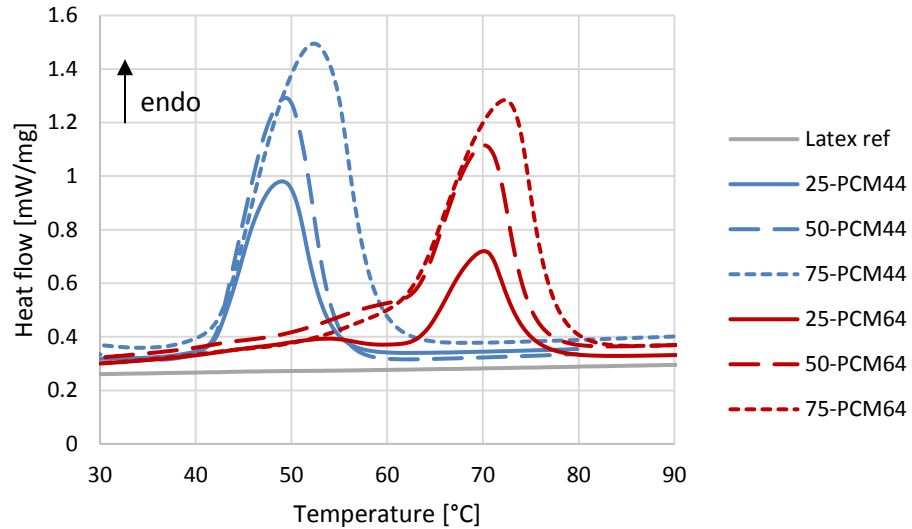
Figure 57. *The effect of PCM microcapsule content on the DSC heating curves of the latex-based SSPCMs.*
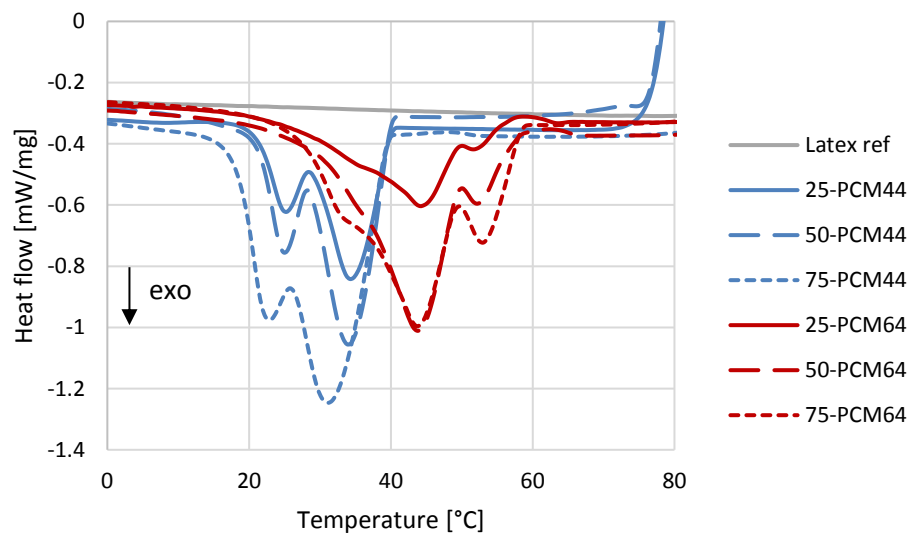

Figure 58. *The effect of PCM microcapsule content on the DSC heating curves of the latex-based SSPCMs.*

Figure 59 shows the DSC heating curves of the NR-based SSPCMs with RT64HC as the PCM. It was found that that the latent heat and the melting temperature increased with increasing PCM content. 25-RT64HC and 75-RT64HC were also tested as unvulcanized to evaluate the effect on vulcanization on the latent heat. It is seen that the latent heats of the unvulcanized samples were notably higher than those of the corresponding vulcanized samples. Thus, the vulcanization of the SSPCMs seemed to lower the latent heat, probably by hindering the thermal movement of the PCM. Figure 60 shows the DSC cooling curves of the SSPCMs. It is seen that the SSPCMs have two overlapping crystallization peaks,

and the latent heat of crystallization increases with increasing PCM content. In addition, vulcanization seems to reduce the latent heat. Differently to melting behavior, no relationship between the crystallization temperature and PCM content of the SSPCM was found.
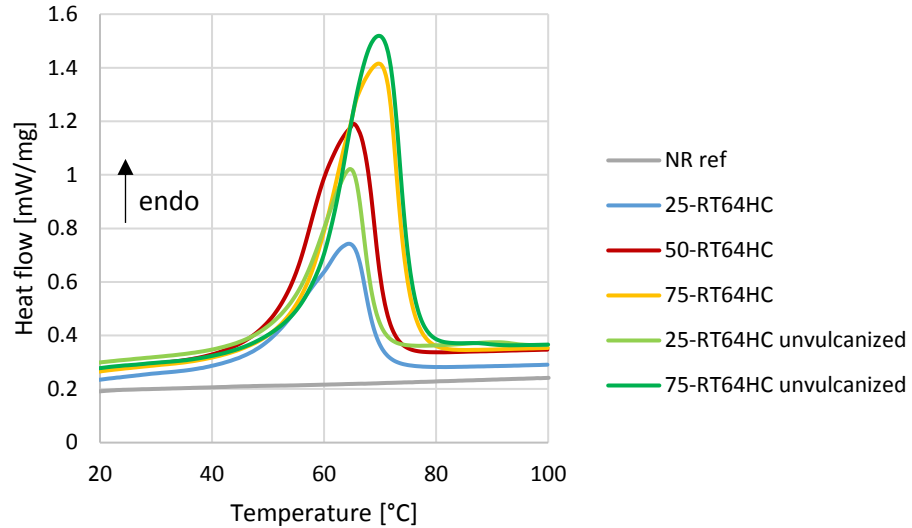

Figure 59. *The effect of PCM content and vulcanization on the DSC heating curves of the NR-based SSPCMs with RT64HC as the PCM.*
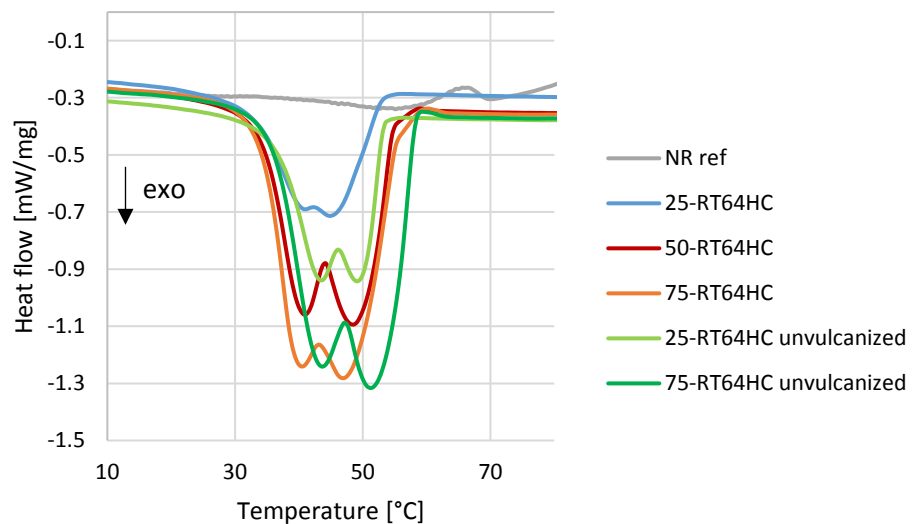

Figure 60. *The effect of PCM content and vulcanization on the DSC cooling curves of the NR-based SSPCMs with RT64HC as the PCM.*

To compare the latent heat and the melting temperature of the SSPCMs to those of the pure PCMs, Figure 61 shows the DSC curves of 50-RT64HC SSPCM and pure RT64HC. It is seen that the latent heat of the SSPCM was significantly lower than that of pure RT64HC. As seen in Table 19, the latent heats of melting and crystallization of 50-RT64HC were 68.2 and -69.6 kJ/kg, while those of pure RT64HC were 231.1 and -224.7

kJ/kg, respectively. Since PCM content of 50 phr is nearly equivalent to weight percentage of 33%, the latent heats of melting and crystallization should theoretically be 76.3 and 74.2 kJ/kg. Thus, the latent heat of 50-RT64HC was slightly lower than theoretically expected. Based on the literature research in Chapter 3, the most probable reason for this was the polymer network of the vulcanized rubber, which hindered the thermal movement of paraffin. It is also seen in Figure 61 that the melting and crystallization temperatures of 50-RT64HC were lower than those of pure RT64HC, as expected.
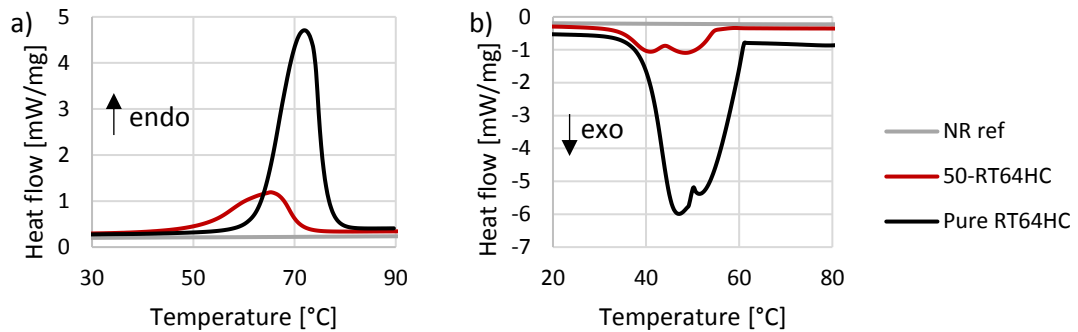

Figure 61. Comparison of the DSC curves of 50-RT64HC and pure RT64HC.

The cyclic stability of 50-RT64HC SSPCM was determined by subjecting the sample to ten successive heating-cooling cycles. The blue curve in Figure 62 represents the second cycle (because the thermal history of the material may distort the results of the first cycle), while the red curve represents the tenth one. It is seen that the latent heat and phase change temperature remain almost unchanged during the ten cycles. In fact, the latent heat of the sample increased slightly during the measurements. Thus, 50-RT64HC was verified to be stable for at least ten thermal cycles.
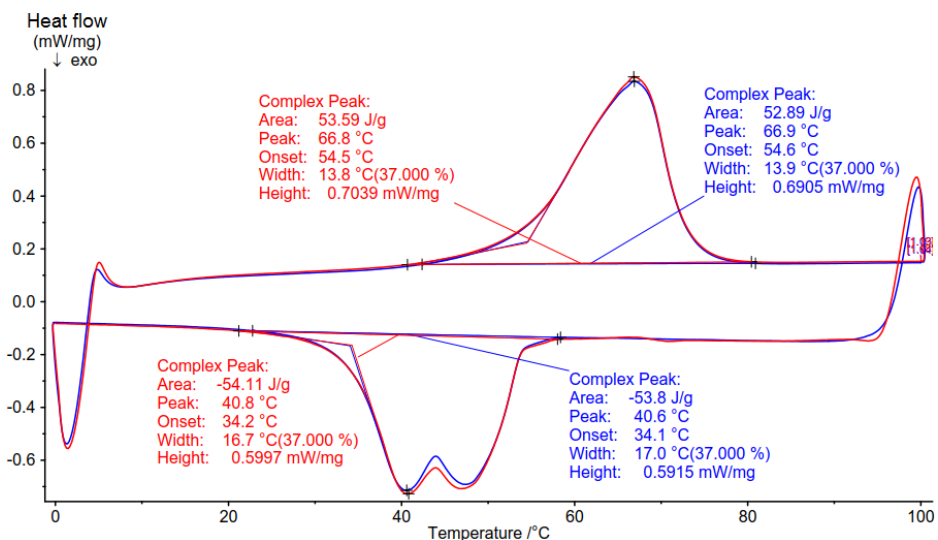

Figure 62. The cyclic stability of 50-RT64HC SSPCM. The blue curve represents the second heating-cooling cycle and the red curve represents the tenth cycle.

Figure 63 shows the DSC heating curves of NR-based SSPCMs with the same amount of different PCMs. Firstly, it is seen that the melting temperatures of the SSPCMs vary notably, ranging from 41 °C (50-RT54HC) to as high as 69 °C (X55). The variation in the melting temperatures may result from the differences in melting temperatures of the pure PCMs. Even though the designed melting temperature of the PCMs varies only 1 °C, the actual difference may be higher (see Table 20). In addition, the rubber matrix may affect differently to the melting temperatures of different PCMs. Considering the relative latent heats of melting of the SSPCMs, it is seen that 50-RT54HC/140, which was vulcanized at 140 °C to avoid thermal decomposition of the PCM, had the highest latent heat (45.8 kJ/kg), while X55 had the lowest one (24.6 kJ/kg). As the latent heat of 50-RT54HC was lower than that of 50-RT54HC/140, it was found that RT54HC decomposed when the SSPCM was vulcanized at 160 °C. Figure 64 shows the DSC cooling curves of the SSPCMs. It is seen that the variation in the crystallization temperatures of the SSPCMs was lower than in melting temperatures. The latent heats of crystallization were close to the latent heats of melting. By comparing Figures 63 and 64, it is seen that 50-X55 showed the most significant supercooling (36.7 °C). By contrast, 50-RT55 showed the least supercooling (14.3 °C).
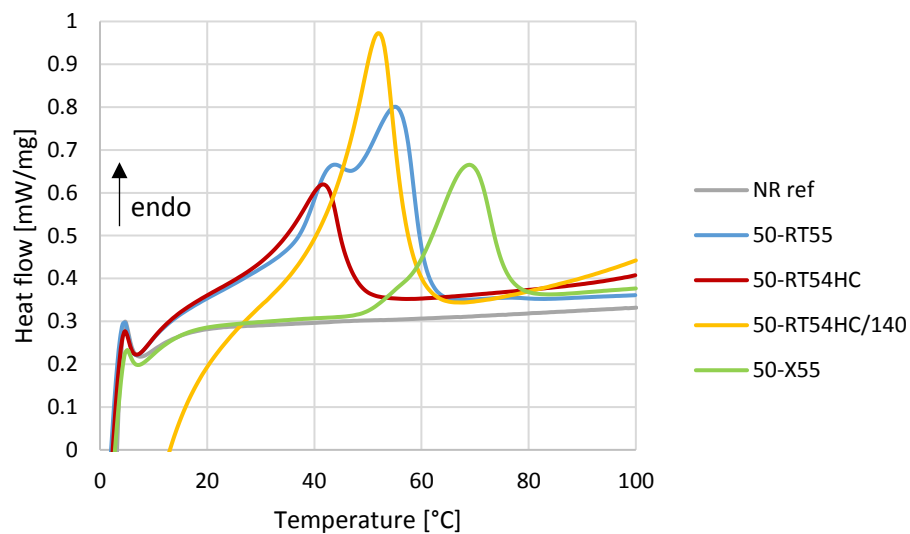

Figure 63. *Comparison of the DSC heating curves of NR-based SSPCMs with the same amount of different PCMs.*
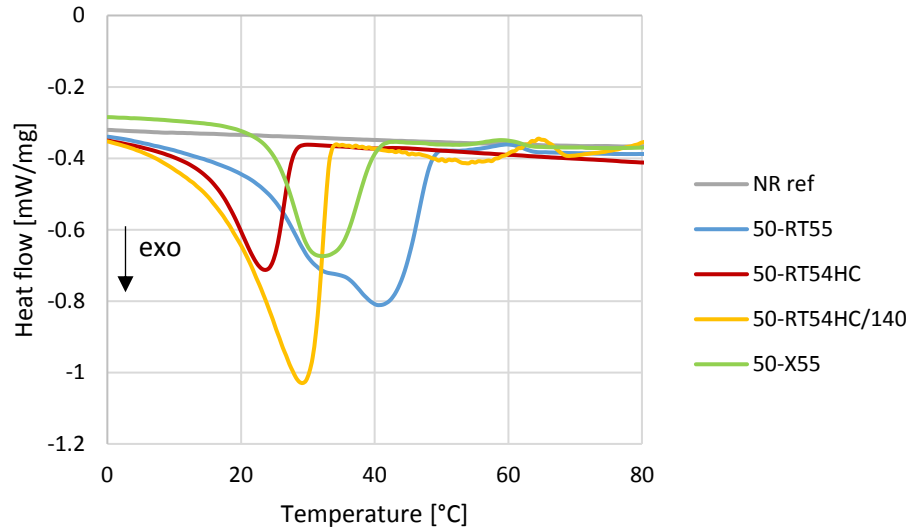
Figure 64. *Comparison of the DSC cooling curves of NR-based SSPCMs with the same amount of different PCMs.*

The DSC heating curves of the SSPCMs with PX52 as the PCM are shown in Figure 65. It is seen that silanization increased the melting temperature of the SSPCMs. In addition, as seen in Table 20, silanization increased the latent heat of fusion. For example, the latent heat of fusion of 50-PX52+silane was 28.2 kJ/kg, while that of 50-PX52 was only 18.7 kJ/kg. Figure 66 shows the DSC cooling curves of the SSPCMs. It is seen that silanization did not have clear effect on the crystallization temperatures of the SSPCMs. On the other hand, silanization increased the latent heat of crystallization.
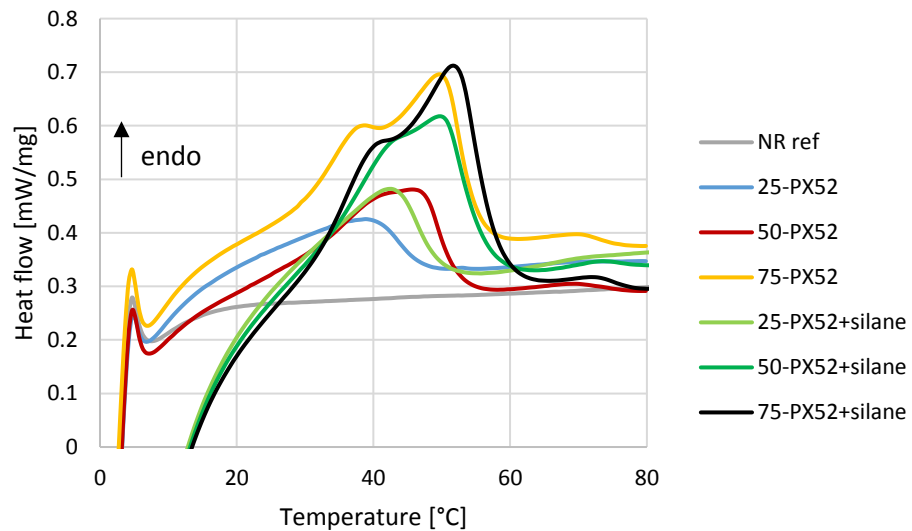

Figure 65. *The effect of silane on the DSC heating curves of NR-based SSPCMs with PX52 as the PCM.*
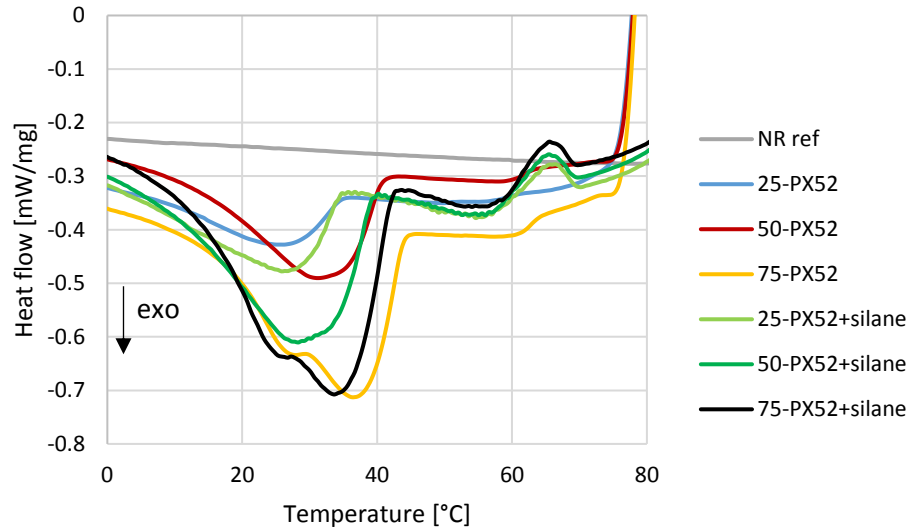
Figure 66. *The effect of silane on the DSC cooling curves of NR-based SSPCMs with PX52 as the PCM.*

Figure 67 shows the effect of the mixing temperature and the polymeric shell material to the DSC curves of the SSPCMs with paraffin as the PCM. It is seen that the mixing temperature did not have notable effect on the latent heat. On the other hand, the SSPCMs with microencapsulated paraffin had slightly higher latent heats than the SSPCM with uncapsulated paraffin. A possible reason for this is that the microencapsulated paraffin dispersed more homogeneously within the matrix. Interestingly, the SSPCMs with microencapsulated paraffin had two overlapping melting peaks, whereas the SSPCM with uncapsulated paraffin had a single, sharper peak. Figure 68 shows the DSC cooling curves of the SSPCMs. The SSPCMs with microencapsulated paraffin had slightly higher latent heats of crystallization than the SSPCM with uncapsulated paraffin.
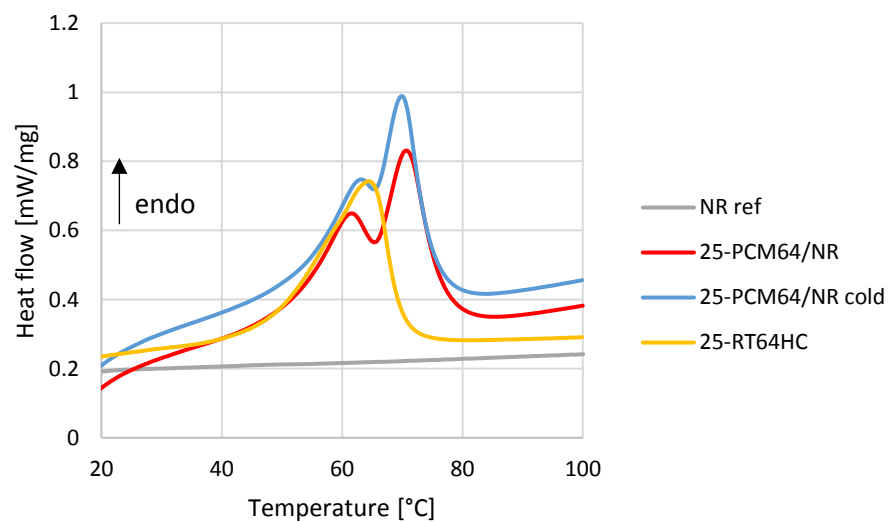

Figure 67. *The effect of shattered microcapsule shell material on the DSC heating curves of the NR-based SSPCMs with paraffin as the PCM.*
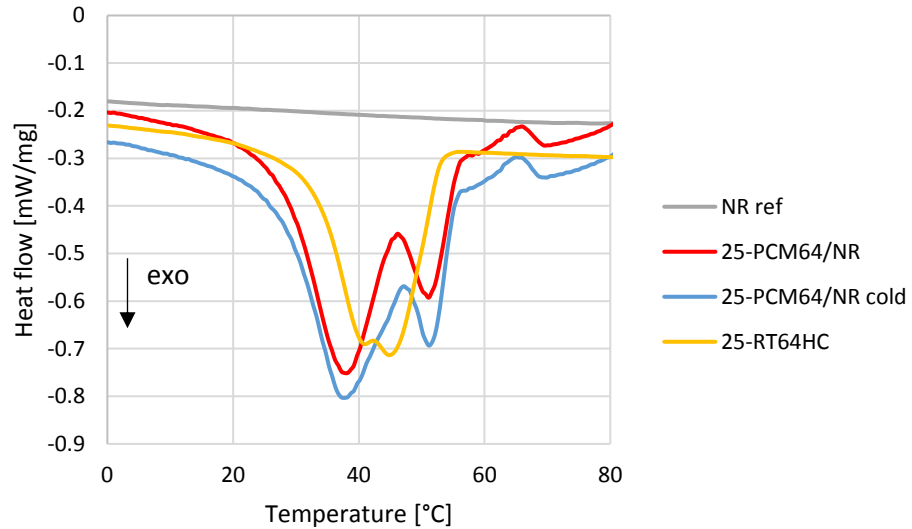
Figure 68. *The effect of shattered microcapsule shell material on the DSC cooling curves of the NR-based SSPCMs with paraffin as the PCM.*

To summarize, the latent heats of the SSPCMs are shown in Figure 69. The latent heat of crystallization, which is exothermic, is presented as a positive value to make the results easier to compare.
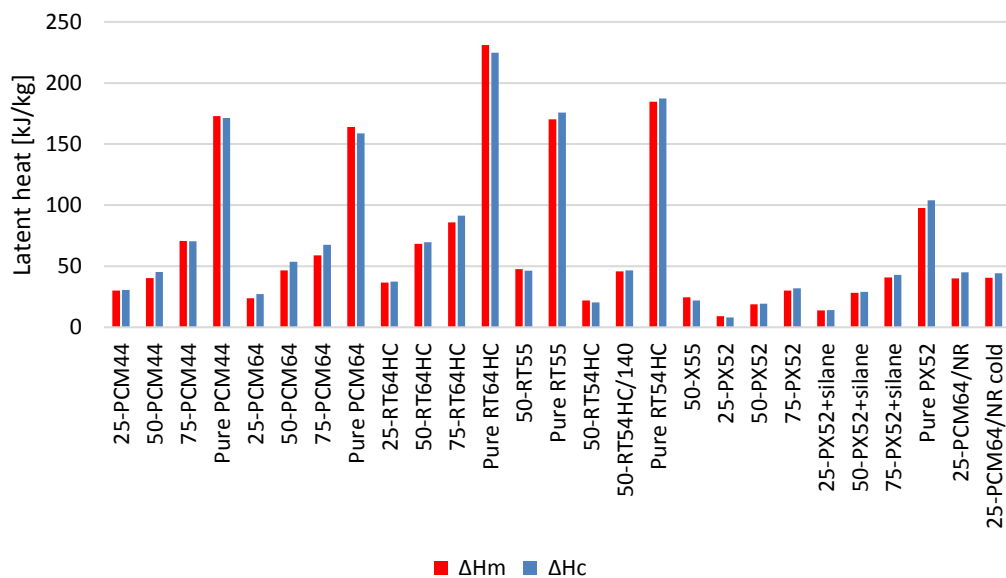

Figure 69. *The latent heat of the SSPCMs and corresponding pure PCMs.*

7.3.2 Thermal buffering capacity

The thermal buffering capacity of several SSPCMs were studied by heating them on a surface with a temperature near their phase change temperature, and recording the changes in temperature with thermal camera. Figure 70 shows thermal camera images of

the SSPCMs with RT64HC as the PCM. The samples were placed from room temperature to the heated surface at 65 °C. It is seen that the reference (pure NR) warmed up fast, and reached an average temperature of 61.9 °C after 2 minutes. By contrast, after the same time the temperatures of the SSPCMs were between 51.8 and 53.5 °C. Thus, the SSPCMs offer far better thermal buffering capacity than pure NR. However, the interpretation of the images was complicated, because the edges of the SSPCM samples curled up, and did not touch the surface after the very beginning. The SSPCM samples did not heat up significantly at the edges during the test duration of 9 minutes, which probably resulted from the curling of the samples. This was verified by the fact that there were no notable differences in the heating of the SSPCMs with different PCM contents.
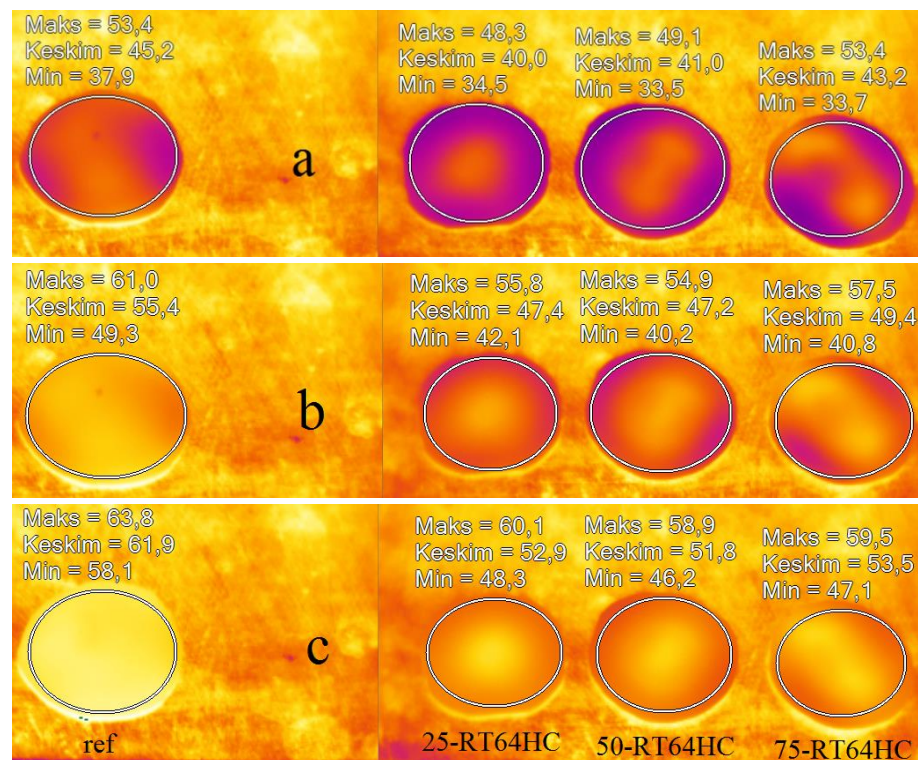

Figure 70. *The thermal camera images of SSPCMs with RT64HC as the PCM after heating at a surface at 65 °C for (a) 30 s, (b) 1 min (c) 2 min.*

It is seen in Figure 71 that the SSPCMs with PX52 as the PCM act somewhat similarly to the SSPCMs with RT64HC as the PCM. The samples were placed from room temperature to a heated surface at 55 °C. Figure 71 shows that the samples warmed up quickly at the center, but curling delayed the heating at the edges of the samples. Moreover, since the thermal conductivity of the SSPCMs is low (more about that in the next subchapter), the heat transfer from the center to the edges was slow, which further delayed the heating of the edges. Thus, it is hard to assess the relative impacts of latent heat storage and curling to the slower heating of the SSPCMs compared to the reference. Moreover, it was found that silane did not have notable effect on the thermal buffering behavior of the SSPCMs.
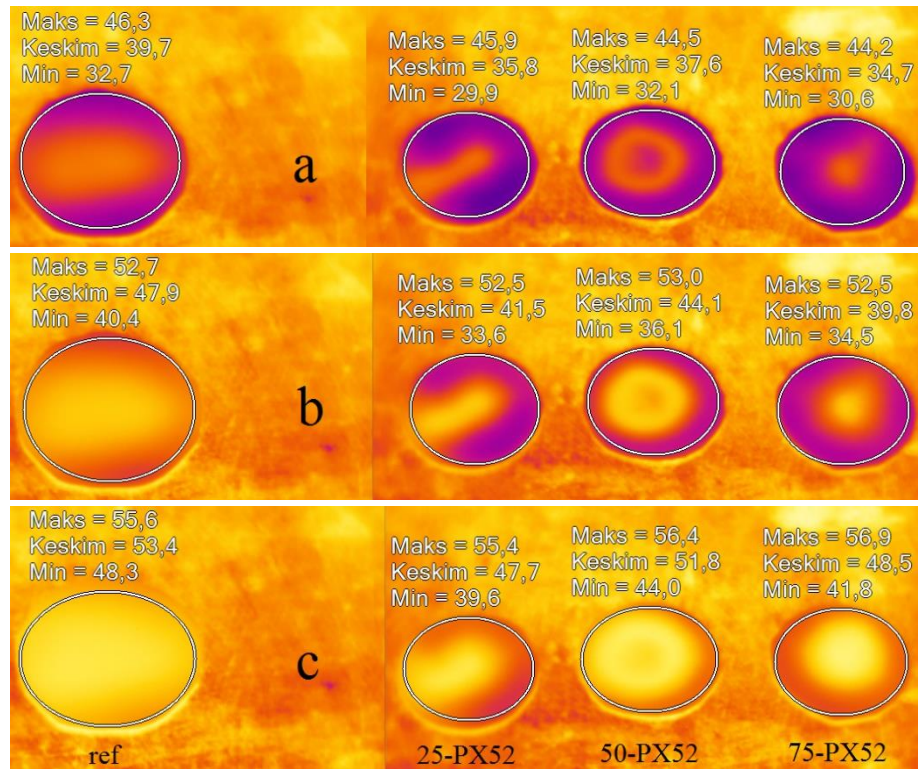
Figure 71. *The thermal camera images of SSPCMs with PX52 as the PCM after heating at a surface at 55 °C for (a) 30 s, (b) 1 min (c) 2 min.*

7.3.3 Thermal conductivity

Figure 72 shows the thermal conductivity of various prepared SSPCMs. The most important phenomenon to notice in the figure is that the thermal conductivity of the SSPCMs was higher below the melting temperature of the PCM than above it. This results from the fact that the thermal conductivity of the PCMs is higher at their solid phase than at their liquid phase.
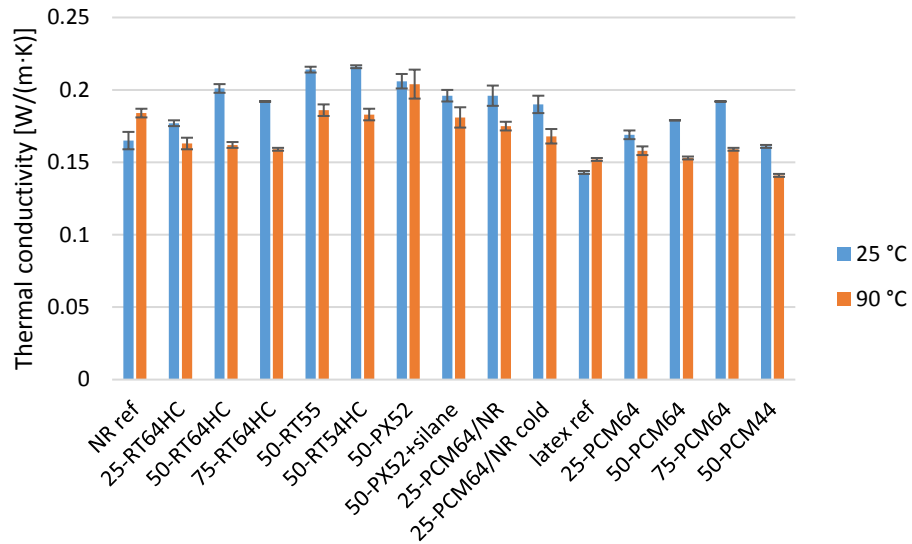
Figure 72. *Thermal conductivity of various prepared SSPCMs.*

To compare the thermal conductivities of the SSPCMs more accurately, the changes in thermal conductivity with respect to the reference were calculated. Figure 73 shows that in the case of the SSPCMs with NR matrix, the thermal conductivity of the SSPCMs at 25 °C was higher than that of pure NR. On the other hand, at 90 °C, when all the PCMs were entirely molten, the thermal conductivity of the SSPCMs was usually lower than that of pure NR. The only exceptions to this are 50-RT55 and 50-PX52, whose thermal conductivity was higher than that of pure NR at both temperatures.
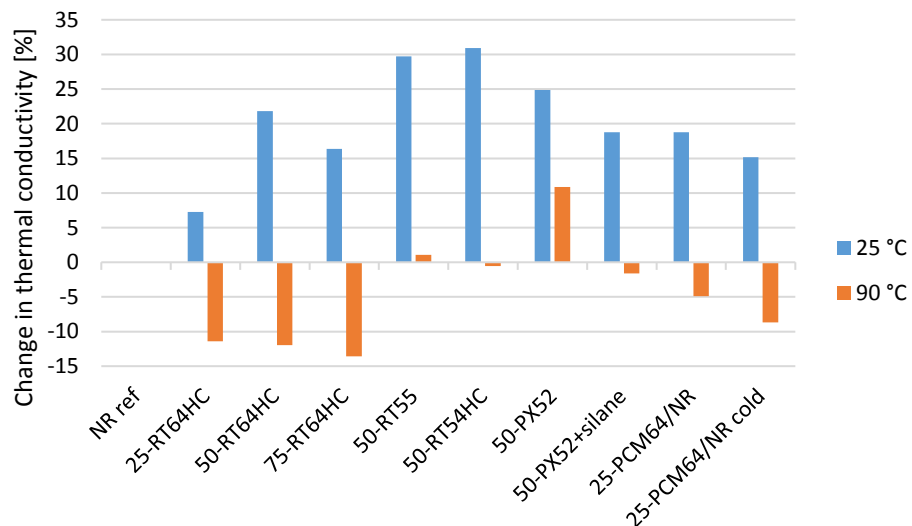

Figure 73. *The change in thermal conductivity of the NR-based SSPCMs compared to the reference.*

Figure 74 shows that the latex-based SSPCMs, with microencapsulated paraffin PCM64, had higher thermal conductivity than the reference at both temperatures. As the paraffin is the same as in RT64HC, the reason for this must be in the microencapsulation. Also,

as seen in Figure 73, the thermal conductivity enhancing effect of PCM64 at 90 °C did not occur in the NR-based SSPCMs (25-PCM64/NR and 25-PCM64/NR cold), probably because the microcapsules were broken during the mixing of these materials.
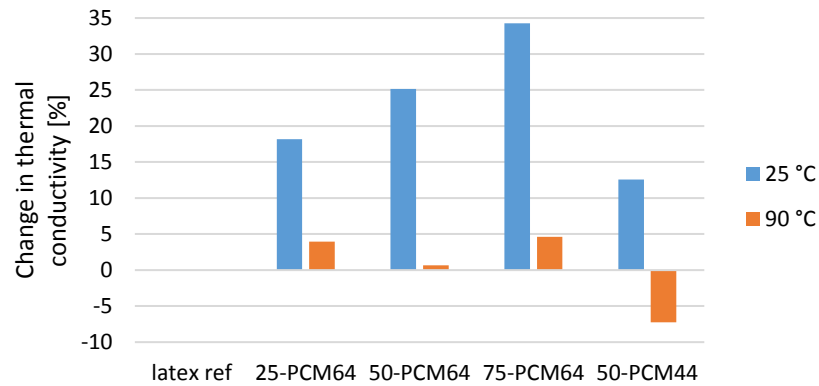

Figure 74. The change in thermal conductivity of the latex-based SSPCMs compared to the reference.

7.4 Mechanical properties

The mechanical properties of the SSPCMs are discussed in the following subchapters through the results of the hardness tests, tensile tests and DMA.

7.4.1 Hardness

In order to create a general view, hardness of all the samples is presented in Figure 75. To distinguish the variables that affect the hardness of the SSPCMs, hardness of the SSPCMs is also discussed through different comparisons.
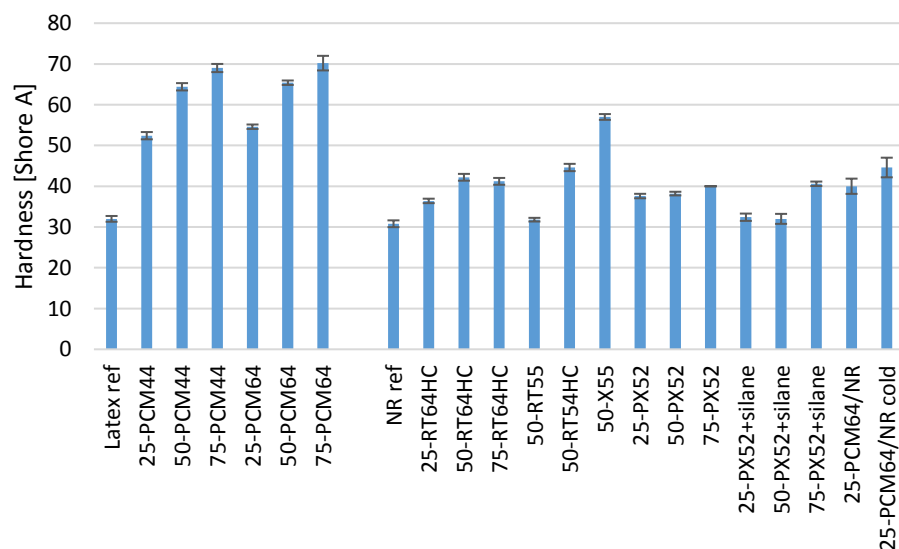

Figure 75. The hardness of the SSPCMs.

The hardness of the SSPCMs with latex matrix is shown in Figure 76. It is seen that the hardness of the SSPCMs with latex matrix increased with increasing PCM microcapsule content. This is actually logical considering the soft and elastic nature of rubber. Moreover, the hardness of the SSPCMs with the same amount of the different PCMs is nearly the same, which is also reasonable since the shell of the PCM microcapsules is of the same material. Since the polymeric shell of the microcapsules is harder than pure paraffin, the microcapsules increase the hardness more than the same amount of uncapsulated paraffin (see Figures 75 and 77).
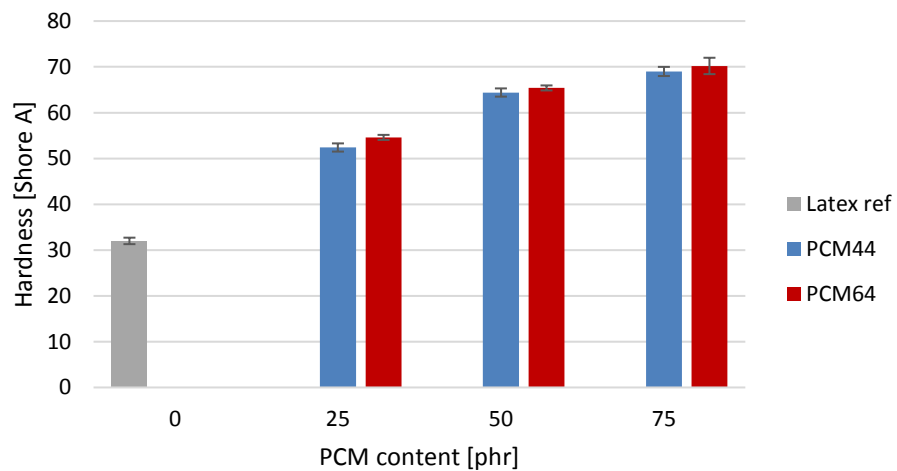

Figure 76. *The effect of the PCM microcapsule content on the hardness of the latex-based SSPCMs.*

The hardness of the NR-based SSPCMs with RT64HC as the PCM is shown in Figure 77. It is seen that the hardness of the SSPCMs increases nearly linearly until PCM content of 50%. On the other hand, the hardness of the 75-RT64HC is surprisingly lower than that of the 50-RT64HC. A probable reason for this is that because the paraffin in 75-RT64HC appeared as large lumps and was not as evenly distributed as in 25-RT64HC and 50-RT64HC, it did not increase the hardness of the NR as significantly.
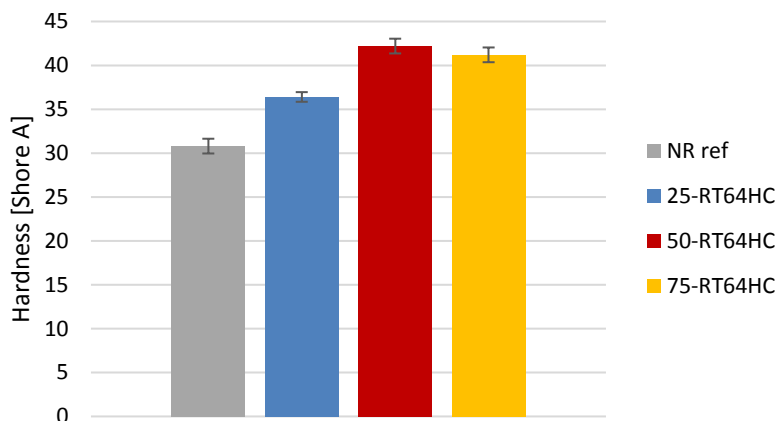
Figure 77. *The effect of the PCM content on the hardness of the NR-based SSPCMs with RT64HC as the PCM.*

Figure 78 shows the comparison of the SSPCMs with PCMs of different classes. The PCM content of all the SSPCMs discussed here was 50 phr. It is seen that paraffin (50-RT55) did not considerably increase the hardness of NR. The hardness of the SSPCM with solid-solid PCM (50-X55) was the highest, while the hardness of the fatty acid - based 50-RT54HC was between the two. In addition, it was notable that the hardness of 50-RT55 was much lower than that of 50-RT64, even though both the SSPCMs have paraffin as PCM. This might have resulted from RT55 being a soft paraffin wax and RT64 a hard paraffin wax, similarly to the LDPE/paraffin and PP/paraffin SSPCMs studied by Krupa et al. [41,42] (see chapters 3.3.2 and 3.3.3).
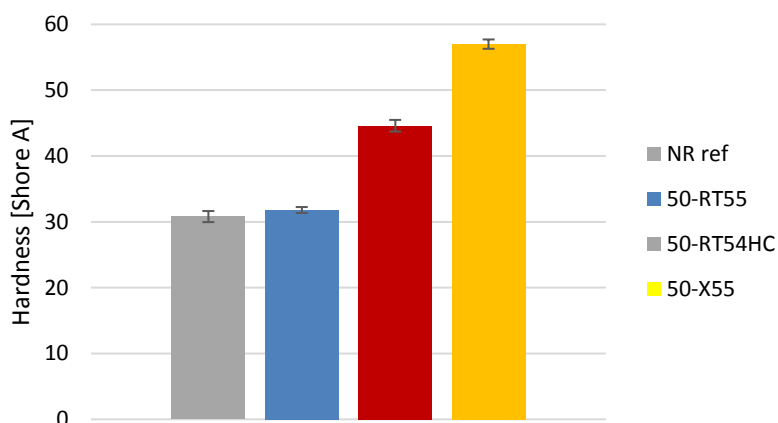
Figure 78. *Comparison of the hardness of the NR-based SSPCMs with the same content of different PCMs.*

The effect of silane to the hardness of the SSPCMs with PX-52 as the PCM is shown in Figure 79. It is seen that with the PCM contents of 25 and 50 phr, the hardness of the PX52-SSPCMs was higher than that of the PX52+silane -SSPCMs. The most probable reason for this is that the silanization required slightly longer mixing time during the preparation, which may have resulted in excessive plasticization of the NR. With the PCM

content of 75 phr, the effect of the silica particles on hardness presumably overcame the plasticization of the NR, which explains the nearly equal hardness of 75-PX52 and 75-PX52+silane.
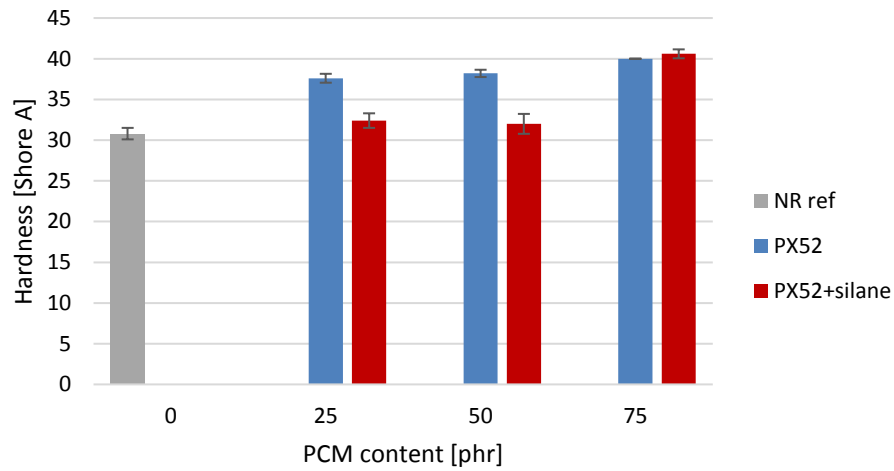
***Figure 79.** The effect of the addition of silane on the hardness of the NR-based SSPCMs with PX52 as the PCM.*

Figure 80 compares the effect of the mixing temperature and the polymeric shell material to the hardness of the SSPCMs with paraffin as the PCM. As seen in Figure 56, the PCM microcapsules did not withstand the shear stresses during the mixing but shattered into pieces. However, the shell material still increased the hardness slightly compared to the SSPCM with uncapsulated paraffin. In addition, cold mixing increased the hardness of the SSPCM as the plasticization of the rubber reduced.

***Figure 80.** The effect of shattered microcapsule shell material on the hardness of the NR-based SSPCMs with paraffin as the PCM.*

7.4.2 Tensile properties

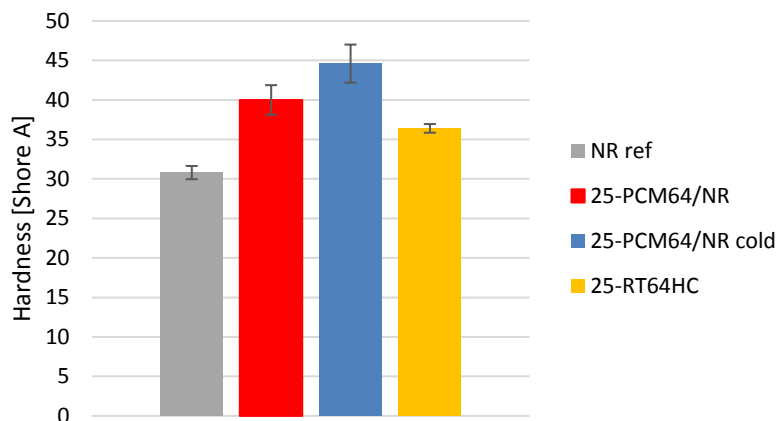The mean stress-strain curves of the latex-based SSPCMs are shown in Figure 81. It is seen that the curves of SSPCMs with the same amount of different PCMs are very close to each other. This was expected as the shell materials of the microcapsules are the same, and the microstructures of the SSPCMs were similar. Moreover, the tensile strength and elongation at break reduced with increasing microcapsule content. Figure 82 shows more clearly the changes in tensile strength with different PCM contents. It is again seen that the tensile strength of the SSPCMs decreased with increasing PCM content, because the adhesion between the PCM capsules and the matrix was not adequately strong. The surprisingly low tensile strength of the reference probably resulted from the porosity in the reference samples, even though the porosity was attempted to reduce by diluting the latex before the vacuum treatment.
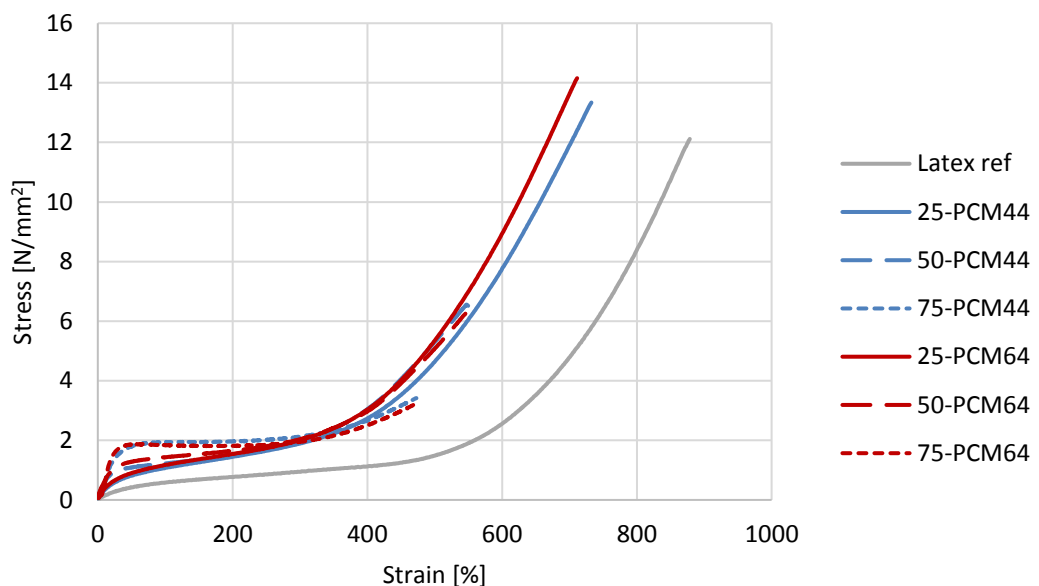

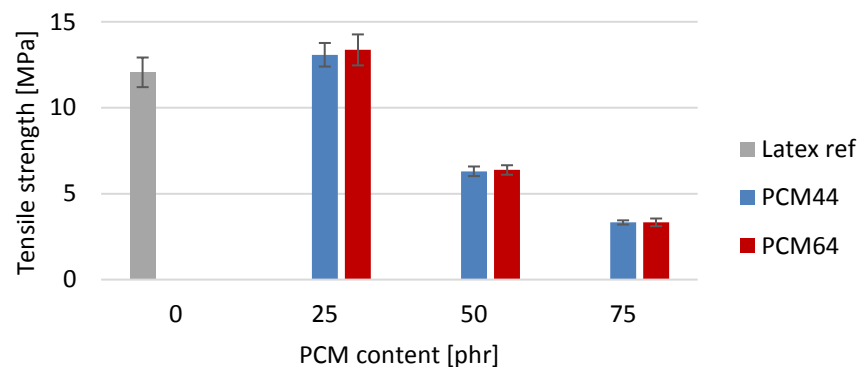*Figure 81. Stress-strain curves of the SSPCMs with latex matrix.*

Figure 82. The effect of PCM microcapsule content on the tensile strength of the SSPCMs with latex matrix.

Figure 83 shows the mean stress-strain curves of the NR-based SSPCMs with RT64HC as the PCM, and Figure 84 shows the effect of the PCM content on the tensile strength and the elongation a break of these SSPCMs. It is seen in Figures 83 and 84 that the tensile properties of the NR/RT64HC SSPCMs generally deteriorate when the PCM content is increased. More specifically, the tensile strength and elongation at break of 75-RT64HC were significantly worse than those of the other materials, which was expected considering that the paraffin appeared as large lumps and was not as evenly distributed within the matrix as in 25-RT64HC and 50-RT64HC. The tensile properties of 50-RT64 HC were relatively close to those of 25-RT64HC. It should be noted that the reference sample did not break during the test, because the measurement range of the tensile testing machine was inadequate. In addition, it is seen in Figure 84 that the standard deviations of the tensile strength of the SSPCMs were larger than those of the corresponding SSPCMs with microencapsulated paraffin as the PCM (see Figure 82). Thus, the dispersion of the paraffin within the matrix was presumably not as homogeneous.
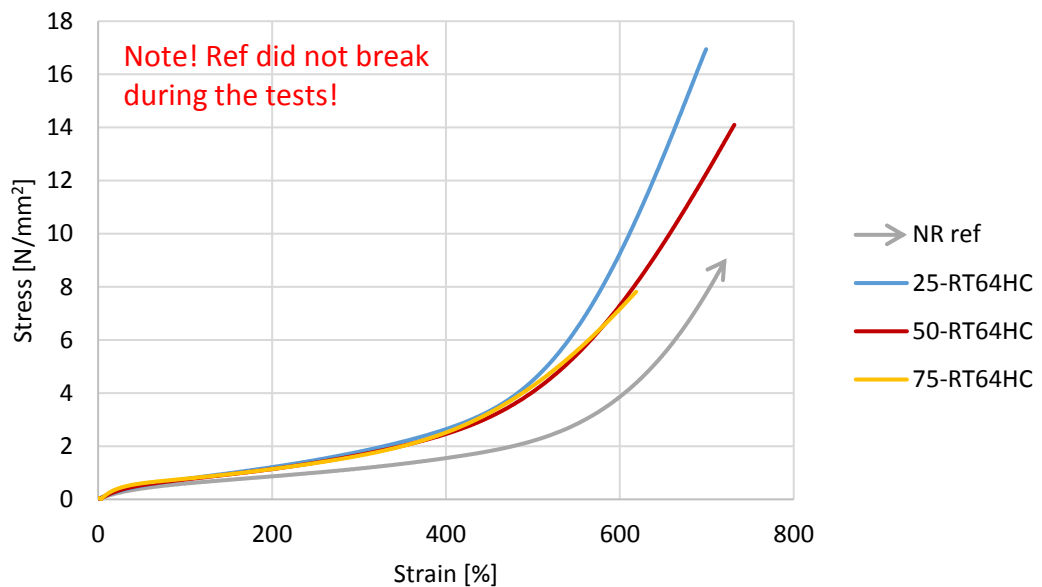

Figure 83. Stress-strain curves of the NR-based SSPCMs with RT64HC as the PCM.
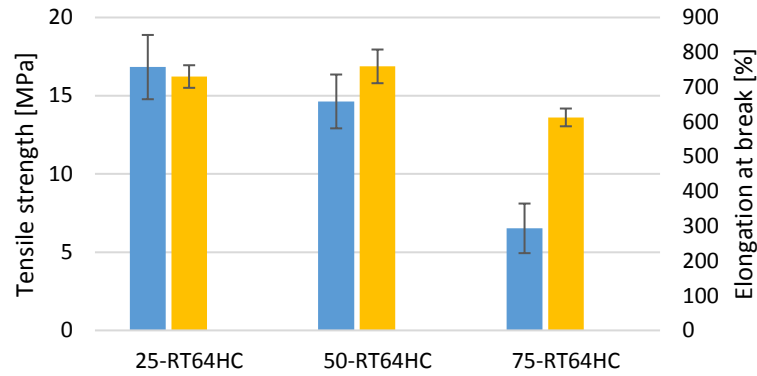
Figure 84. The effect of the PCM content on the tensile strength (blue) and elongation at break (yellow) of the NR-based SSPCMs with RT64HC as the PCM.

The tensile properties of NR-based SSPCMs with the same amount of different PCMs are compared in Figure 85. It is seen that the SSPCM with paraffin as PCM (50-RT55) possessed the best combination of tensile strength and elongation at break. In fact, 50-RT55 acted even more elastically in the tensile test than pure NR. It should be noted that the reference and 50-RT55 did not break during the test due to insufficient measurement range of the tensile testing machine. On the other hand, the tensile strength of the SSPCMs with fatty acid (50-RT54HC) and NPG-based solid-solid PCM (50-X55) were low. This was probably partly due to inhomogeneity of 50-X55 and porosity of 50-RT54HC.

Because the reference and 50-RT55 -samples did not break during the tests, the mechanical properties were compared in more detail by studying the stress required to strain the samples by 100% and by 300%. Figure 85 shows that 50-RT54HC and 50-X55 were stiffer than pure NR, while 50-RT55 was less stiff. These results match well with the results of the hardness tests (Figure 78). It seems that RT55 plasticized the NR matrix, while RT54HC and X55 made it stiffer. It should be noted that the standard deviation of the results of 50-X55 is relatively large, because the dispersion of X55 was not homogenous.
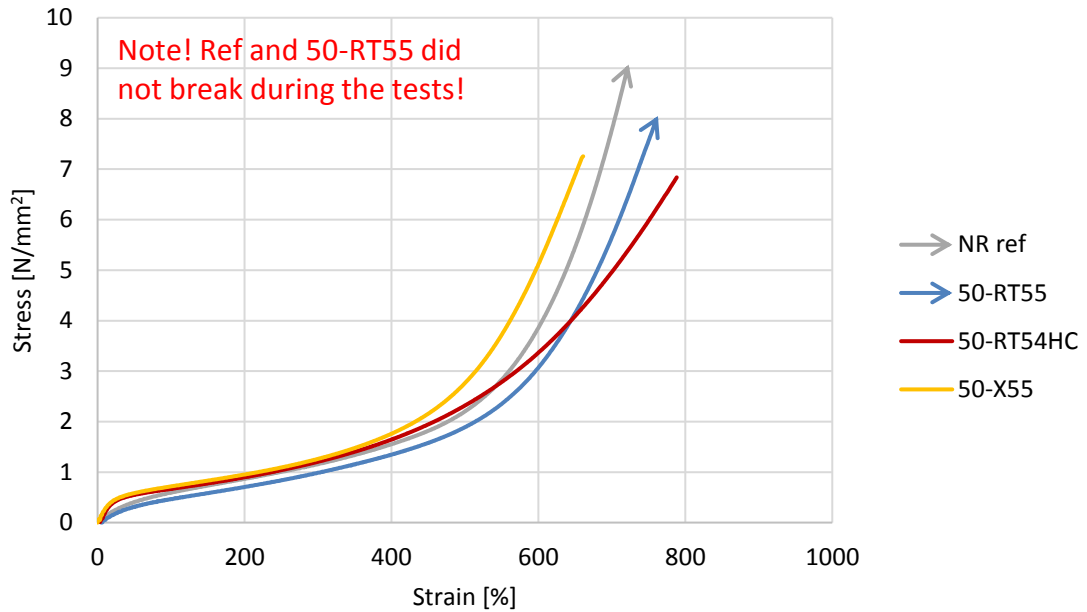
Figure 85. Stress-strain curves of the NR-based SSPCMs with the same amount of different PCMs.
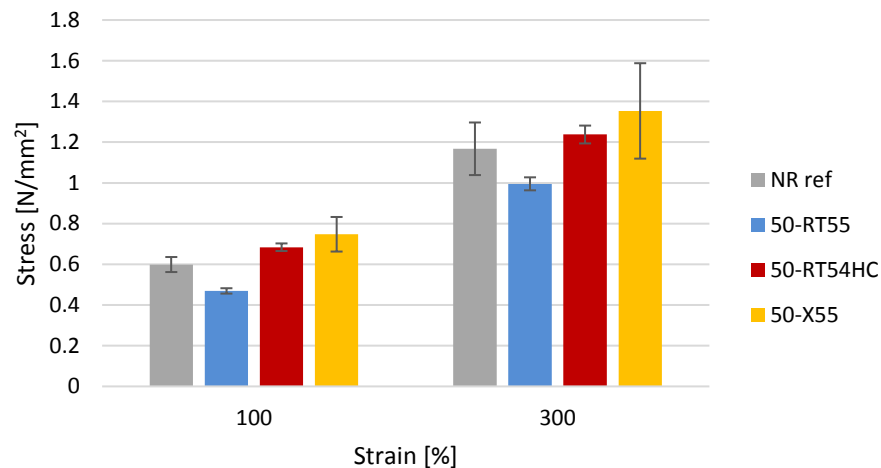
Figure 86. The stiffness of NR-based SSPCMs with the same amount of different PCMs.

The effect of silane on the tensile properties of the SSPCMs with PX52 as the PCM is shown in Figure 87. It is seen that all the SSPCMs were stiffer than pure NR. SSPCMs with and without silane had similar tensile curves with PCM contents of 25 and 75 phr. However, with PCM content of 50 phr the SSPCM without silane seemed to be much stiffer than the SSPCM with silane. The same is seen in Figure 88, which compares the stresses required to strain the SSPCMs. With PCM content of 25 phr, the stresses were close to each other with both the strains, indicating that the stiffness of the SSPCMs with and without silane were nearly equal. With PCM content of 50 phr, the SSPCM without silane was notably stiffer than the SSPCM with silane. With PCM content of 75 phr, the SSPCM with silane was stiffer than the SSPCM without silane, especially with the higher

strain of 300%. The most probable reasons for these contradictory results are the inhomogeneity of the samples (especially 50-PX52, see Figure 55c) and the longer mixing time of the SSPCMs including silane, which may have led to the plasticization and lower stiffness of 25-PX52+silane and 50-PX52+silane.
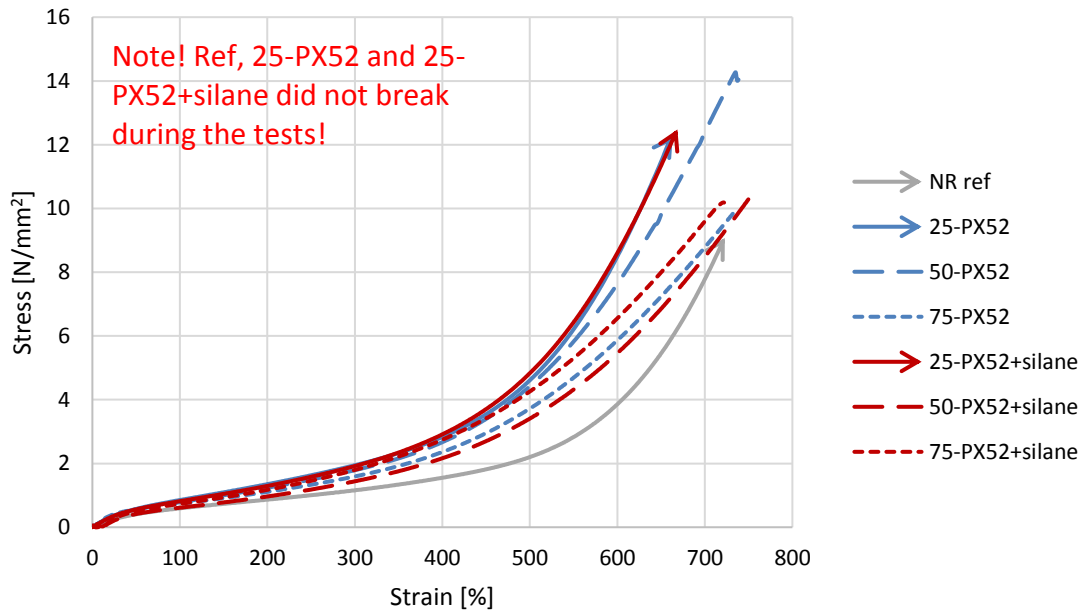
Figure 87. Stress-strain curves of the NR-based SSPCMs with PX52 as the PCM.
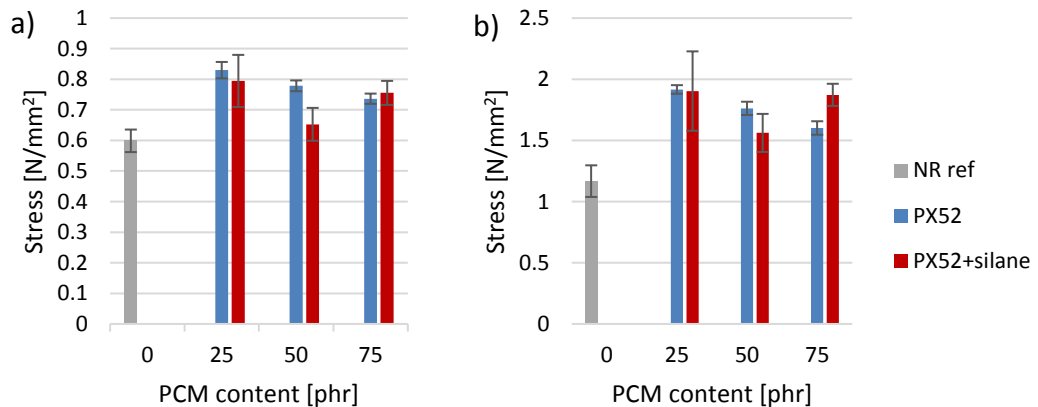
Figure 88. The effect of silane on the stiffness of NR-based SSPCMs with PX52 as the PCM. The samples were strained by (a) 100% and (b) 300%.

The effect of the mixing temperature and the polymeric shell material to the tensile properties of the SSPCMs with paraffin as the PCM is compared in Figure 89. It is seen that the curves of 25-RT64HC and 25-PCM64/NR, in which the only difference was the shattered shell material on 25-PCM64/NR, were quite similar. However, as 25-PCM64/NR did not break during the test, its tensile strength was higher. 25-PCM64/NR

cold was stiffer than these two materials, probably because NR did not plasticize as much during the mixing because the mixing temperature was lower. Figure 90 compares the stresses required to strain the SSPCMs. The same observations are made than in the tensile curves. Of these SSPCMs, 25-PCM64/NR cold was the stiffest, because cold mixing prevented excessive plasticization and the shattered polymer shells reinforced the material. Also 25-PCM64/NR was stiffer than 25-RT64HC, because of the reinforcing effect of shattered polymer shells, which were finely and homogeneously dispersed in the rubber (see Figure 56a).

Figure 89. The effect of shattered microcapsule shell material on the stress-strain curve of the NR-based SSPCMs with paraffin as the PCM.

Figure 90. The effect of shattered microcapsule shell material on the stiffness of the NR-based SSPCMs with paraffin as the PCM.

7.4.3 Dynamical mechanical properties

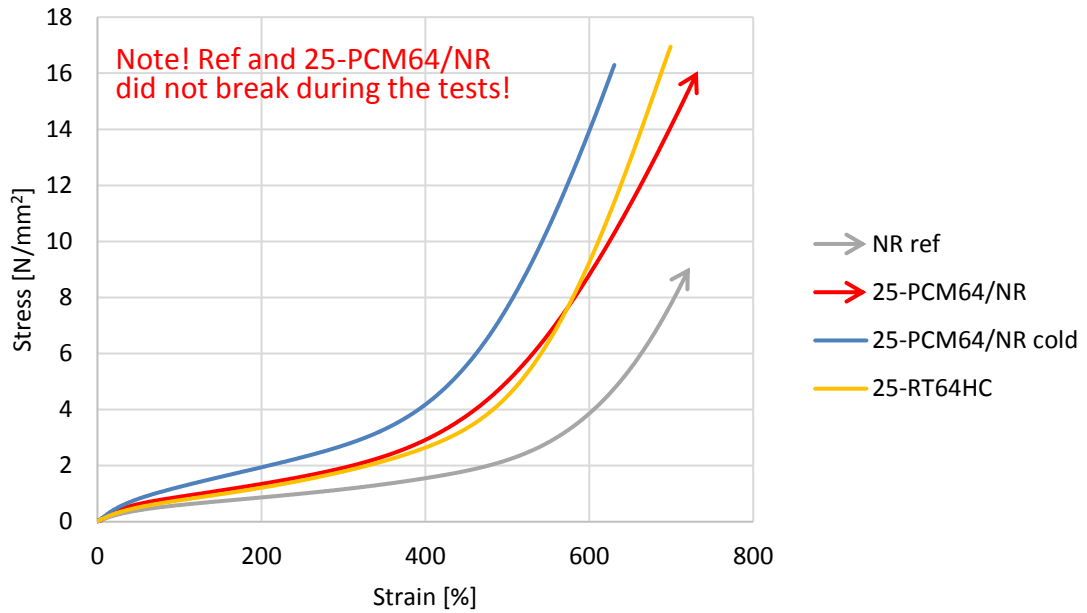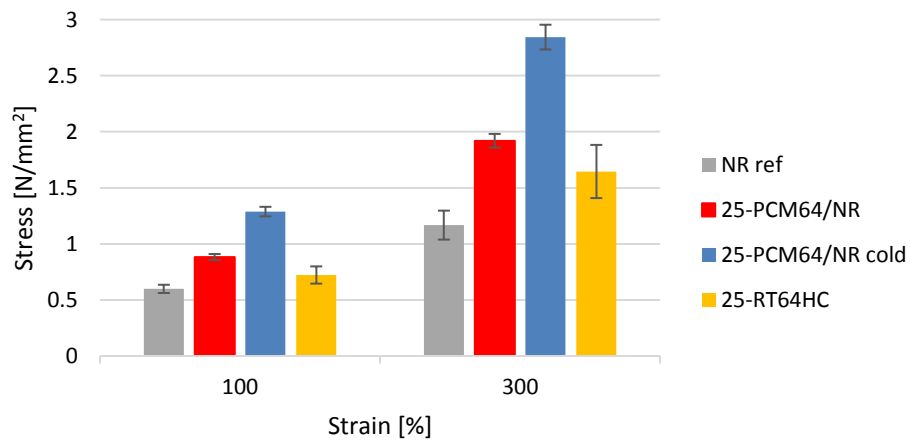The effect of the PCM microcapsule content on the storage modulus and tan δ of latex-based SSPCMs is shown in Figure 91. It is seen in Figure 91a that the addition of PCM microcapsules did not change the glass transition temperature of NR (steep decrease in the storage modulus curve). On the other hand, it increased the modulus of the rubbery plateau, which is the region between the recrystallization temperature and the melting of the PCM slightly above 50 °C. Thus, the increase in PCM content may be considered to increase the stiffness of NR at this temperature region, which is consistent with the tensile test results at low strains (see Figure 81). When the PCM started to melt, the storage modulus of the SSPCMs decreased. The decrease was more rapid when the PCM content was increased. However, because the microcapsules did not melt, but only the PCM inside them, the microcapsules still increased the modulus of NR after the melting of the PCM. It can hence be said that the PCM microcapsules increased the stiffness of the latex at the usage temperatures of the SSPCMs. It is seen in Figure 91b that the increase in the PCM content resulted in decrease in the height of tan δ peak at the recrystallization temperature of NR. By contrast, at temperatures above 0 °C, tan δ increased with increasing PCM content, indicating an increase in the damping capacity of the SSPCMs. Above the melting temperature of the PCM, tan δ of all the SSPCMs decreased and approached that of pure NR.
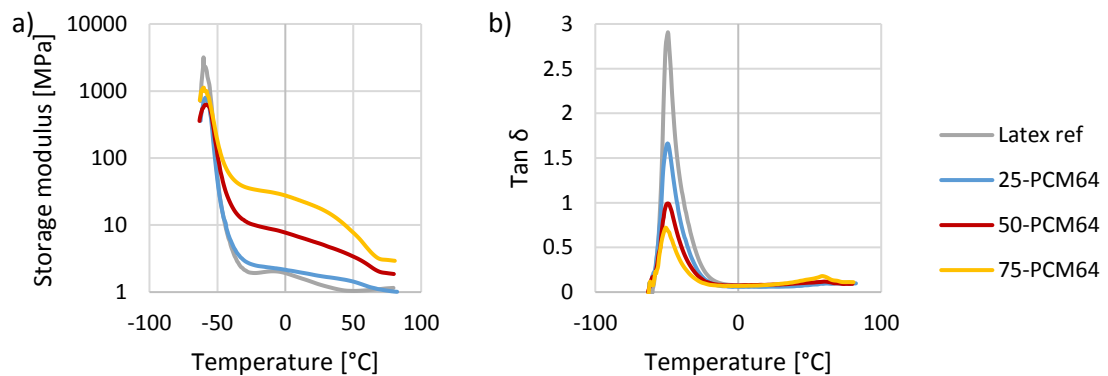
Figure 91. *The effect of PCM microcapsule content on (a) storage modulus and (b) tan δ of latex-based SSPCMs.*

Figure 92 shows the effect of the PCM content on the storage modulus and tan δ of NR-based SSPCMs with RT64HC as the PCM. It is seen in Figure 92a that the increase in PCM content increased the storage modulus of the rubbery plateau, even though the increment was not as significant as in the case of PCM microcapsules in the latex-based SSPCMs. In addition, the decrease in the storage modulus at the melting temperature of the PCM was steeper. With PCM contents of 50 and 75 phr the storage modulus at temperatures higher than the melting point of the PCM was lower than that of the

reference. Figure 92b shows that the height of the tan δ peak decreased with increasing PCM content, even though the decline was less significant than in the case of the latex-based SSPCMs. Furthermore, at temperatures above 0 °C, tan δ increased with increasing PCM content.
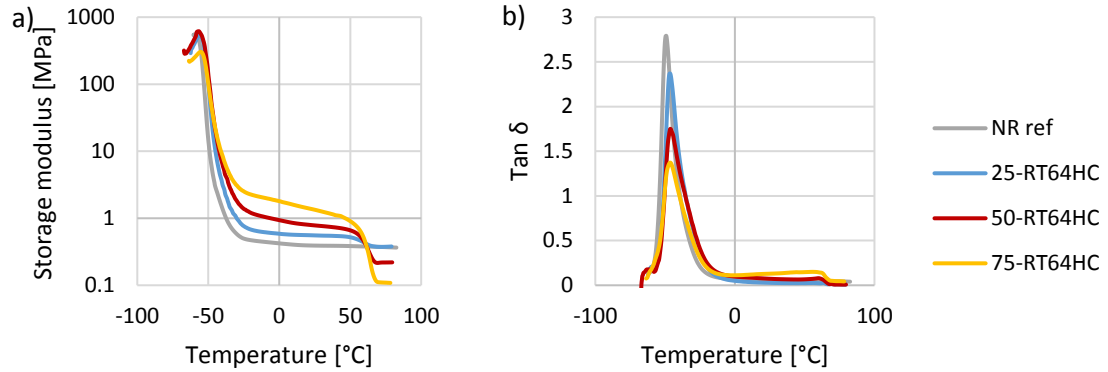
Figure 92. *The effect of PCM content on (a) storage modulus and (b) tan δ of latex-based SSPCMs with RT64HC as the PCM.*

Figure 93 shows the comparison of dynamical mechanical properties of SSPCMs with paraffin (50-RT55) and fatty acid (50-RT54HC as the PCM). It is seen that the storage modulus curves of these two SSPCMs differed significantly, as the modulus of the rubbery plateau of 50-RT54HC was much higher than that of 50-RT55. This result is analogous to the tensile test results (see Figure 85). The tan δ peak of 50-RT54HC was lower than that of 50-RT55. In addition, at temperatures above 0 °C, tan δ of 50-RT54HC was higher than that of 50-RT55.
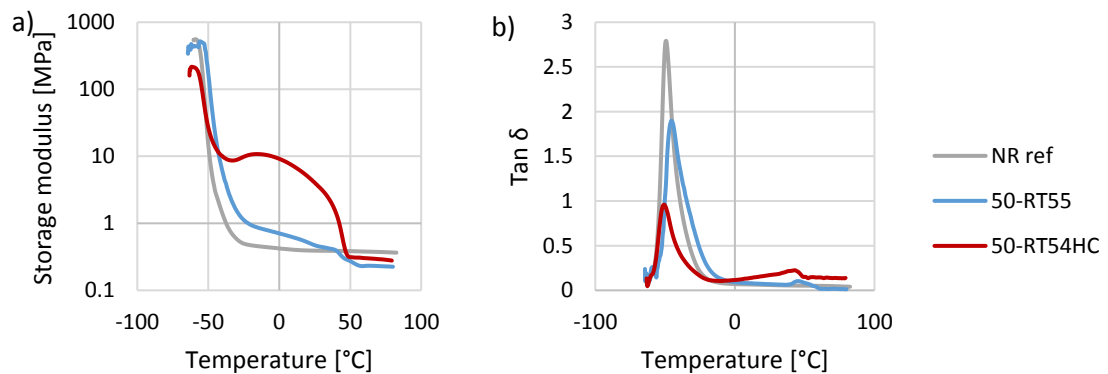
Figure 93. *Comparison of (a) storage modulus and (b) tan δ of 50-RT55 and 50-RT54HC.*

The effect of the addition of silane on dynamical mechanical properties on SSPCMs with PX52 as the PCM is shown in Figure 94. It is seen that silane did not have notable effect on storage modulus or tan δ curves of the SSPCMs.
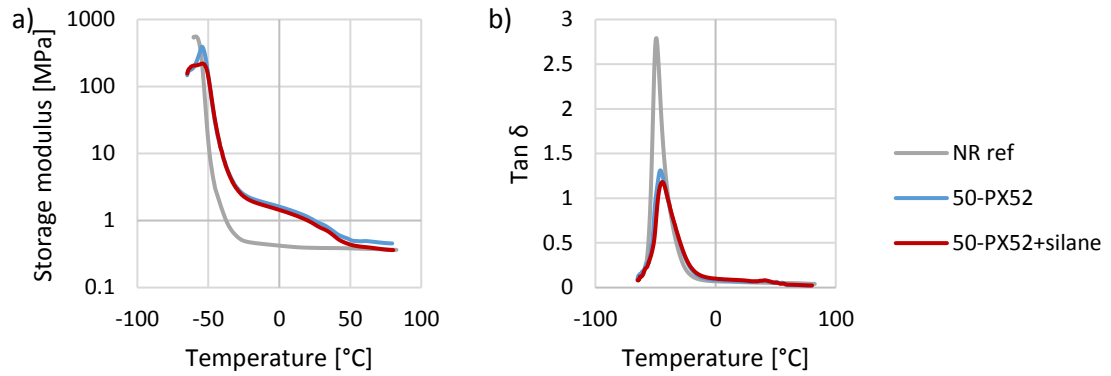
Figure 94. *The effect of silane on (a) storage modulus and (b) tan δ of NR-based SSPCMs with PX52 as the PCM.*

Figure 95 shows the effect of shattered microcapsule shell material and the mixing temperature on dynamical mechanical properties of the SSPCMs with paraffin as the PCM. It is seen that the shattered shell material increases the storage modulus of the rubbery plateau, which is consistent with the tensile test results (see Figure 89). On the other hand, either the shell material or the mixing temperature did not have notable effect on the tan δ curves of the SSPCMs.

Figure 95. *The effect of shattered microcapsule shell material and mixing temperature on (a) storage modulus and (b) tan δ of NR-based SSPCMs with paraffin as the PCM.*

7.5 Summary

As a summary of the results presented in this chapter, Table 21 shows the quantitative results of all the samples.

Table 21. The summary table of the results. Marking ↑ indicates that the measurement range of the tensile test machine was insufficient, and the samples did not break.

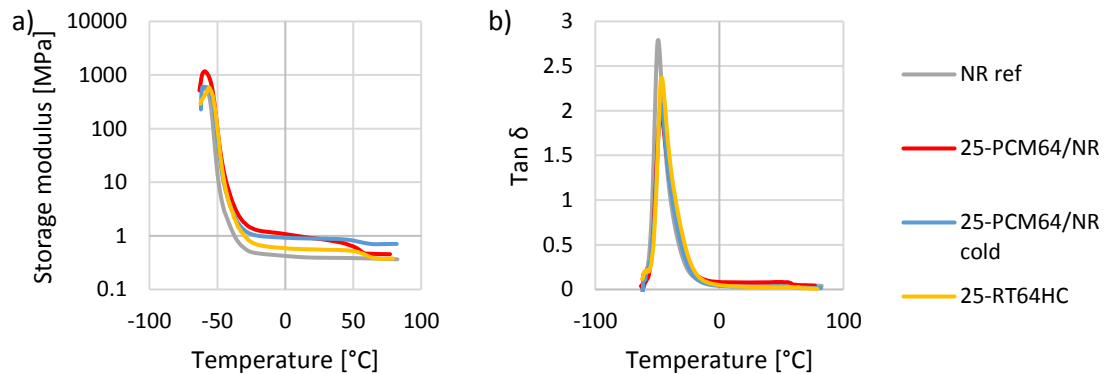| Sample	T_m (°C)	ΔH_m (kJ/kg)	T_c (°C)	ΔH_c (kJ/kg)	Thermal conductivity (25 °C) [W/(m·K)]	Thermal conductivity (90 °C) [W/(m·K)]	Hardness (Shore A)	Tensile strength (MPa)	Elongation at break (%)
Latex ref					0.143 ± 0.001	0.152 ± 0.001	32.0 ± 0.8	12.1 ± 0.9	883 ± 29
25-PCM44	49.1	30.1	34.3	-30.5	0.161 ± 0.001	0.141 ± 0.001	52.4 ± 0.9	13.1 ± 0.7	726 ± 11
50-PCM44	49.4	46.3	33.9	-45.2			64.4 ± 0.9	6.3 ± 0.3	542 ± 19
75-PCM44	52.4	70.8	31.1	-70.4			69.0 ± 1.0	3.3 ± 0.2	456 ± 20
Pure PCM44	53.2	172.8	30.2	-171.2					
25-PCM64	70.1	23.7	44.2	-27.1	0.169 ± 0.003	0.158 ± 0.003	54.6 ± 0.6	13.4 ± 1.0	696 ± 17
50-PCM64	70.1	46.7	43.8	-53.7	0.179 ± 0.000	0.153 ± 0.001	65.4 ± 0.6	6.4 ± 0.3	549 ± 17
75-PCM64	72.3	58.9	43.7	-67.6	0.192 ± 0.000	0.159 ± 0.001	70.2 ± 1.8	3.3 ± 0.3	491 ± 13
Pure PCM64	73.0	163.9	36.1	-158.8					
NR ref					0.165 ± 0.006	0.184 ± 0.003	30.8 ± 0.9	↑	↑
25-RT64HC	64.4	36.6	44.8	-37.4	0.177 ± 0.002	0.163 ± 0.004	36.4 ± 0.6	16.8 ± 2.1	730 ± 33
50-RT64HC	65.3	68.2	48.4	-69.6	0.201 ± 0.003	0.162 ± 0.002	38.0 ± 0.8	14.6 ± 1.8	759 ± 49
75-RT64HC	69.7	85.8	46.9	-91.5	0.192 ± 0.000	0.159 ± 0.001	42.2 ± 0.9	6.5 ± 1.6	613 ± 26
Pure RT64HC	72.0	231.1	47.2	-224.7			41.2 ± 0.9		
50-RT55	55.0	47.5	40.7	-46.3	0.214 ± 0.002	0.186 ± 0.004	31.8 ± 0.5	↑	↑
50-RT54HC	41.4	22.0	23.6	-20.3	0.216 ± 0.001	0.183 ± 0.004	44.6 ± 0.9	6.9 ± 1.8	778 ± 55
50-RT54HC/140	52.0	45.8	29.3	-46.6					
50-X55	68.9	24.6	32.2	-21.9			57.0 ± 0.8	8.1 ± 0.9	663 ± 57
Pure RT55	59.9	170.3	40.5	-175.8					
Pure RT54HC	64.8	184.7	38.2	-187.3					
25-PX52	38.9	9.0	26.2	-8.0	0.206 ± 0.005	0.204 ± 0.010	37.6 ± 0.6	↑	↑
50-PX52	45.9	18.7	31.1	-19.3			38.2 ± 0.5	14.3 ± 0.8	747 ± 24
75-PX52	49.8	30.0	36.6	-32.0			40.0 ± 0.0	9.9 ± 0.4	728 ± 20
25-PX52+silane	42.4	13.9	26.5	-14.1	0.196 ± 0.004	0.181 ± 0.007	32.4 ± 0.9	↑	↑
50-PX52+silane	49.7	28.2	28.6	-29.1			32.0 ± 1.3	9.4 ± 1.4	736 ± 20
75-PX52+silane	51.6	40.7	33.4	-42.8			40.6 ± 0.6	9.8 ± 0.9	700 ± 26
Pure PX52	54.2	97.7	36.1	-103.9					
25-PCM64/NR	70.6	40.0	37.9	-44.9	0.196 ± 0.007	0.175 ± 0.003	40.0 ± 1.9	↑	↑
25-PCM64/NR cold	69.9	40.5	37.9	-44.2	0.190 ± 0.006	0.168 ± 0.005	44.6 ± 2.4	14.9 ± 1.5	619 ± 51

8. CONCLUSION

The goal of this thesis was to prepare SSPCMs with NR and latex matrixes, to study their mechanical and thermal properties and to find the most compatible PCM/matrix combinations as well as the optimal PCM contents of the SSPCMs.

The microencapsulated paraffins with transition temperatures of 44 and 64 °C (PCM44 and PCM64 were the only PCMs mixed with latex matrix, because the water-based microcapsule slurry was easily mixed with the latex. The preparation of the latex-based SSPCMs was easy even at the highest PCM microcapsule content of 75 phr. However, the increase in PCM content resulted in significant reduction in the mechanical properties of the SSPCMs, since the adhesion between the microcapsules and the matrix was inadequate. Consequently, the PCM content of 75 phr was found to be too high to be used in practical applications requiring mechanical strength, even though it would have offered the highest heat storage capacity and thermal conductivity. Generally, the heat storage capacities of the latex-based SSPCMs were lower than those of the corresponding NR-based SSPCMs, because the actual PCM content was lower due to the microencapsulation. Considering both the mechanical properties and heat storage capacity, 50 phr was found to be the best PCM content tried for the latex-based SSPCMs. Unfortunately, the mechanical properties of the latex-based SSPCMs were generally lower than those of the NR-based SSPCMs.

The PCM content had similar effects on the NR-based SSPCMs than on the latex-based SSPCMs. Higher PCM content resulted in deterioration of the mechanical properties, even though the deterioration was not as abrupt as in the case of latex-based SSPCMs. As expected, the increase in PCM content resulted in higher heat storage capacity. The best PCM content was found to be 50 phr, as it offered good mechanical properties, satisfactory heat storage capacity and it was also verified to possess cyclic stability.

Considering the compatibility of different PCM groups with NR matrix, paraffin was found to be the most suitable PCM group. The mechanical properties, especially tensile strength, of the SSPCM with paraffin as the PCM (50-RT55), were superior to those of other PCM groups. 50-RT55 retained well the mechanical properties of NR, as the high tensile strength was combined with high elasticity and low hardness. In addition, the latent heat of 50-RT55 was higher than that of the other SSPCMs. Considering SSPCMs with fatty acid as the PCM (50-RT54HC), the vulcanization temperature of 160 °C was found to be too high, as the fatty acid decomposed and lost its heat storage capacity. Better heat storage capacity was achieved by lowering the vulcanization temperature. Unfortunately, the SSPCM was still very porous. NPG-based solid-solid PCM (X55) was found to be incompatible with NR, since both the mechanical properties and latent heat of 50-X55

were insufficient. The failure to mix salt hydrate (SP58) with NR was unfortunate, since SP58 had the highest latent heat of the pure PCMs.

Silane was added to the SSPCMs with paraffin bound within silica (PX52) as the PCM to enhance the dispersion of PCM and the adhesion between the PCM and the matrix, and to subsequently improve the mechanical properties of the SSPCMs. The addition of silane was found to result in more homogeneous microstructure of the SSPCM. However, the effect of silane on the mechanical properties was contradictory, as the addition of silane improved the mechanical properties of 75-PX52 but deteriorated those of 25-PX52 and especially of 50-PX52. That probably resulted from the longer mixing time of the SSPCMs including silane, which may have caused excessive plasticization of the rubber. PX52 could be added to NR at higher contents, since the mechanical properties of 75-PX52+silane were still satisfactory, indicating good adhesion between the PCM and the matrix. Moreover, silanization seemed to enhance the latent heat of the SSPCMs. However, the latent heats of these SSPCMs were still poor, because silica comprised the majority of PX52. Consequently, the amount of the actual PCM in the SSPCMs was low.

Also microencapsulated paraffin PCM64 was mixed with NR to see if the capsules withstood the mixing and vulcanization processes without breaking. Even though the capsules were broken, the shattered shell material seemed to improve the mechanical properties of the SSPCM. In addition, the SSPCMs with microencapsulated paraffin had higher latent heats than the SSPCM with uncapsulated paraffin, probably because the microencapsulated paraffin dispersed more homogeneously within the matrix.

In conclusion, paraffin was found to be the most compatible PCM group with NR matrix. The optimal paraffin content was found to be 50 phr, because 50-RT64HC possessed the best combination of mechanical strength and latent heat storage capacity. In addition, the thermal properties of the SSPCM with fatty acid (50-RT54HC), vulcanized at 140 °C, seemed promising. However, decomposition of fatty acid during vulcanization resulted in severe porosity, which deteriorated the mechanical properties of the SSPCM. Also microencapsulated paraffin was found to be compatible with NR.

The biggest challenge in the effective utilization of SSPCMs with NR matrix is their low thermal conductivity, which reduces the efficiency of the SSPCMs. Previous studies show that the thermal conductivity of SSPCMs with plastic matrix may be improved by adding thermally conductive fillers. However, the effect of these on rubber-based SSPCMs have not been studied. Considering that, future research should be focused on the enhancement of the thermal conductivity of the NR-based SSPCMs. In addition, the improvement of the latent heat storage capacity of the SSPCMs could be achieved by increasing the PCM content. However, this should be done without deteriorating the mechanical properties, which requires more advanced preparation techniques. If these enhancements can be made, the SSPCMs with NR matrix could be useful in applications making use of the mechanical characteristics and damping capability of rubber accompanied with increased

heat storage capacity. These SSPCMs could be used for example in architectural membranes to decrease the heat losses and improve the thermal comfort inside buildings. Another possible application is in spacecraft to provide thermal control. In addition, these SSPCMs could be used in cooling and thermal buffering systems of industrial machines.

REFERENCES

[1]   H. Mehling, L.F. Cabeza, Heat and cold storage with PCM, Springer Berlin Heidelberg, 2008, 308 p.

[2]   Review on sustainable thermal energy storage technologies, Part I: heat storage materials and techniques, 1998, pp. 1127-1138.

[3]   M.M. Farid, A.M. Khudhair, S.A.K. Razack, S. Al-Hallaj, A review on phase change energy storage: materials and applications, Energy Conversion and Management, Vol. 45, No. 9, 2004, pp. 1597-1615.

[4]   A.M. Khudhair, M.M. Farid, A review on energy conservation in building applications with thermal storage by latent heat using phase change materials, Energy Conversion and Management, Vol. 45, No. 2, 2004, pp. 263-275.

[5]   F. Agyenim, N. Hewitt, P. Eames, M. Smyth, A review of materials, heat transfer and phase change problem formulation for latent heat thermal energy storage systems (LHTESS), Renewable and Sustainable Energy Reviews, Vol. 14, No. 2, 2010, pp. 615-628.

[6]   B. Cárdenas, N. León, High temperature latent heat thermal energy storage: Phase change materials, design considerations and performance enhancement techniques, Renewable and Sustainable Energy Reviews, Vol. 27, 2013, pp. 724-737.

[7]   D. Zhou, C.Y. Zhao, Y. Tian, Review on thermal energy storage with phase change materials (PCMs) in building applications, Applied Energy, Vol. 92, 2012, pp. 593-605.

[8]   G. Alva, L. Liu, X. Huang, G. Fang, Thermal energy storage materials and systems for solar energy applications, Renewable and Sustainable Energy Reviews, Vol. 68, 2017, pp. 693-706.

[9]   P.B. Salunkhe, P.S. Shembekar, A review on effect of phase change material encapsulation on the thermal performance of a system, Renewable and Sustainable Energy Reviews, Vol. 16, No. 8, 2012, pp. 5603-5616.

[10]   M.M. Kenisarin, K.M. Kenisarina, Form-stable phase change materials for thermal energy storage, Renewable and Sustainable Energy Reviews, Vol. 16, No. 4, 2012, pp. 1999-2040.

[11] Y. Hong, G. Xin-shi, Preparation of polyethylene–paraffin compound as a form-stable solid-liquid phase change material, Solar Energy Materials and Solar Cells, Vol. 64, 2000, pp. 37-44.

[12] A. Sari, Form-stable paraffin/high density polyethylene composites as solid–liquid phase change material for thermal energy storage: preparation and thermal properties, Energy Conversion and Management, Vol. 45, No. 13–14, 2004, pp. 2033-2042.

[13] M. Karkri, M. Lachheb, Z. Nógellová, B. Boh, B. Sumiga, M.A. AlMaadeed, A. Fethi, I. Krupa, Thermal properties of phase-change materials based on high-density polyethylene filled with micro-encapsulated paraffin wax for thermal energy storage, Energy and Buildings, Vol. 88, 2015, pp. 144-152.

[14] Y.P. Zhang, K.P. Lin, R. Yang, H.F. Di, Y. Jiang, Preparation, thermal performance and application of shape-stabilized PCM in energy efficient buildings, Energy and Buildings, Vol. 38, No. 10, 2006, pp. 1262-1269.

[15] M. Xiao, B. Feng, K. Gong, Preparation and performance of shape stabilized phase change thermal storage materials with high thermal conductivity, Energy Conversion and Management, Vol. 43, No. 1, 2002, pp. 103-108.

[16] S. Peng, A. Fuchs, R.A. Wirtz, Polymeric phase change composites for thermal energy storage, Journal of Applied Polymer Science, Vol. 93, No. 3, 2004, pp. 1240-1251.

[17] Q. Zhang, Y. Zhao, J. Feng, Systematic investigation on shape stability of high-efficiency SEBS/paraffin form-stable phase change materials, Solar Energy Materials and Solar Cells, Vol. 118, 2013, pp. 54-60.

[18] L.F. Cabeza, Advances in Thermal Energy Storage Systems - Methods and Applications, Elsevier, 2015, 572 p.

[19] A.S. Fleischer, Thermal energy storage using phase change materials; fundamentals and applications, SpringerBriefs in Applies Sciences and Technology, 2015, 94 p.

[20] K. Pielichowska, K. Pielichowski, Phase change materials for thermal energy storage, Progress in Materials Science, Vol. 65, 2014, pp. 67-123.

[21] A. Sharma, V.V. Tyagi, C.R. Chen, D. Buddhi, Review on thermal energy storage with phase change materials and applications, Renewable and Sustainable Energy Reviews, Vol. 13, No. 2, 2009, pp. 318-345.

[22] G.A. Lane, Solar Heat Storage: Latent Heat Materials, CRC Press, 1983, 248 p.

[23] M.A. White, Heat storage systems, McGraw-Hill Education, web page. Available (accessed 31.10.2017): http://accessscience.com/content/heat-storage-systems/801980.

[24] W.M. Groenewoud, Characterisation of Polymers by Thermal Analysis, Elsevier B.V., 2001, 390 p.

[25] [25] Choudhury, N.R., De, P.P. & Dutta, N.K. (ed.). 2010. Thermal Analysis of Rubbers and Rubbery Materials. Smithers Rapra Technology. 543 p.

[26] K.Z. Ahmed, Application of Phase Change Materials, web page. Available (accessed 03.08.2017): http://textilecentre.blogspot.com/2016/05/application-of-phase-change-materials.html.

[27] Z. Khan, Z. Khan, A. Ghafoor, A review of performance enhancement of PCM based latent heat storage system within the context of materials, thermal stability and compatibility, Energy Conversion and Management, Vol. 115, 2016, pp. 132-158.

[28] A. Fallahi, G. Guldentops, M. Tao, S. Granados-Focil, S. Van Dessel, Review on solid-solid phase change materials for thermal energy storage: Molecular structure and thermal properties, Applied Thermal Engineering, Vol. 127, 2017, pp. 1427-1441.

[29] A. Abhat, Low temperature latent heat thermal energy storage: Heat storage materials, Solar Energy, Vol. 30, No. 4, 1983, pp. 313-332.

[30] G. Wettermark, B. Carlsson, H. Stymme, Storage of heat, Swedish Council for Building Research, 1979, 163 p.

[31] S. Tao, S. Wei, Y. Yulan, Characterization of expanded graphite microstructure and fabrication of composite phase-change material for energy storage, Journal of Materials in Civil Engineering, Vol. 27, No. 4, 2015.

[32] A. Sari, Thermal reliability test of some fatty acids as PCMs used for solar thermal latent heat storage applications, Energy Conversion and Management, Vol. 44, No. 14, 2003, pp. 2277-2287.

[33] S. Ushak, M. Suárez, S. Véliz, A.G. Fernández, E. Flores, H.R. Galleguillos, Characterization of calcium chloride tetrahydrate as a phase change material and thermodynamic analysis of the results, Renewable Energy, Vol. 95, 2016, pp. 213-224.

[34] S. Phadungphatthanakoon, S. Poompradub, S.P. Wanichwecharungruang, Increasing the thermal storage capacity of a phase change material by

encapsulation: Preparation and application in natural rubber, ACS Applied Materials and Interfaces, Vol. 3, No. 9, 2011, pp. 3691-3696.

[35]   G. Song, S. Ma, G. Tang, Z. Yin, X. Wang, Preparation and characterization of flame retardant form-stable phase change materials composed by EPDM, paraffin and nano magnesium hydroxide, Energy, Vol. 35, No. 5, 2010, pp. 2179-2183.

[36]   C.Y. Luo, J.D. Zuo, Property of POE, EVA and EPDM encapsulating paraffin as form stable phase change materials, Materials Research Innovations, Vol. 17, 2013, pp. 58-61.

[37]   Y. Wang, S. Wang, J. Wang, R. Yang, Preparation, stability and mechanical property of shape-stabilized phase change materials, Energy and Buildings, Vol. 77, 2014, pp. 11-16.

[38]   B. Pause, 6 - High-performance architectural membranes: Phase-change materials, in: J.I.d. Llorens (ed.), Fabric Structures in Architecture, Woodhead Publishing, 2015, pp. 187-199.

[39]   T.R. Crompton, Thermal Methods of Polymer Analysis, Smithers Rapra Technology, 2013, 216 p.

[40]   Y. Tang, D. Su, X. Huang, G. Alva, L. Liu, G. Fang, Synthesis and thermal properties of the MA/HDPE composites with nano-additives as form-stable PCM with improved thermal conductivity, Applied Energy, Vol. 180, 2016, pp. 116-129.

[41]   I. Krupa, G. Miková, A.S. Luyt, Phase change materials based on low-density polyethylene/paraffin wax blends, European Polymer Journal, Vol. 43, No. 11, 2007, pp. 4695-4705.

[42]   I. Krupa, G. Miková, A.S. Luyt, Polypropylene as a potential matrix for the creation of shape stabilized phase change materials, European Polymer Journal, Vol. 43, No. 3, 2007, pp. 895-907.

[43]   C. Alkan, K. Kaya, A. Sari, Preparation, Thermal Properties and Thermal Reliability of Form-Stable Paraffin/Polypropylene Composite for Thermal Energy Storage, Journal of Polymers and the Environment, Vol. 17, No. 4, 2009, pp. 254.

[44]   A. Sari, K. Kaygusuz, Studies on poly(vinyl chloride)/fatty acid blends as shape-stabilized phase change material for latent heat thermal energy storage, Indian Journal of Engineering and Materials Sciences, Vol. 13, 2006, pp. 253-258.

[45]   A. Sari, K. Kaygusuz, Poly(vinyl alcohol)/Fatty Acid Blends for Thermal Energy Storage, Energy Sources, 2007, pp. 873-883.

[46]   C. Alkan, A. Sari, Fatty acid/poly(methyl methacrylate) (PMMA) blends as form-stable phase change materials for latent heat thermal energy storage, Solar Energy, Vol. 82, No. 2, 2008, pp. 118-124.

[47]   L. Wang, D. Meng, Fatty acid eutectic/polymethyl methacrylate composite as form-stable phase change material for thermal energy storage, Applied Energy, Vol. 87, No. 8, 2010, pp. 2660-2665.

[48]   A. Sari, C. Alkan, A. Karaipekli, A. Önal, Preparation, characterization and thermal properties of styrene maleic anhydride copolymer (SMA)/fatty acid composites as form stable phase change materials, Energy Conversion and Management, Vol. 49, No. 2, 2008, pp. 373-380.

[49]   J. Zeng, F. Zhu, S. Yu, Z. Xiao, W. Yan, S. Zheng, L. Zhang, L. Sun, Z. Cao, Myristic acid/polyaniline composites as form stable phase change materials for thermal energy storage, Solar Energy Materials and Solar Cells, Vol. 114, 2013, pp. 136-140.

[50]   J.L. Zeng, J. Zhang, Y.Y. Liu, Z.X. Cao, Z.H. Zhang, F. Xu, L.X. Sun, Polyaniline/1-tetradecanol composites, Journal of Thermal Analysis and Calorimetry, Vol. 91, No. 2, 2008, pp. 455-461.

[51]   F. Zhu, L. Zhang, J. Zeng, L. Zhu, Z. Zhu, X. Zhu, R. Li, Z. Xiao, Z. Cao, Preparation and thermal properties of palmitic acid/polyaniline/copper nanowires form-stable phase change materials, Journal of Thermal Analysis and Calorimetry, Vol. 115, No. 2, 2014, pp. 1133-1141.

[52]   S. Jegadheeswaran, S.D. Pohekar, Performance enhancement in latent heat thermal storage system: A review, Renewable and Sustainable Energy Reviews, Vol. 13, No. 9, 2009, pp. 2225-2244.

[53]   W. Mhike, W.W. Focke, J.P. Mofokeng, A.S. Luyt, Thermally conductive phase-change materials for energy storage based on low-density polyethylene, soft Fischer–Tropsch wax and graphite, Thermochimica Acta, Vol. 527, 2012, pp. 75-82.

[54]   W. Cheng, R. Zhang, K. Xie, N. Liu, J. Wang, Heat conduction enhanced shape-stabilized paraffin/HDPE composite PCMs by graphite addition: Preparation and thermal properties, Solar Energy Materials and Solar Cells, Vol. 94, No. 10, 2010, pp. 1636-1642.

[55]   Z. Liu, R. Yang, Synergistically-Enhanced Thermal Conductivity of Shape-Stabilized Phase Change Materials by Expanded Graphite and Carbon Nanotube, Applied Sciences, Vol. 7, No. 6, 2017, pp. 574.

[56] Y. Tang, Y. Jia, G. Alva, X. Huang, G. Fang, Synthesis, characterization and properties of palmitic acid/high density polyethylene/graphene nanoplatelets composites as form-stable phase change materials, Solar Energy Materials and Solar Cells, Vol. 155, 2016, pp. 421-429.

[57] B. Pause, Membranes with thermo-regulating properties for architectural application, International Conference on Adaptable Building Structures, 03.07.2006.

[58] W. Wu, N. Liu, W. Cheng, Y. Liu, Study on the effect of shape-stabilized phase change materials on spacecraft thermal control in extreme thermal environment, Energy Conversion and Management, Vol. 69, 2013, pp. 174-180.